UNIVERSITY OF CALIFORNIA SAN DIEGO

Mechanisms of regulation of cytoplasmic dynein by Lis1

A dissertation submitted in partial satisfaction of the
requirements for the degree Doctor of Philosophy

in

Biology

by

John P. Gillies

Committee in charge:

Professor Samara Reck-Peterson, Chair
Professor Kevin Corbett
Professor Enfu Hui
Professor Andres Leschziner
Professor Karen Oegema
Professor Jin Zhang

2021

The dissertation of John P. Gillies is approved, and it is acceptable in quality and form for publication on microfilm and electronically:

_____

_____

_____

_____

_____

_____

Chair

University of California San Diego

2021

TABLE OF CONTENTS

LIST OF FIGURES

ACKNOWLEDGMENTS

First and foremost I would like to thank my advisor Sam Reck-Peterson. She has been an exceptional mentor, not only in science but in leadership, communication and compassion as well. She was always willing to make time to help me with a problem I was facing, but was never overbearing and allowed me to push my projects forward. Her ability to create such a collaborative lab environment is truly admirable, and it made it a joy to come to work every day.

I would also like to thank my committee members, Kevin Corbett, Enfu Hui, Andres Leschziner, Karen Oegema and Jin Zhang for providing me guidance, insights and critical feedback. I would particularly like to thank Andres for being an incredible collaborator throughout both of my projects. I would also like to thank my undergraduate mentor Andrew Marcus for giving me the opportunity to conduct research for the first time and for encouraging me to attend grad school.

I have had the opportunity to work with an amazing group of scientists in both the Reck-Peterson and Leschziner labs, and each of them has helped me along the way as well as made for such a fun lab environment. I would particularly like to thank Morgan and Zaw for being amazing mentors, collaborators, and friends. I would also like to thank Salo for all his advice on experiments, writing and presentations, it’s just too bad we never got that chance to collaborate on a project.

Finally, I would like to thank my family. I would not be where I am today without the love and support of my mom and dad. I would like to thank my older

sister Taryn for inspiring me to follow her into biology and for warning me about grad school even though I didn't listen. Last but not least I would like to thank my wife Kaitlyn. She has supported me every step of the way, and I could not have done any of it without her.

Chapter 2, in full, is a reprint of Htet, ZM*; Gillies, JP*; Baker, RW.; Leschziner, AE; DeSantis, ME; Reck-Peterson, SL. LIS1 promotes the formation of activated cytoplasmic dynein-1 complexes. Nat. Cell Biol. 22, 518–525 (2020). The dissertation author was the co-primary author of this work.

Chapter 3, in full, is a manuscript in preparation: Gillies, JP*; Reimer, JM*; Lahiri I; Karasmanis E; Htet ZM; Leschziner, AE; Reck-Peterson, SL. Structural Basis for Cytoplasmic Dynein-1 Regulation by Lis1. (In preparation). The dissertation author was the co-primary author of this work.

VITA

Education

University of California San Diego, San Diego, California 2016-2021
PhD, Biology

University of Oregon, Eugene, Oregon 2016
Bachelor of Science in Biochemistry, *summa cum laude*

Research Experience

Graduate Student 2017-2021
University of California San Diego
Reck-Peterson Lab

Undergraduate Research 2013-2016
University of Oregon
Marcus Lab

Honors and Achievements

ARCS Scholar 2019
NSF Graduate Research Fellowship Program Honorable Mention 2018
Ruth Stern Fellowship 2017
Molecular Biophysics Training Grant 2017
Goldwater Scholar 2015
Arnold and Mabel Beckman Foundation Scholar 2014-2015

Presentation

Biophysical Society Meeting 2019
Poster

American Society of Cell Biology Meeting 2018-2019
Microsymposium talk and poster 2018, Poster 2019

Molecular Biophysics Training Grant Retreat 2017-2018
Poster; received best poster award 2017 and 2018

Publications

Zaw Min Htet#, **John P. Gillies#**, Richard W. Baker, Andres E. Leschziner, Morgan E. DeSantis*, Samara L. Reck-Peterson*. (2019). Lis1 promotes the formation of maximally activated cytoplasmic dynein-1 complexes. In press at Nature Cell Biology. doi:10.1101/683052 #co-first authors *co-corresponding authors

Wonbae Lee#, **John P. Gillies#**, Davis Jose, Brett A. Israels, Peter H. von Hippel, & Andrew H. Marcus. (2016). Single-molecule FRET studies of the cooperative and non-cooperative binding kinetics of the bacteriophage T4 single-stranded DNA binding protein (gp32) to ssDNA lattices at replication fork junctions. Nucleic Acids Research, 44(22), 10691-10710. #co-first authors

ABSTRACT OF THE DISSERTATION

Mechanisms of regulation of cytoplasmic dynein by Lis1

by

John P. Gillies

Doctor of Philosophy in Biology

University of Calfornia San Diego, 2021

Professor Samara Reck-Peterson, Chair

Cytoplasmic dynein-1 (dynein) is a molecular motor that drives nearly all minus-end-directed microtubule-based transport in human cells, performing functions ranging from retrograde axonal transport to mitotic spindle assembly. For human dynein to be motile it must form an activated complex with two cofactors, dynactin and one of a set of coiled-coil containing activating adaptor proteins. In cells dynein requires additional cofactors, including the conserved dynein regulator

Lis1. Lis1 is critical for all of dynein's known functions and is unique among dynein's regulators because it is the only one which binds directly to the motor domain. This makes it important to consider Lis1 regulation both of activated dynein complexes as well as regulation of the dynein motor itself. In this thesis I present work studying the mechanisms of dynein regulation by Lis1 using a combination of biochemistry, single molecule imaging, cell biology, and cryo-electron microscopy. In chapter 2 we investigated the role of Lis1 in the context of activated dynein complexes containing dynactin, an activating adaptor and one or two dynein dimers and found that Lis1 aids the formation of these complexes. Interestingly, Lis1 is not required for the motility of these complexes once they form. Lis1 aids dynein in overcoming its auto-inhibition and assume the correct configuration for proper addition into the complex before Lis1 dissociates as the complex moves along microtubules. In chapter 3 we solved a 3.1Å structure of a dynein-Lis1 complex, which we used to understand how Lis1 directly influences the mechanochemistry of the dynein motor. Lis1 has two opposing modes of regulating the dynein motor, either increasing or decreasing dynein's microtubule binding affinity. We found novel contact sites important for both modes of regulation *in vitro* in single molecule assays and *in vivo* in *Saccharomyces cerevisiae*. Overall, this work reveals the complicated nature of dynein regulation by Lis1 and allows us to make a unified model, which is presented in chapter 4.

Chapter 1:

Introduction to the regulation of

Cytoplasmic Dynein-1 by Lis1

1.1 Cytoplasmic Dynein-1

Cell division, development and the transport of cellular cargo are fundamental processes that require the microtubule cytoskeleton and associated motor proteins. Microtubules are polarized structures that have plus ends generally oriented toward the plasma membrane and minus ends usually found near the center of the cell. The motor proteins dynein and kinesin couple ATP hydrolysis to movement along these microtubule tracks. There are ~40 kinesins that are responsible for transporting cellular cargos towards the plus end of microtubules, but minus-end-directed transport is carried out by only one motor, cytoplasmic dynein-1 (dynein hereafter)[1]. This means that dynein is responsible for the movement of hundreds of different cargos, including endosomes, peroxisomes, mitochondria, and other membrane-bound compartments. Additionally, dynein has been linked to the motility of mRNAs and is hijacked by viruses to transport viral components[2]. Dynein is found in many eukaryotes and is often essential; for example, dynein knockout causes embryonic lethality in mice[3]. Notably, dynein genes are not found in plants and some algae, which instead use minus-end directed kinesins. Mutations in dynein have been linked to a variety of neurological diseases, such as spinal muscular atrophy with lower extremity predominance, Charcot-Marie-Tooth disease, Perry syndrome, and lissencephaly[4].

In contrast to kinesin and myosin motors, which share a common ancestor related to G-proteins, dynein is a member of the AAA+ family of ATPases. Dynein is also larger and more complicated in terms of accessory chains than either

kinesin or myosin; dynein is a 1.4 MDa complex composed of two copies each of six polypeptide chains (Figure 1.1a). The dynein motor is composed of six AAA domains, with AAA1, 3 and 4 capable of binding and hydrolyzing ATP[5]. The primary site of ATP hydrolysis is AAA1, which is required for dynein motility[6,7]. Mutations that block binding or hydrolysis in AAA3 impair dynein motility, as do mutations in AAA4 albeit to a much lesser extent[7–11]. On average dynein only hydrolyzes one ATP per step, indicating a regulatory role for AAA3 and 4[9,12–14].

Dynein from *Saccharomyces cerevisiae* is a processive motor (i.e., able to take multiple steps along microtubules without dissociating completely). This is true for full length dynein as well as dynein with a truncated tail dimerized with GST that does not require the dynein accessory chains[12]. However, *in vivo* dynein requires many additional co-factors to function[15]. Also, unlike yeast dynein, mammalian dynein is not processive in the absence of other regulators in vitro. Mammalian dynein in vitro requires interaction with at least two factors, dynactin and an activating adaptor, to form the minimal processive dynein complex[16,17] (Figure 1.1b). This is partially due to dynein existing in an auto-inhibited state called the phi particle that must be opened before it can be become active[18] (Figure 1.1c). Recently it was shown that some activating adaptors can recruit a second dynein to the complex, which results in faster velocities[19,20] (Figure 1.1c).

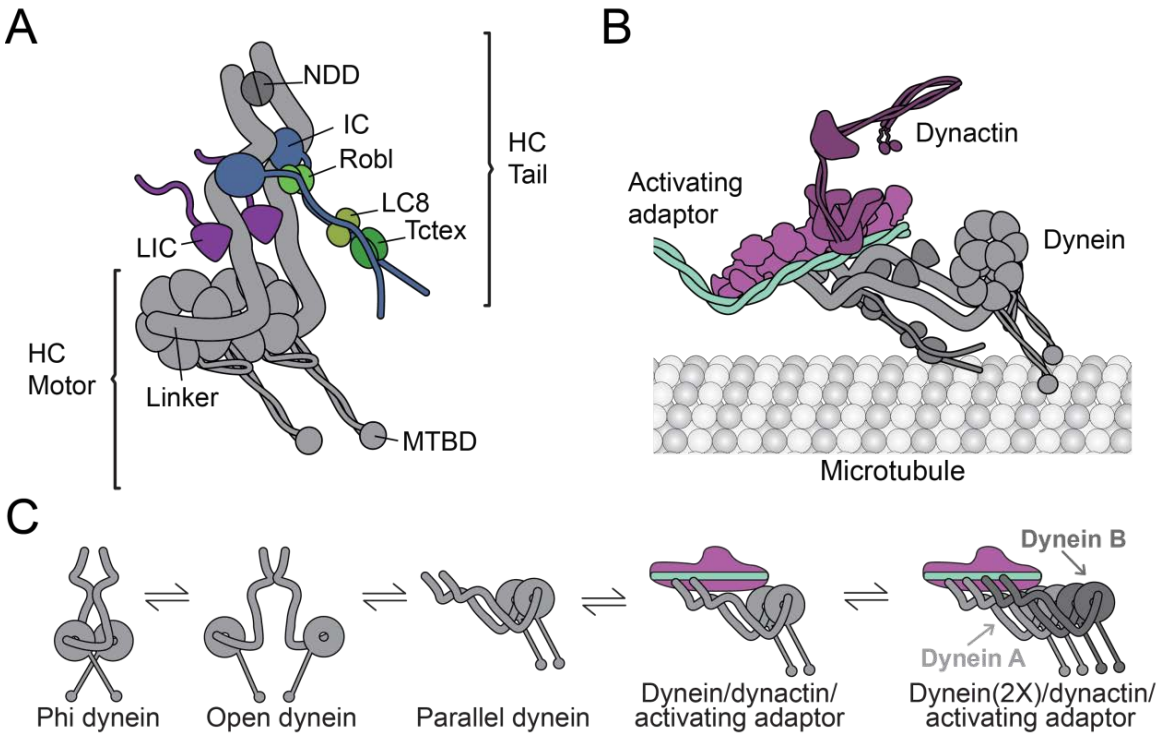

Figure 1.1. Activation of dynein by dynactin and activating adaptors. A. Cartoon of cytoplasmic dynein 1. The dynein heavy chain (HC) contains a C-terminal motor domain composed of 6 AAA+ ATPase domains with a microtubule-binding domain (MTDB) at the end of a long coiled- coil stalk.The HCs are linked together via an N- terminal dimerization domain (NDD) that is part of the HC tail, which also binds the intermediate chains (IC) and light intermediate chains (LIC). The ICs have extended N termini that bind dimers of the light chains Roadblock (Robl), LC8 and Tctex. **B.** Cartoon of an activated dynein complex composed of dynein, dynactin, and an activating adaptor. **C.** Schematic of the current model for dynein activation. Dynein (grey) is autoinhibited in the Phi conformation, and then opens and finally adopts a parallel conformation that is seen in the activated dynein complex, which includes dynactin (purple) and an activating adaptor (green). Activated dynein complexes can contain two dynein dimers (dynein A and B, far right).

In vivo dynein also requires an additional regulatory molecule, the protein Lis1. Lis1 is required for nearly all dynein functions, and loss of Lis1 results in debilitating neurodevelopmental defects[21]. Lis1 is unique among dynein's regulators because it is the only one known to bind directly to the motor domain[5,22–24]. Lis1 regulation is particularly interesting because it has implications both for the mechanochemical regulation of dynein as well as for the formation of activated complexes containing dynein, dynactin and activating adaptors.

1.2 Lis1 is a conserved regulator of dynein

LIS1 was first discovered as the primary gene mutated in type-1 lissencephaly, a neurodevelopmental disorder that results in a smooth cerebral surface and abnormal neuronal migration[25]. It was later linked to the dynein pathway in fungal genetic screens probing nuclear migration and positioning[26]. This link was later confirmed in metazoans through genetic studies in *Drosophila melanogaster*[27,28]. Shortly after, mammalian Lis1 was shown to colocalize with dynein in vivo and directly interact with it in vitro[29–31]. In highly polarized cells, such as neurons or filamentous fungi, Lis1 is required for the transport of endosomes, peroxisomes, lysosomes, mitochondria and mRNA[32–38]. Lis1 has a conserved function in nuclear and centrosomal positioning in organisms from fungi to humans[26,39–42].

One required function of Lis1 seems to be initiating transport by aiding dynein recruitment to cargo. For example, in A. nidulans Lis1 is not observed on

moving endosomes and loss of Lis1 reduces the number of moving endosomes but does not reduce the velocity of those that do move, suggesting that once dynein is on the cargo Lis1 is no longer required[33]. Similarly, Lis1 is required to recruit dynein to mRNA complexes in Drosophila[32] and in mouse dorsal root ganglion neurons Lis1 knockdown reduces the retrograde movement of lysosomes[35]. In HeLa cells Lis1 is necessary for dynein recruitment to membranes[43,44], suggesting that recruiting dynein to cargo is a conserved function of Lis1.

1.3 Molecular mechanism of dynein regulation by Lis1

Lis1 is the only known dynein regulator to bind to the motor domain, and it is therefore important to consider Lis1's regulation of dynein's mechanochemical cycle. Lis1 is a functional dimer, with each monomer consisting of an N-terminal LisH dimerization domain, a coiled coil, a disordered loop, and a β-propeller containing seven WD repeats[45,46]. Lis1 binds at two sites on dynein, one site at AAA3/AAA4 ($site_{ring}$) and one on the dynein stalk ($site_{stalk}$)[22–24].

Dynein microtubule binding

Lis1 has been shown to induce a high microtubule binding affinity of dynein in organisms ranging from yeast to humans[22,47–49]. This state correlates with Lis1 bound only at $site_{ring,}$ which induces an open conformation in dynein's ring[22,24]. In vivo this is likely important for maintaining dynein at plus ends for cargo loading,

such as offloading onto the cortex in *S. cerevisiae* or attachment to vesicular cargo for long distance transport.

Lis1 bound to $site_{stalk}$ as well as $site_{ring}$ induces the opposite effect, decreasing dynein's affinity for the microtubule. This occurs when dynein's AAA3 domain is bound to ATP. This state can be observed using a dynein that has a mutation in its Walker B motif in AAA3, which allows it to bind ATP but not hydrolyze it. It can also be observed using ATP and vanadate, which mimic the ADP.Pi state in AAA3. Binding of Lis1 at both binding sites induces a closed state in dynein's ring and prevents the sliding of the coiled coils in dynein's stalk that result in high MT affinity. In *S. cerevisiae* this release from microtubules is required for dynein's transport to the plus ends of microtubules[24].

Dynein ATPase rate

Lis1 does not significantly affect the ATPase rate of dynein[22,47,48]. The majority of dynein's ATPase activity is attributed to AAA1 both in the presence and absence of Lis1[23]. This is a surprising contrast to mutations in dynein that increase its microtubule binding affinity, such as the AAA4 arginine finger mutant[22,50] or a mutant that inhibits linker docking at AAA5[51]; both of these dynein mutants result in prolonged microtubule attachment, but they also both display severely reduced ATPase rate[50,51]. This distinction in the mechanism of Lis1 led to an analogy of a clutch; Lis1 binding serves to disconnect the flow of structural changes from dynein's motor to the microtubule binding domain[22].

Dynein velocity

An increase in dynein's microtubule binding affinity results in a decrease in velocity because each dynein motor remains bound to the microtubule longer between steps. Addition of Lis1 to dynein therefore results in a decrease in dynein velocity[22–24]. Although human dynein is not processive on its own as discussed above, teams of dynein attached to a surface are able to move microtubules. In this assay Lis1 decreases the velocity of human dynein as well[47,49,52,53]. Interestingly, when Lis1 is added to activated dynein complexes containing dynein, dynactin and an activating adaptor it increases their velocity, in contrast to its effect on dynein alone.

1.4 Outstanding questions

We wanted to investigate how Lis1 increases the velocity of activated dynein complexes, which is the topic of chapter 2. In agreement with previous studies[49,54] we found that Lis1 increases the velocity of activated dynein complexes. We show that this is due to Lis1 aiding the recruitment of two dynein dimers to the complex. Interestingly, Lis1 does not remain as a stable member of this complex but instead dissociates once it is moving on microtubules. We propose that Lis1 helps release dynein auto-inhibition and favors a dynein conformation primed for inclusion in the activated dynein complex.

The contact sites required for Lis1's regulation of the dynein mechanochemical cycle have not been fully mapped because previous structures

were not of high enough resolution to unambiguously determine the orientation of the Lis1 ß-propeller. In chapter 3 we use a new 3.1Å structure of Lis1 bound to dynein to disrupt all of the observed dynein-Lis1 interactions as well as the interaction between the Lis1 ß-propellers and then determine the effects on dynein's mechanochemistry and functions in vivo. We found novel interactions that contribute to both modes of Lis1 regulation.

1.5 References

1. Vale, R. D. The molecular motor toolbox for intracellular transport. *Cell* **112**, 467–480 (2003).

2. Reck-Peterson, S. L., Redwine, W. B., Vale, R. D. & Carter, A. P. The cytoplasmic dynein transport machinery and its many cargoes. *Nat. Rev. Mol. Cell Biol.* (2018) doi:10.1038/s41580-018-0004-3.

3. Harada, A., Takei, Y., Kanai, Y., Tanaka, Y., Nonaka, S. & Hirokawa, N. Golgi vesiculation and lysosome dispersion in cells lacking cytoplasmic dynein. *J. Cell Biol.* **141**, 51–59 (1998).

4. Lipka, J., Kuijpers, M., Jaworski, J. & Hoogenraad, C. C. Mutations in cytoplasmic dynein and its regulators cause malformations of cortical development and neurodegenerative diseases. *Biochem. Soc. Trans.* **41**, 1605–12 (2013).

5. Cianfrocco, M. a., DeSantis, M. E., Leschziner, A. E. & Reck-Peterson, S. L. Mechanism and Regulation of Cytoplasmic Dynein. *Annu. Rev. Cell Dev. Biol.* **31**, annurev-cellbio-100814-125438 (2015).

6. Gibbons, I. R., Lee-Eiford, A., Mocz, G., Phillipson, C. A., Tang, W. J. & Gibbons, B. H. Photosensitized cleavage of dynein heavy chains. Cleavage at the 'V1 site' by irradiation at 365 nm in the presence of ATP and vanadate. *J. Biol. Chem.* **262**, 2780–2786 (1987).

7. Kon, T., Nishiura, M., Ohkura, R., Toyoshima, Y. Y. & Sutoh, K. Distinct functions of nucleotide-binding/hydrolysis sites in the four AAA modules of cytoplasmic dynein. *Biochemistry* **43**, 11266–11274 (2004).

8. Kon, T., Mogami, T., Ohkura, R., Nishiura, M. & Sutoh, K. ATP hydrolysis cycle-dependent tail motions in cytoplasmic dynein. *Nat. Struct. Mol. Biol.* **12**, 513–519 (2005).

9. DeWitt, M. A., Cypranowska, C. A., Cleary, F. B., Belyy, V. & Yildiz, A. The AAA3 domain of cytoplasmic dynein acts as a switch to facilitate microtubule release. *Nat. Struct. Mol. Biol.* **22**, 73–80 (2015).

10. Silvanovich, A., Li, M., Serr, M., Mische, S. & Hays, T. S. The Third P-loop Domain in Cytoplasmic Dynein Heavy Chain Is Essential for Dynein Motor Function and ATP-sensitive Microtubule Binding. *Mol. Biol. Cell* **14**, 1355–1365 (2003).

11. Cho, C., Reck-Peterson, S. L. & Vale, R. D. Regulatory ATPase sites of cytoplasmic dynein affect processivity and force generation. *J. Biol. Chem.* **283**, 25839–25845 (2008).

12. Reck-Peterson, S. L., Yildiz, A., Carter, A. P., Gennerich, A., Zhang, N. & Vale, R. D. Single-Molecule Analysis of Dynein Processivity and Stepping Behavior. *Cell* **126**, 335–348 (2006).

13. Mallik, R., Carter, B. C., Lex, S. A., King, S. J. & Gross, S. P. Cytoplasmic dynein functions as a gear in response to load. *Nature* **427**, 649–652 (2004).

14. Toba, S., Watanabe, T. M., Yamaguchi-Okimoto, L., Toyoshima, Y. Y. & Higuchi, H. Overlapping hand-over-hand mechanism of single molecular motility of cytoplasmic dynein. *Proc. Natl. Acad. Sci. U. S. A.* **103**, 5741–5745 (2006).

15. Reck-peterson, S. L., Redwine, W. B., Vale, R. D. & Carter, A. P. The Cytoplasmic Dynein Transport Machinery and its Many Cargos.

16. McKenney, R. J., Huynh, W., Tanenbaum, M. E., Bhabha, G. & Vale, R. D. Activation of cytoplasmic dynein motility by dynactin-cargo adapter complexes. *Science (80-.).* **345**, 337–41 (2014).

17. Schlager, M. A., Hoang, H. T., Urnavicius, L., Bullock, S. L. & Carter, A. P. In vitro reconstitution of a highly processive recombinant human dynein complex. *EMBO J.* **33**, 1855–68 (2014).

18. Zhang, K., Foster, H. E., Rondelet, A., Lacey, S. E., Bahi-Buisson, N., Bird, A. W. & Carter, A. P. Cryo-EM Reveals How Human Cytoplasmic Dynein Is Auto-inhibited and Activated. *Cell* **169**, 1303-1314.e18 (2017).

19. Urnavicius, L., Lau, C. K., Elshenawy, M. M., Morales-Rios, E., Motz, C., Yildiz, A. & Carter, A. P. Cryo-EM shows how dynactin recruits two dyneins

for faster movement. *Nature* **554**, 202–206 (2018).

20. Grotjahn, D. A., Chowdhury, S., Xu, Y., McKenney, R. J., Schroer, T. A. & Lander, G. C. Cryo-electron tomography reveals that dynactin recruits a team of dyneins for processive motility. *Nat. Struct. Mol. Biol.* **25**, 203–207 (2018).

21. Franker, M. A. M. & Hoogenraad, C. C. Microtubule-based transport -basic mechanisms, traffic rules and role in neurological pathogenesis. *J. Cell Sci.* **126**, 2319–2329 (2013).

22. Huang, J., Roberts, A. J., Leschziner, A. E. & Reck-Peterson, S. L. Lis1 acts as a 'clutch' between the ATPase and microtubule-binding domains of the dynein motor. *Cell* **150**, 975–986 (2012).

23. Toropova, K., Zou, S., Roberts, A. J., Redwine, W. B., Goodman, B. S., Reck-Peterson, S. L. & Leschziner, A. E. Lis1 regulates dynein by sterically blocking its mechanochemical cycle. *Elife* **3**, 1–25 (2014).

24. DeSantis, M. E., Cianfrocco, M. A., Htet, Z. M., Tran, P. T., Reck-Peterson, S. L. & Leschziner, A. E. Lis1 Has Two Opposing Modes of Regulating Cytoplasmic Dynein. *Cell* **170**, 1197-1208.e12 (2017).

25. Reiner, O., Carrozzo, R., Shen, Y., Wehnert, M., Faustinella, F., Dobyns, W. B., Caskey, C. T. & Ledbetter, D. H. Isolation of a Miller-Dieker lissencephaly gene containing G protein beta-subunit-like repeats. *Nature* **364**, 717–721 (1993).

26. Xiang, X., Osmani, A. H., Osmani, S. A., Xin, M. & Morris, N. R. NudF, a nuclear migration gene in Aspergillus nidulans, is similar to the human LIS-1 gene required for neuronal migration. *Mol. Biol. Cell* **6**, 297–310 (1995).

27. Liu, Z., Xie, T. & Steward, R. Lis1, the Drosophila homolog of a human lissencephaly disease gene, is required for germline cell division and oocyte differentiation. *Development* **126**, 4477–4488 (1999).

28. Liu, Z., Steward, R. & Luo, L. Drosophila Lis1 is required for neuroblast proliferation, dendritic elaboration and axonal transport. *Nat. Cell Biol.* **2**, 776–783 (2000).

29. Faulkner, N. E., Dujardin, D. L., Tai, C. Y., Vaughan, K. T., O'connell, C. B., Wang, Y. L. & Vallee, R. B. A role for the lissencephaly gene Lis1 in mitosis and cytoplasmic dynein function. *Nat. Cell Biol.* **2**, 784–791 (2000).

30. Sasaki, S., Shionoya, A., Ishida, M., Gambello, M. J., Yingling, J., Wynshaw-Boris, A. & Hirotsune, S. A LIS1/NUDEL/cytoplasmic dynein heavy chain

complex in the developing and adult nervous system. *Neuron* **28**, 681–696 (2000).

31. Smith, D. S., Niethammer, M., Ayala, R., Zhou, Y., Gambello, M. J. & Tsai, L. Regulation of cytoplasmic dynein behaviour and microtubule organization by mammalian Lis1. *Nat. Cell Biol.* **2**, 767–775 (2000).

32. Dix, C. I., Soundararajan, H. C., Dzhindzhev, N. S., Begum, F., Suter, B., Ohkura, H., Stephens, E. & Bullock, S. L. Lissencephaly-1 promotes the recruitment of dynein and dynactin to transported mRNAs. *J. Cell Biol.* **202**, 479–494 (2013).

33. Egan, M. J., Tan, K. & Reck-Peterson, S. L. Lis1 is an initiation factor for dynein-driven organelle transport. *J. Cell Biol.* **197**, 971–982 (2012).

34. Lenz, J. H., Schuchardt, I., Straube, A. & Steinberg, G. A dynein loading zone for retrograde endosome motility at microtubule plus-ends. *EMBO J.* **25**, 2275–2286 (2006).

35. Moughamian, A. J., Osborn, G. E., Lazarus, J. E., Maday, S. & Holzbaur, E. L. F. Ordered recruitment of Dynactin to the microtubule plus-end is required for efficient initiation of retrograde axonal transport. *J. Neurosci.* **33**, 13190–13203 (2013).

36. Shao, C. Y., Zhu, J., Xie, Y. J., Wang, Z., Wang, Y. N., Wang, Y., Su, L. Da, Zhou, L., Zhou, T. H. & Shen, Y. Distinct Functions of Nuclear Distribution Proteins LIS1, Ndel1 and NudCL in Regulating Axonal Mitochondrial Transport. *Traffic* **14**, 785–797 (2013).

37. Yi, J. Y., Ori-McKenney, K. M., McKenney, R. J., Vershinin, M., Gross, S. P. & Vallee, R. B. High-resolution imaging reveals indirect coordination of opposite motors and a role for LIS1 in high-load axonal transport. *J. Cell Biol.* **195**, 193–201 (2011).

38. Zhang, J., Zhuang, L., Lee, Y., Abenza, J. F., Peñalva, M. A. & Xiang, X. The microtubule plus-end localization of Aspergillus dynein is important for dynein-early-endosome interaction but not for dynein ATPase activation. *J. Cell Sci.* **123**, 3596–3604 (2010).

39. Lee, W. L., Oberle, J. R. & Cooper, J. A. The role of the lissencephaly protein Pac1 during nuclear migration in budding yeast. *J. Cell Biol.* **160**, 355–364 (2003).

40. Tsai, J. W., Bremner, K. H. & Vallee, R. B. Dual subcellular roles for LIS1 and dynein in radial neuronal migration in live brain tissue. *Nat. Neurosci.* **10**, 970–979 (2007).

41. Sitaram, P., Anderson, M. A., Jodoin, J. N., Lee, E. & Lee, L. A. Regulation of dynein localization and centrosome positioning by lis-1 and asunder during drosophila spermatogenesis. *Dev.* **139**, 2945–2954 (2012).

42. Cockell, M. M., Baumer, K. & Gönczy, P. lis-1 is required for dynein-dependent cell division processes in C. elegans embryos. *J. Cell Sci.* **117**, 4571–4582 (2004).

43. Lam, C., Vergnolle, M. A. S., Thorpe, L., Woodman, P. G. & Allan, V. J. Functional interplay between LIS1, NDE1 and NDEL1 in dynein-dependent organelle positioning. *J. Cell Sci.* **123**, 202–212 (2010).

44. Splinter, D., Razafsky, D. S., Schlager, M. A., Serra-Marques, A., Grigoriev, I., Demmers, J., Keijzer, N., Jiang, K., Poser, I., Hyman, A. A., Hoogenraad, C. C., King, S. J. & Akhmanova, A. BICD2, dynactin, and LIS1 cooperate in regulating dynein recruitment to cellular structures. *Mol. Biol. Cell* **23**, 4226–4241 (2012).

45. Kim, M. H., Cooper, D. R., Oleksy, A., Devedjiev, Y., Derewenda, U., Reiner, O., Otlewski, J. & Derewenda, Z. S. The structure of the N-terminal domain of the product of the lissencephaly gene Lis1 and its functional implications. *Structure* **12**, 987–998 (2004).

46. Tarricone, C., Perrina, F., Monzani, S., Massimiliano, L., Kim, M. H., Derewenda, Z. S., Knapp, S., Tsai, L. H. & Musacchio, A. Coupling PAF signaling to dynein regulation: Structure of LIS1 in complex with PAF-acetylhydrolase. *Neuron* **44**, 809–821 (2004).

47. Yamada, M., Toba, S., Yoshida, Y., Haratani, K., Mori, D., Yano, Y., Mimori-Kiyosue, Y., Nakamura, T., Itoh, K., Fushiki, S., Setou, M., Wynshaw-Boris, A., Torisawa, T., Toyoshima, Y. Y. & Hirotsune, S. LIS1 and NDEL1 coordinate the plus-end-directed transport of cytoplasmic dynein. *EMBO J.* **27**, 2471–2483 (2008).

48. McKenney, R. J., Vershinin, M., Kunwar, A., Vallee, R. B. & Gross, S. P. LIS1 and NudE induce a persistent dynein force-producing state. *Cell* **141**, 304–314 (2010).

49. Baumbach, J., Murthy, A., McClintock, M. A., Dix, C. I., Zalyte, R., Hoang, H. T. & Bullock, S. L. Lissencephaly-1 is a context-dependent regulator of the human dynein complex. *Elife* **6**, 1–31 (2017).

50. Zhuang, L., Zhang, J. & Xiang, X. Point mutations in the stem region and the fourth AAA domain of cytoplasmic dynein heavy chain partially suppress the phenotype of NUDF/LIS1 loss in Aspergillus nidulans. *Genetics* **175**, 1185–1196 (2007).

51. Schmidt, H., Gleave, E. S. & Carter, A. P. Insights into dynein motor domain function from a 3.3-Å crystal structure. *Nat. Struct. Mol. Biol.* **19**, 492–497 (2012).

52. Torisawa, T., Nakayama, A., Furuta, K., Yamada, M., Hirotsune, S. & Toyoshima, Y. Y. Functional dissection of LIS1 and NDEL1 towards understanding the molecular mechanisms of cytoplasmic dynein regulation. *J. Biol. Chem.* **286**, 1959–1965 (2011).

53. Wang, S., Ketcham, S. A., Schon, A., Goodman, B., Wang, Y., Yates, J., Freire, E., Schroer, T. A. & Zheng, Y. Nudel/NudE and Lis1 promote dynein and dynactin interaction in the context of spindle morphogenesis. *Mol. Biol. Cell* **24**, 3522–3533 (2013).

54. Gutierrez, P. A., Ackermann, B. E., Vershinin, M. & McKenney, R. J. Differential effects of the dynein-regulatory factor Lissencephaly-1 on processive dynein-dynactin motility. *J. Biol. Chem.* **292**, 12245–12255 (2017).

Chapter 2:

Lis1 promotes the formation of activated cytoplasmic dynein-1 complexes

2.1 Abstract

Cytoplasmic dynein-1 is a molecular motor that drives nearly all minus-end-directed microtubule-based transport in human cells, performing functions ranging from retrograde axonal transport to mitotic spindle assembly[1,2]. Activated dynein complexes consist of one or two dynein dimers, the dynactin complex, and an "activating adaptor", with faster velocity seen when two dynein dimers are present[3-6]. Little is known about the assembly process of this massive ~4MDa complex. Here, using purified recombinant human proteins, we uncover a role for the dynein-binding protein Lis1 in promoting the formation of activated dynein/ dynactin complexes containing two dynein dimers. Complexes activated by proteins representing three families of activating adaptors: BicD2, Hook3, and Ninl all show enhanced motile properties in the presence of Lis1. Activated dynein complexes do not require sustained Lis1 binding for fast velocity. Using cryo-electron microscopy we show that human Lis1 binds to dynein at two sites on dynein's motor domain. Our work suggests that Lis1 binding at these sites functions in multiple stages of assembling the motile dynein/ dynactin/ activating adaptor complex.

2.2 Introduction

Cytoplasmic dynein-1 (dynein) is responsible for the long-distance transport of nearly all cargos that move towards the minus ends of microtubules[2]. Mutations in components of the dynein machinery cause neurodevelopmental and neurodegenerative diseases[7]. Activated human dynein is a large multi-subunit

complex composed of one or two dynein dimers (each dynein dimer contains two motor subunits and two copies each of five additional subunits), the dynactin complex (composed of 23 polypeptides) and a dimeric, coiled-coil-containing activating adaptor (Figure 2.1a)[2-6,8]. The dynein motor subunit, or heavy chain, is an ATPase containing six AAA+ domains and a microtubule-binding domain that emerges from a long coiled-coil "stalk" (Figure 2.1b).

Though yeast dynein is capable of moving processively on its own *in vitro*[9], mammalian dynein is largely immotile in the absence of dynactin and an activating adaptor[3,4,10]. However, dynein activation *in vivo* is likely conserved across eukaryotes as dynactin subunits and a candidate activating adaptor (Num1) are required for dynein function in yeast[11]. Activating adaptors also link dynein/ dynactin to its cargos[2,8]. Nearly a dozen activating adaptors have been described; they share little sequence identity, but contain a long stretch of predicted coiled-coil that spans the ~40 nm length of dynactin[2,8]. All activated dynein complexes that have been investigated structurally can bind two dynein dimers[5,6] (Figure 2.1a).

Mammalian dynein in the absence of these other components adopts a conformation known as "Phi"[12,13]. Phi dynein is autoinhibited and cannot interact with microtubules productively[12]. The current model for dynein activation proposes that Phi dynein must first adopt an "Open" conformation and ultimately a "Parallel" conformation that is observed when it is bound to dynactin and an activating adaptor (Figure 2.1a)[5,6]. Little is known about how dynein switches between the

Figure 2.1. Lis1 increases microtubule binding and velocity of activated dynein complexes. a. Current model for dynein activation. Dynein is autoinhibited in the Phi conformation, opens, and then adopts a parallel conformation in the activated dynein complex, which can contain two dynein dimers (A and B). **b.** Schematic of the AAA+ ATPase dynein heavy chain. The two Lis1 binding sites, "$Site_{ring}$" and "$Site_{stalk}$" are shown. Microtubule binding domain (MTBD). **c.** Activating adaptor constructs used in this study. Dashed lines highlight the regions that were truncated. **d, e.** Binding density (mean ± s.e.m.) of full-length recombinant human dynein with its associated intermediate, light intermediate and light chains (d) or dynein/ dynactin/ activating adaptor complexes (e) on microtubules in the absence (white circle) or presence (black circle) of 300 nM Lis1. Data was normalized to a density of 1.0 in the absence of Lis1. **f.** Single-molecule velocity of dynein/ dynactin/ activating adaptor complexes in the absence (white circles) or presence (black circles) of 300 nM Lis1. The median and interquartile range are shown. **g.** Single-molecule velocity of dynein/ dynactin/ Hook3 complexes in a higher ionic strength buffer (67.5 mM compared to 37.5 mM in our standard buffer) in the absence (white circle) or presence (black circle) of 300 nM Lis1. The median and interquartile range are shown. **h.** Percent processive runs of dynein/ dynactin/ Hook3 complexes in standard and higher (grey panel) ionic strength motility buffer in the absence (white circles) or presence (black circles) of 300 nM Lis1. Statistical analysis was performed on data pooled from all replicates with a chi-squared test. **i.** Peroxisome relocation assay. The peroxisomal protein, Pex3, is fused to mEmerald and FKBP and BicD2-S is fused to FRB. Rapalog induces the association of FKBP and FRB. **j.** Peroxisome velocity in human U2OS cells with scrambled or Lis1 siRNA knockdown with two independent siRNAs. The median and interquartile range are shown.

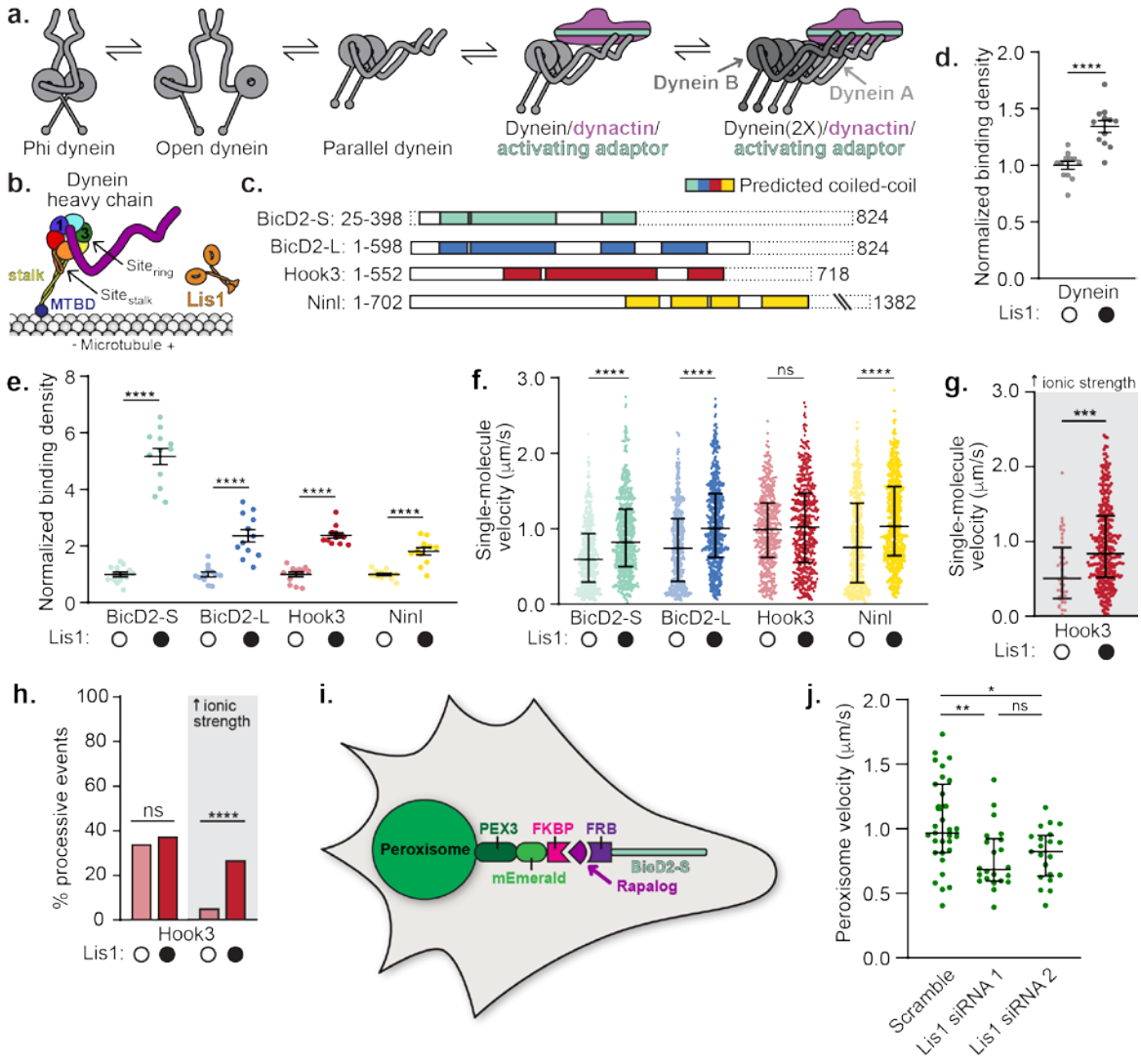
a.
Phi dynein
Open dynein
Parallel dynein
Dynein/dynactin/
activating adaptor
Dynein B
Dynein A
Dynein(2X)/dynactin/
activating adaptor
b.
Dynein
heavy chain
stalk
Site ring
Site stalk
MTBD
Lis1
- Microtubule +
c.
Predicted coiled-coil
BicD2-S: 25-398
824
BicD2-L: 1-598
824
Hook3: 1-552
718
NinI: 1-702
1382
d.
Normalized binding density
Dynein
Lis1:
e.
Normalized binding density
BicD2-S
BicD2-L
Hook3
NinI
Lis1:
f.
Single-molecule
velocity (μm/s)
BicD2-S
BicD2-L
Hook3
NinI
Lis1:
g.
↑ ionic strength
Single-molecule
velocity (μm/s)
Hook3
Lis1:
h.
% processive events
↑ ionic
strength
ns
Hook3
Lis1:
i.
Peroxisome
PEX3
FKBP
FRB
mEmerald
BicD2-S
Rapalog
j.
Peroxisome velocity (μm/s)
Scramble
Lis1 siRNA 1
Lis1 siRNA 2

autoinhibited Phi conformation and the Open and Parallel conformations that lead to the assembly of the motile activated dynein complex.

Genetic studies in model organisms place the dynein-binding protein Lis1 in the dynein pathway[14-16]. Given that deletion or mutations in Lis1 phenocopy deletion or mutation of dynein or dynactin subunits in these organisms[14-16], Lis1 is considered a positive regulator of dynein's cellular activities. Activities that require Lis1 range from organelle trafficking (e.g.[17-20]) to nuclear migration/positioning (e.g.[15,21-23]) to RNA localization (e.g.[24]). The *LIS1* gene is mutated in the neurodevelopmental disease type-1 lissencephaly[25], and was first directly linked to dynein through genetic studies in *Aspergillus nidulans*[15]. Lis1 is a dimer of β-propellers[26,27] and yeast Lis1 binds dynein at two distinct sites on the dynein motor domain: dynein's ATPase ring at AAA3 and AAA4 ("site$_{ring}$") and dynein's stalk ("site$_{stalk}$") (Figure 2.1b)[28-30]. In yeast, binding of Lis1 to dynein at site$_{ring}$ causes tight microtubule binding and decreases velocity[29,30], whereas binding at both sites leads to weak microtubule binding and increases velocity[30]. Lis1 also increases the binding of mammalian dynein to microtubules[31,32] and increases the velocity of mammalian dynein/ dynactin complexes containing the BicD2 activating adaptor[33,34]. How Lis1 exerts these effects on mammalian dynein is unknown. It is also unknown if Lis1 has the same effects on dynein/ dynactin bound to other activating adaptors.

2.3 Results

To determine how Lis1 regulates activated human dynein complexes, we purified full-length recombinant human dynein in the presence of its accessory chains ("dynein")[3] and human Lis1 from insect cells, dynactin from human HEK293T cells[35], and the human activating adaptors BicD2, Hook3, and Ninl from *E. coli* (Supplementary Data Figure 2.1a). Since some activating adaptors are known to be autoinhibited[36], we used well-characterized carboxy-terminal truncations of BicD2, Hook3 and Ninl[3,4,35] (Figure 2.1c). We made two truncations of BicD2: BicD2-S (aa 25-398), which activates dynein in vitro[3,4] and BicD2-L (aa 1- 598), which activates dynein in cells[18,37].

We first determined the effects of Lis1 on the microtubule binding properties of dynein alone and dynein/ dynactin bound to different activating adaptors using a single-molecule assay[30]. Lis1 increased the microtubule binding density of dynein alone (Figure 2.1d and Supplementary Data Figure 2.1b), consistent with studies of yeast[29,30] and mammalian[31,32] dynein. Lis1 also increased the microtubule binding density of dynein/ dynactin complexes bound by the activating adaptors BicD2-S, BicD2-L, Hook3, and Ninl (Figure 2.1e and Supplementary Data Figure 2.1b).

Next, we examined how Lis1 affected the motile properties of activated dynein complexes. While Lis1 inhibits the motility of human dynein alone in microtubule gliding assays[31,33,38,39], in agreement with some previous studies[33,34] we found that Lis1 increased the velocity of dynein/ dynactin / BicD2-S complexes

(Figure 2.1f, Supplementary Data Figure 2.1c). We also found that Lis1 increased the velocity of dynein/ dynactin activated by BicD2-L and Ninl in our standard motility assay buffer (Figure 2.1f, Supplementary Data Figure 2.1c). Lis1 also increased the percentage of processive runs for dynein/ dynactin activated by BicD2-S, BicD2-L and Ninl (Supplementary Data Figure 2.1d). While Hook3-activated dynein complexes were not affected by Lis1 in these conditions (Figure 2.1f), increasing the ionic strength of our assay buffer led to increased velocity and an increase in processive runs of these complexes in the presence of Lis1 (Figure 2.1g,h). We interpret this difference in sensitivity to the ionic strength of our assay conditions as an indication that Hook3 may have a higher affinity for dynactin, the dynein tails, or the dynein light intermediate chains compared to BicD2 and Ninl. These data show that Lis1 increases both microtubule binding and motility of dynein/ dynactin complexes bound by activating adaptors from three different families and allude to a role for Lis1 in activated dynein/ dynactin complex formation.

We next asked if Lis1 had a similar effect on dynein velocity in cells using a well-established peroxisome relocation assay (Figure 2.1i)[37,40]. We co-transfected human U2OS cells with: 1) the rapamycin binding protein FRB fused to BicD2-S and 2) another rapamycin binding protein FKBP fused to mEmerald and the peroxisome targeting protein Pex3 (Figure 2.1i). In U2OS cells peroxisomes rarely move, but upon the addition of rapalog, which causes FRB and FKBP to interact, we observed many processive runs. This is an indication that BicD2-S recruits and

activates dynein/ dynactin[40]. We observed a significant decrease in peroxisome velocity when Lis1 expression was knocked down with siRNA (Figure 2.1j, Supplementary Data Figure 2.1e-g), suggesting that Lis1 also increases the velocity of dynein complexes in a cellular environment.

We next sought to determine where Lis1 binds human dynein. Experiments with yeast proteins showed that Lis1 binds dynein at two sites on the dynein motor domain ($site_{ring}$ and $site_{stalk}$[29,30]), although previous studies with mammalian protein fragments reported interactions with other regions of dynein[41,42]. We used cryo-electron microscopy (cryo-EM) to identify the Lis1 binding sites on human dynein. We purified monomeric human dynein motor domains and mixed them with dimeric human Lis1 in the presence of ATP-vanadate. This ATP analog was previously shown to promote an interaction between mammalian dynein and Lis1[32] and causes dynein's linker to adopt a bent position[43] that would prevent the linker from sterically interfering with Lis1 binding at $site_{ring}$. We generated two-dimensional (2D) class averages of the dynein/ Lis1 complex that showed high-resolution features in both dynein and Lis1 (Figure 2.2a).

To determine whether the binding sites for Lis1 are similar in human and yeast dynein, we compared our experimental class averages with calculated 2D projections of a model of human dynein bound to Lis1 (Figure 2.2b). To make this model we combined the structure of human dynein-2 bound to ATP-vanadate (PDB: 4RH7[44]) with a homology model of human Lis1 bound to dynein at the two binding sites observed with the yeast proteins (PDB: 5VLJ[30]) (Figure 2.2b). To

Figure 2.2. Human Lis1 binds the human dynein motor domain at AAA3/4 and the stalk. a. 2D class averages of human dynein monomers bound to human Lis1 dimers in the presence of ATP-vanadate. **b.** Best-matching projections of a model combining human dynein-2 bound to ATP-vanadate (PDB: 4RH7) with homology models of human Lis1 at the locations where Lis1 binds to yeast dynein in the presence of ATP-vanadate (PDB: 5VLJ). The two Lis1's ("$Site_{ring}$" and "$Site_{stalk}$") identified in yeast dynein, dynein's AAA ring, stalk and buttress are labeled. **c.** Projections of 4RH7 alone in the same orientations as those shown in (b). **d**. Homology model of human Lis1 (from SWISS-MODEL) showing the five residues mutated to alanine in "Lis1-5A". **e.** Single-molecule velocity of dynein/ dynactin/ BicD2-S complexes in the absence (white circles) or presence (black circles) of Lis1 or Lis1-5A. The median and interquartile range are shown. **f.** Percent processive runs of dynein/ dynactin/ Hook3 complexes in a higher ionic strength buffer in the absence (white circles) or presence (black circles) of 300 nM Lis1 or Lis1-5A. Data in the presence of 300 nM Lis1 was also presented in Figure 2.1h. Statistical analysis was performed on data pooled from all replicates with a chi-squared test. **g.** Single-molecule velocity of dynein/ dynactin/ BicD2-S complexes in the absence (white circles) or presence (black circles) of 300 nM Lis1 dimer or 600 nM Lis1ΔN. Since Lis1ΔN is largely monomeric (Supplementary data Figure 2e), 300 nM Lis1 dimer is roughly equivalent to 600 nM Lis1ΔN. The median and interquartile range are shown.

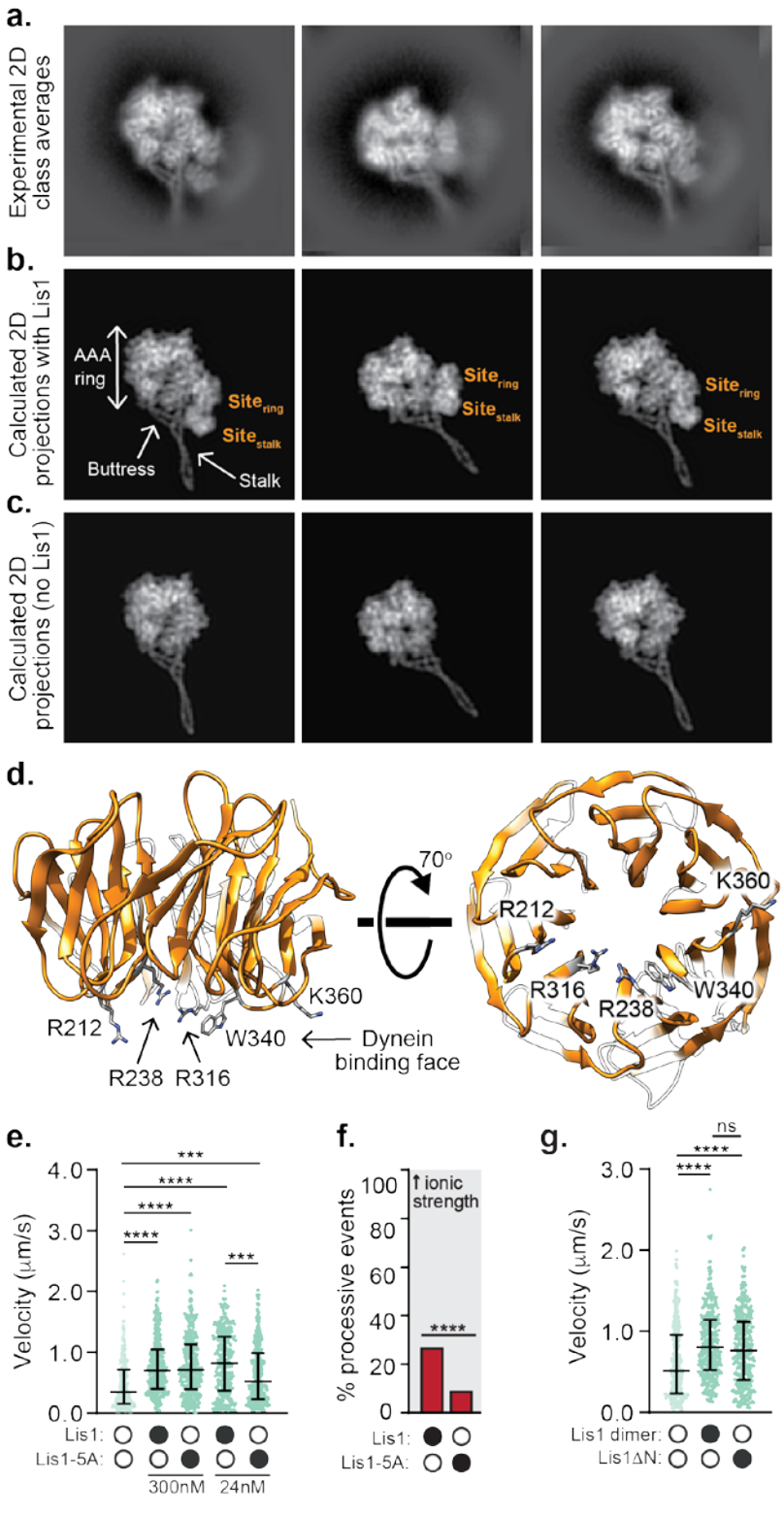
a.
Experimental 2D class averages
b.
Calculated 2D projections with Lis1
AAA ring
Site ring
Site stalk
Buttress
Stalk
c.
Calculated 2D projections (no Lis1)
d.
70°
K360
R212
R316
W340
R238
R212
W340
Dynein binding face
R238
R316
e.
Velocity (μm/s)
4.0
3.0
2.0
1.0
0.0
***
****
****
****
***
Lis1:
Lis1-5A:
300nM
24nM
f.
% processive events
100
80
60
40
20
0
↑ ionic strength
****
Lis1:
Lis1-5A:
g.
Velocity (μm/s)
3.0
2.0
1.0
0.0
ns
****
****
Lis1 dimer:
Lis1ΔN:

highlight the densities corresponding to Lis1, we also calculated 2D projections of human dynein-2 alone (Figure 2.2c). The correspondence between our data and the model with two Lis1s bound (Figure 2.2a,b) suggests that the yeast and human Lis1 binding sites are in similar regions of the dynein motor domain on the ring at AAA3/4 and on the stalk. The strong preferred orientation adopted by the sample prevented us from obtaining a 3D reconstruction and mapping the exact sites of interaction on either human dynein or Lis1. The stoichiometry of this complex is 1 dynein monomer to 1.2 Lis1 dimers ± 0.3 (Supplementary Data Figure 2.2a), suggesting that the majority of dynein monomers are bound to a single Lis1 dimer.

Mutation of five amino acids on the dynein binding face of yeast Lis1 disrupts the interaction between dynein[28]. We made the equivalent mutations in human Lis1 ("Lis1-5A"; Figure 2.2d). To determine if Lis1-5A could enhance the velocity of activated dynein complexes we focused on complexes activated by BicD2-S, as Lis1 had the greatest effect on these complexes (Figure 2.1g). We found that 300 nM Lis1-5A still enhanced the velocity of dynein/ dynactin/ BicD2-S complexes. We hypothesized that Lis1-5A might still weakly interact with dynein. Thus, we lowered the concentration of Lis1 and Lis1-5A to 24 nM; under these conditions wild-type Lis1 more potently increased dynein velocity compared to Lis1-5A (Figure 2.2e and Supplementary Data Figure 2.2b). We also found that Lis1-5A was less potent at enhancing processive runs of dynein/ dynactin/ Hook3 complexes compared to wild-type Lis1 in a higher ionic strength buffer (Figure

2.2f) and the velocity of these runs was no longer increased (Supplementary Data Figure 2.2c and 2d).

Since Lis1 is a dimer, we wondered whether Lis1's effects on activated dynein/ dynactin complexes required dimerization. To test this, we purified human Lis1 lacking its amino-terminal high affinity LisH dimerization domain[26], which we refer to as Lis1ΔN. Similar to the equivalent yeast construct, which is a monomer by gel filtration analysis[29], the human construct is mostly monomeric (Supplementary Data Figure 2.2e). However, with the human construct a small amount of dimer is also observed (Supplementary Data Figure 2.2e), likely due to an interaction between Lis1's two β-propellers, as seen by Cryo-EM here and previously[30]. Lis1ΔN still increased dynein/ dynactin/ BicD2-S velocity at the same molar ratio of dynein to Lis1 β-propellers (Figure 2.2g), indicating that the high affinity LisH dimerization domain is not required for Lis1 to increase dynein's velocity.

As activated dynein complexes containing two dynein dimers are faster than those containing a single one[5], we hypothesized that Lis1 may play a role in promoting the recruitment of a second dynein dimer to the dynein/ dynactin complex. To determine if Lis1 enhances the formation of dynein/ dynactin complexes *in vitro* we measured the formation of activated dynein complexes by mixing dynein and dynactin with an excess of BicD2-S conjugated to magnetic beads. We then quantified the percentage of dynein bound to the BicD2-S beads (Figure 2.3a). The presence of Lis1 increased the percentage of dynein bound to

Figure 2.3. Lis1 recruits a second dynein dimer to dynein/ dynactin/ BicD2-S complexes. a. Schematic of the dynein/ dynactin complex formation assay. **b, c.** Percent dynein bound to BicD2-S-coupled beads (mean ± s.e.m.) in the presence (b) or absence (c) of dynactin and in the absence (white circle) or presence (black circle) of 150 nM Lis1. **d.** Schematic depicting the maximum probability of forming various dynein/ dynactin/ BicD2-S complexes containing two dynein dimers. The maximum probability of colocalization was 45% (grey dashed line shown in f and g) given our labeling efficiency (see Methods). **e.** Representative kymographs showing the colocalization of TMR- and Alexa647-labeled dynein in moving dynein/ dynactin/ BicD2-S complexes in the presence of 300 nM Lis1. Each channel is shown separately (left and middle panels) and the merged TMR- and Alexa647-channels in pseudocolor (right panel). Scale bars are 10 µm (x) and 20 sec (y). Data is quantified in Figure 2.3f. **f.** Percent two-color dynein/ dynactin/ BicD2-S runs in the absence (white circle) or presence (black circle) of 300 nM Lis1. Statistical analysis was performed using a chi-squared test.

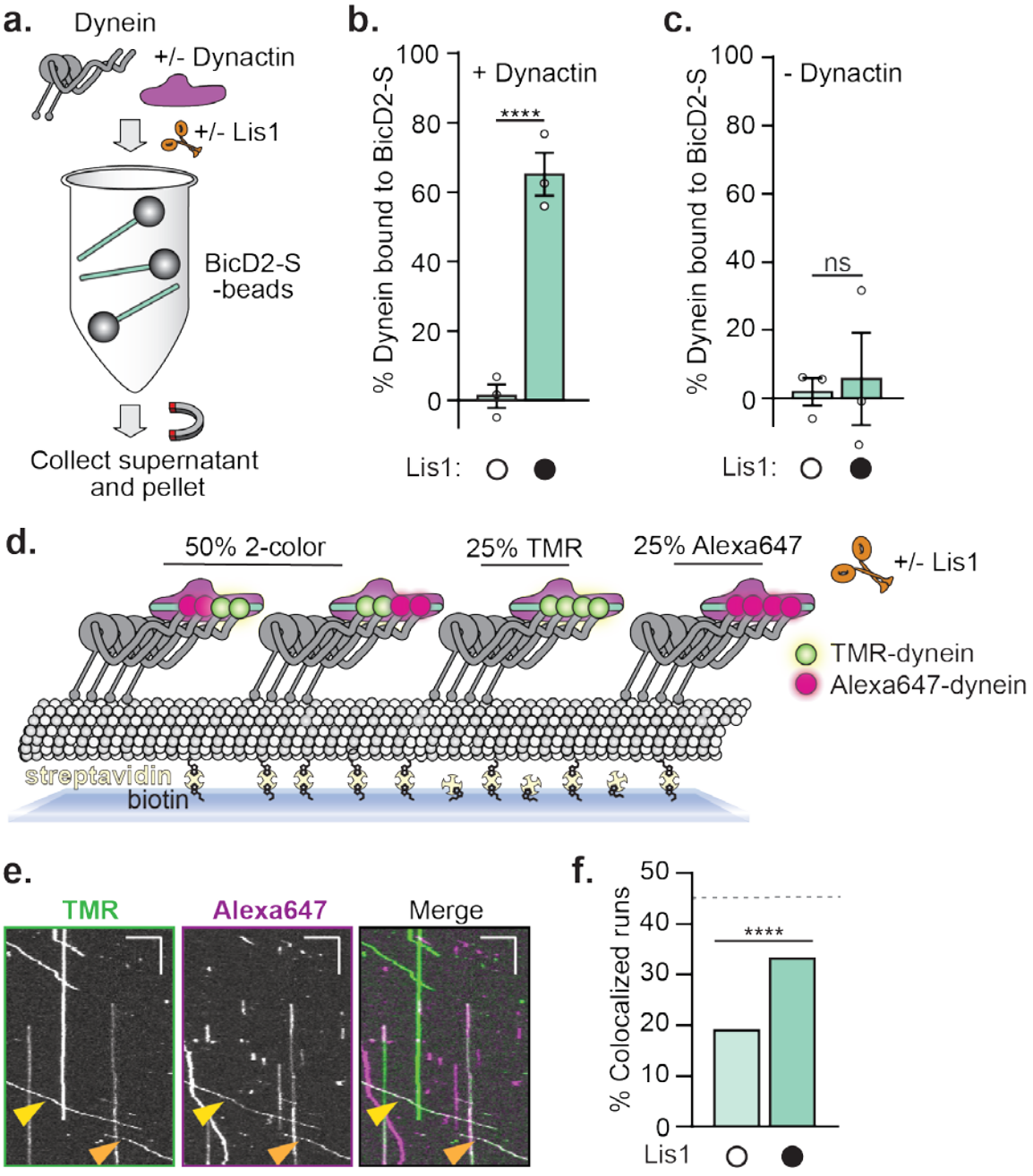
a.
Dynein
+/- Dynactin
+/- Lis1
BicD2-S
-beads
Collect supernatant
and pellet
b.
+ Dynactin
****
% Dynein bound to BicD2-S
100
80
60
40
20
0
Lis1:
c.
- Dynactin
ns
% Dynein bound to BicD2-S
100
80
60
40
20
0
Lis1:
d.
50% 2-color
25% TMR
25% Alexa647
+/- Lis1
TMR-dynein
Alexa647-dynein
streptavidin
biotin
e.
TMR
Alexa647
Merge
f.
% Colocalized runs
50
40
30
20
10
0
****
Lis1

BicD2-S beads (Figure 2.3b) and dynactin was required for this effect (Figure 2.3c).

To directly test if Lis1 promotes the recruitment of a second dynein dimer to the activated complex we performed two-color single-molecule assays. To do this we added equimolar amounts of dynein labeled with either TMR or Alexa647 to dynactin and BicD2-S and quantified the percentage of moving two-color complexes. If all moving dynein complexes contained two dynein dimers, 50% of events would show co-localization (Figure 2.3d). The presence of Lis1 significantly increased the number of moving two-color dynein/ dynactin/ BicD2-S complexes (Figure 2.3e,f). Two-color complexes moved faster in both the presence and absence of Lis1 (Supplementary Data Figure 2.3a). One-color complexes in the presence of Lis1 also moved faster, presumably because half of these events contained two dynein dimers labeled with the same color (Supplementary Data Figure 2.3a). We conclude that Lis1 promotes the recruitment of a second dynein dimer to activated dynein complexes.

We wondered if Lis1 must remain bound to moving activated dynein complexes to sustain fast velocity. To address this, we sought to determine if TMR-labeled Lis1 co-migrated with moving dynein/ dynactin/ BicD2-S complexes tagged with Alexa647. Most of our earlier experiments used 300 nM Lis1, a concentration that is too high to visualize single Lis1 molecules. Therefore, we lowered the Lis1 concentration to 50 nM, which is still well above the concentration where a maximal increase in dynein velocity by Lis1 is observed (Figure 2.4a and

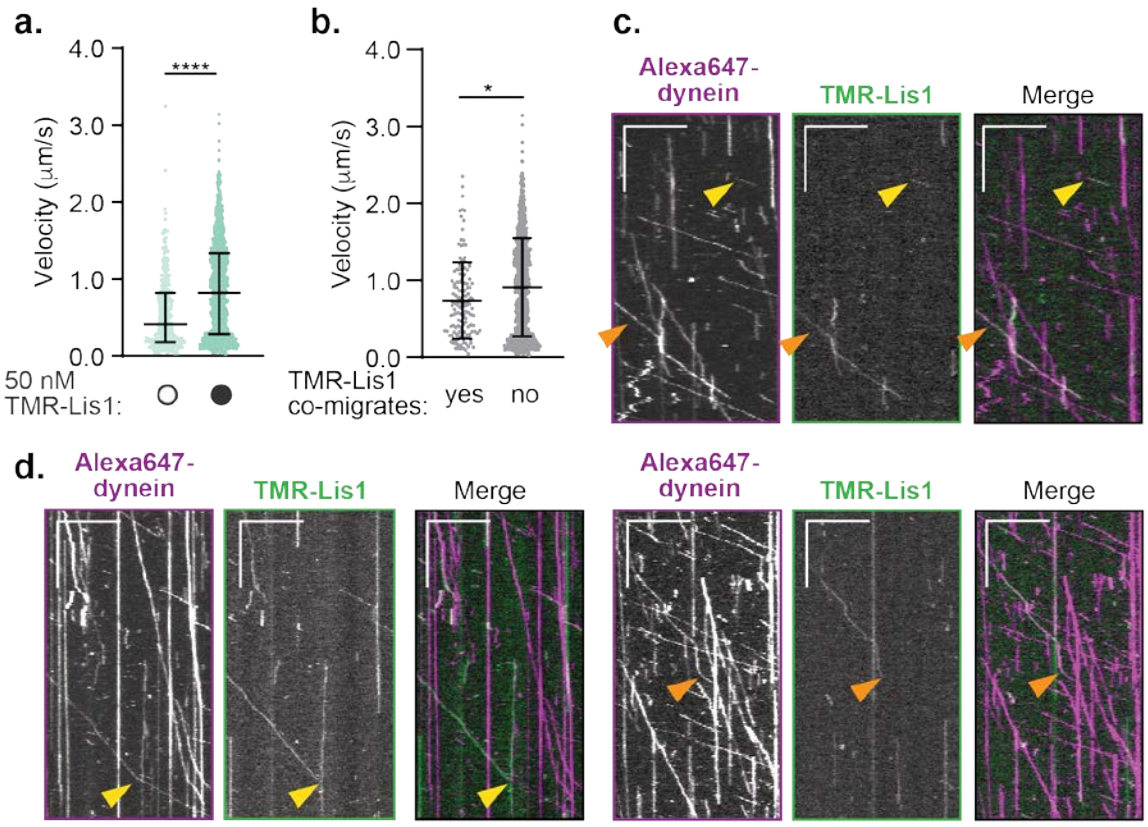

Figure 2.4. Lis1 is not required to sustain fast velocity of activated dynein complexes. a. Single-molecule velocity of dynein/ dynactin/ BicD2-S complexes in the absence (white circle) or presence (black circle) of 50 nM TMR-Lis1. The median and interquartile range are shown. **b.** Single-molecule velocity of Alexa647-dynein/ dynactin/ BicD2-S complexes in the presence of 50 nM TMR-Lis1 either co-migrating with TMR-Lis1 (yes) or not (no). The median and interquartile range are shown. **c.** Representative kymographs of the Alexa647-dynein and TMR-Lis1 channels (left and middle panels) and the merged images in pseudocolor (right panel). Arrowheads indicate colocalized runs. Scale bars are 10 μm (x) and 20 sec (y). Data is quantified in Figure 2.4b. **d.** Kymographs showing examples of dynein's velocity changing upon loss of the TMR-Lis1 signal. The Alexa647-dynein and TMR-Lis1 channels are shown (left and middle panels) and the merged images in pseudocolor (right panel). Arrowheads indicate instances of velocity change. Four such events were observed. Scale bars are 10 μm (x) and 20 sec (y). Data is quantified in Figure 2.4b.

Supplementary Data Figure 2.2b). Single-molecule motility assays with TMR-Lis1 and Alexa647-dynein/ dynactin/ BicD2-S complexes showed that only 16.8 ± 1.9% of dynein runs co-migrated with Lis1, with co-migrating runs moving slower than those with no detectable Lis1 (Figure 2.4b,c). Occasionally the disappearance of the TMR-Lis1 signal coincided with an increase in speed of a dynein/ dynactin/ BicD2-S run (Figure 2.4d), similar to a previous report[34]. As shown previously[32], we found that human Lis1 in the absence of dynein does not bind to microtubules (Supplementary Data Figure 2.4a), suggesting that the effects of Lis1 we observe on dynein activity and complex assembly are not due to an interaction between Lis1 and microtubules. We also found that Lis1-5A increased the velocity of activated dynein complexes significantly less than wild-type Lis1 (Supplementary Data Figure 2.4b) and we observed no colocalization of TMR-Lis1-5A with Alexa647-dynein (Supplementary Data Figure 2.4c). These results suggest that the presence of Lis1 is not required for sustained fast velocity of activated dynein complexes. Our results showing that activated dynein complexes move faster when Lis1 is no longer co-migrating are consistent with contemporaneous work[45], but differ from other reports[33,34], perhaps due to differences in assay conditions or protein source.

We next explored which step(s) Lis1 affects in the dynein complex assembly pathway (Figure 2.1a). Because the site$_{ring}$ Lis1 binding site on dynein is not accessible in Phi dynein (Figure 2.5a), we wondered if Lis1 had higher affinity for a dynein mutant that does not form the Phi particle (K1610E and R1567E[12],

Figure 2.5. Lis1 preferentially binds to Open dynein and enhances the formation of complexes containing two Open dynein dimers. a. One of the dynein protomers in the Phi conformation (PDB: 5NVU) was aligned to the structure of yeast dynein (AAA3-Walker B) bound to Lis1 in the presence of ATP-vanadate (PDB: 5VLJ). The inset shows the cryo-EM map for the yeast structure with Lis1 docked at $Site_{ring}$ and highlights the steric incompatibility between the Phi conformation and binding of Lis1 at this site. **b.** Determination of the binding affinity of Lis1 for wild-type (WT) dynein (blue, K_d = 144 nM ± 25) and Open dynein (green, K_d = 80 nM ± 8.1). **c.** Percent (mean ± s.e.m.) of WT dynein (blue) and Open dynein (green) bound to BicD2-S conjugated to beads in the absence (white circles) or presence (black circles) of 150 nM Lis1. Data with WT dynein in the presence and absence of Lis1 is also presented in Figure 2.3b. Statistical analysis was performed using a two-tailed unpaired t test with Bonferroni corrected significance levels for two comparisons. **d.** Single-molecule velocity of dynein/ dynactin/ BicD2-S complexes with WT dynein (blue) and Open dynein (green) in the absence (white circles) or presence (black circles) of 300 nM Lis1. The median and interquartile range are shown. Data with WT dynein with and without Lis1 was also presented in Figure 2.1f. **e.** Percent two-color colocalized runs with activated dynein complexes with Open dynein in the absence (white circle) or presence (black circle) of 300 nM Lis1. Statistical analysis was performed using a chi-squared test. The labeling efficiency for both TMR- and Alexa-647 dynein in this experiment was 100%. **f.** Model for the roles of Lis1 in forming activated dynein complexes.

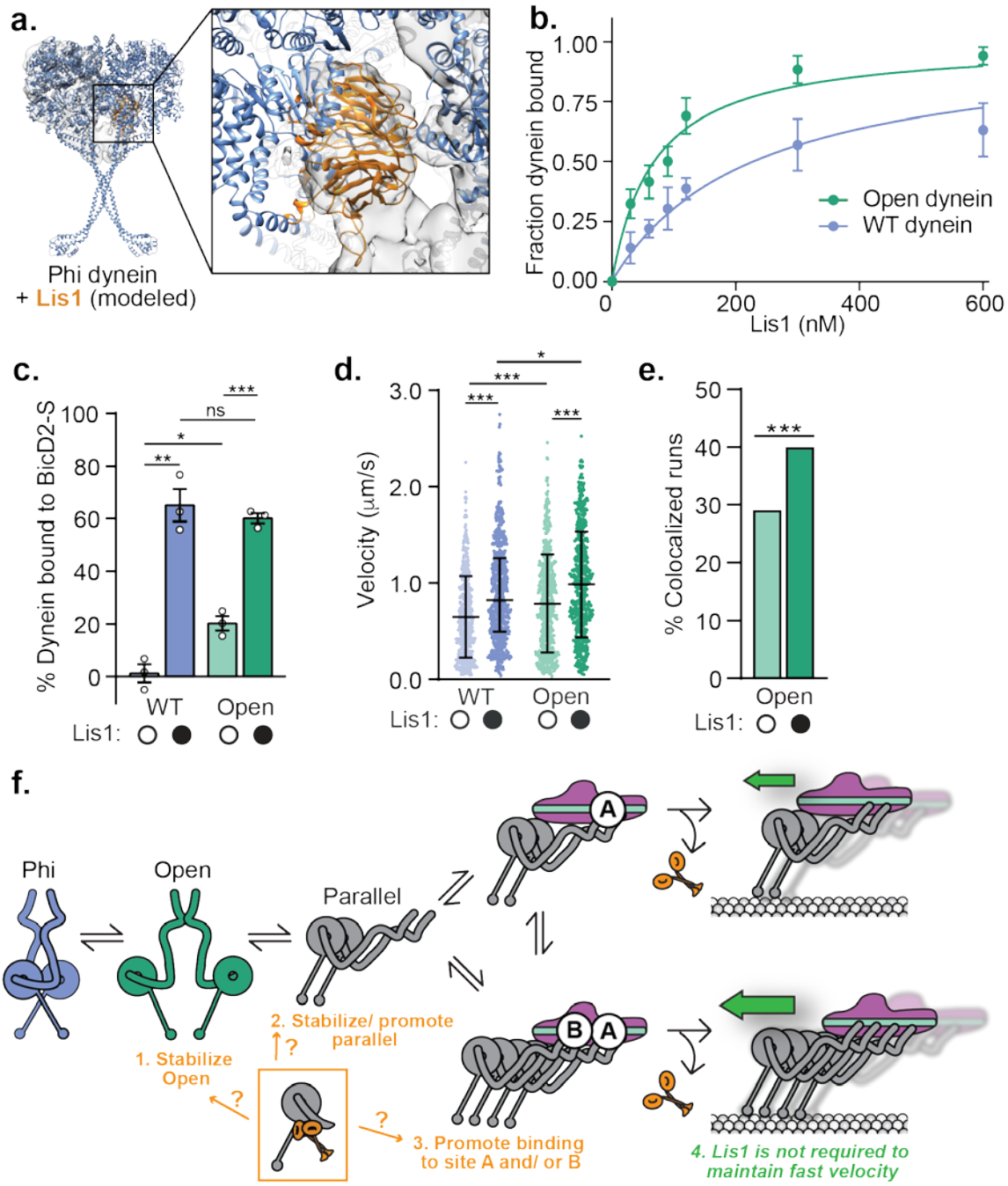
a.
Phi dynein
+ Lis1 (modeled)
b.
Fraction dynein bound
1.00
0.75
0.50
0.25
0.00
0
200
400
600
Lis1 (nM)
Open dynein
WT dynein
c.
% Dynein bound to BicD2-S
100
80
60
40
20
0
ns
*
**
***
WT
Open
Lis1:
d.
Velocity (μm/s)
3.0
2.0
1.0
0.0
*
***
***
***
WT
Open
Lis1:
e.
% Colocalized runs
50
40
30
20
10
0
***
Open
Lis1:
f.
Phi
Open
Parallel
A
B
A
1. Stabilize
Open
2. Stabilize/ promote
parallel
?
?
?
3. Promote binding
to site A and/ or B
4. Lis1 is not required to
maintain fast velocity

"Open dynein"). Indeed, we found that Lis1 had a higher affinity for Open dynein (Figure 2.5b). We hypothesize that binding of Lis1 to dynein at site$_{ring}$ alters the equilibrium between Phi and Open dynein to favor the Open conformation.

We next considered two possibilities: first, that Lis1's only role is to stabilize dynein's open conformation; and second, that in addition to this role Lis1 also promotes activated complex formation. To do this we examined Open dynein complexes in the absence of Lis1 and found that Open dynein/ dynactin/ BicD2-S complexes were more likely to form and moved faster compared to complexes containing wild-type dynein (Figure 2.5c,d)[12]. We then asked if Lis1 altered the motile properties of complexes containing Open dynein. We found that Lis1 further increased complex formation and the velocity of Open dynein/ dynactin/ BicD2-S complexes (Figure 2.5d). Lis1 also increased the percentage of complexes containing two dynein dimers when Open dynein was used (Figure 2.5e). Previous studies showed that the Open dynein mutant does not form Phi particles[12]. Assuming this is the case in our experiments, the ability of Lis1 to further activate Open dynein suggests that Lis1's effect on complex formation may have additional roles beyond altering the equilibrium between Phi and Open dynein.

2.4 Discussion

Together our work suggests that Lis1 promotes the formation of human dynein/ dynactin/ activating adaptor complexes containing two dynein dimers. Experiments in human cells[18], *Drosophila* embryos[24], *Xenopus* extracts[39], *Aspergillus nidulans*[46], and yeast[47] showed that Lis1 is required for the interaction

of dynein and dynactin with each other and/or with their cargos. Our work offers a biochemical explanation for this requirement for Lis1. Our data suggest that Lis1 promotes complex formation by favoring a conformation of dynein that drives association with dynactin and an activating adaptor. First, Lis1 may promote the Open dynein conformation (Figure 2.5f, step 1). We propose this based on our data showing that Open dynein has a higher affinity for Lis1 and because the structure of Phi dynein is incompatible with Lis1 binding at site$_{ring}$. Recent work in *Aspergillus nidulans*[46] and *Saccharomyces cerevisiae*[47] also supports this. Second, Lis1 may favor a conformation of dynein that is primed to assemble the fully activated complex (Figure 2.5f, step 2). Our data showing that Open dynein is further activated by Lis1 supports this. Third, Lis1 favors the formation of dynein complexes containing two dynein dimers, which move faster (Figure 2.5f, step 3). Our single-molecule experiments measuring the velocity of activated dynein complexes in the presence of Lis1 and our experiments showing that Lis1 promotes the recruitment of two dynein dimers support this. Because we also observe these effects with Lis1ΔN the underlying mechanism does not rely on the high affinity Lis1H dimerization domain, although interactions between the Lis1 β-propellers could play a role. Finally, once a fully activated dynein/ dynactin/ activating adaptor complex is formed, Lis1 dissociates from moving complexes (Figure 2.5f, step 4). This component of our model is based on our data showing that most moving dynein complexes do not remain bound to Lis1 and those that

do, move slower. Contemporaneous work made complementary findings that supports steps 3 and 4 of our model[45].

How does our current work and other recent studies[45-47] relate to previous mechanistic studies of yeast Lis1, which showed how allosteric effects of Lis1 binding to dynein's motor domain controlled dynein's microtubule binding affinity[28-30]? This earlier work was done in the absence of dynactin and an activating adaptor because yeast dynein is a processive motor on its own[9], allowing the dissection of dynein function in a minimal system (however, dynactin and a candidate activating adaptor, Num1, are required for yeast dynein function *in vivo*). Here we show that human Lis1 binds to two sites on human dynein's motor domain, which are similar to the yeast binding sites[28-30]. Vertebrate Lis1 increases dynein's affinity for microtubules and slows microtubule gliding velocity[31-33,39], again mirroring findings in yeast. Thus, the Lis1 binding sites on dynein and some of the consequences of these interactions on dynein's mechanochemical cycle are conserved.

Lis1's ability to regulate dynein's mechanochemistry may be important for its role in assembling activated dynein complexes. For example, dynein idling on the microtubule (caused by tight microtubule binding induced by Lis1), could be well-suited for aiding in the challenging kinetics of loading two dynein motors on to dynactin before transport begins. In support of this, Lis1 has a role in localizing dynein to microtubule plus ends[21,48] or initiating transport from microtubule plus ends[19,20,49], where tight microtubule binding and reduced motility is likely important

for maintaining dynein at these sites. Binding of Lis1 to dynein at microtubule plus ends could promote the Open dynein conformation, lead to tight microtubule binding of dynein, and ultimately favor the formation of activated dynein/ dynactin/ activator complexes containing two dynein dimers. Lis1 binding to dynein may have additional allosteric affects that promote the formation of the full activated dynein/ dynactin complex, perhaps influencing the conformation of the dynein tails that interact with dynactin and activating adaptors. A contemporaneous study suggests that Lis1's regulation of yeast dynein involves an interaction between Lis1 and microtubules[47]. However, much of the past work with yeast proteins[28-30] cannot be accounted for by this model. Furthermore, we and others[32] have shown that mammalian Lis1 does not interact with microtubules.

Finally, we have shown that proteins representing three distinct families of activating adaptors, BicD2, Hook3, and Ninl, all move faster in the presence of Lis1. This raises the possibility that activated dynein complexes in cells contain two dynein dimers. We hypothesize that related activating adaptors or candidate activating adaptors will also use Lis1 to form activated complexes. In humans there are additional BicD, Hook and Ninl family members, as well as a number of known and candidate activating adaptors[2,8]. Thus, we predict that Lis1 will play a role in the cell biological processes that additional dynein activating adaptors facilitate.

Author Contributions

ZMH, JPG, MED, AEL and SRP designed the experiments. ZMH, JPG, MED and RWB performed the experiments. ZMH, JPG, MED, AEL and SRP wrote the manuscript. All authors interpreted the data and reviewed and edited the manuscript.

2.5 Methods

Cloning, plasmid construction, and mutagenesis

The pDyn1 plasmid (the pACEBac1 expression vector containing insect cell codon optimized dynein heavy chain (*DYNC1H1*) fused to a His-ZZ-TEV tag on the amino-terminus and a carboxy-terminal SNAPf tag (New England Biolabs)) and the pDyn2 plasmid (the pIDC expression vector with codon optimized *DYNC1I2*, *DYNC1LI2*, *DYNLT1*, *DYNLL1*, and *DYNLRB1*) were recombined in vitro with a Cre recombinase (New England Biolabs) to generate the pDyn3 plasmid. The presence of all six dynein chains was verified by PCR. pDyn1, pDyn2 and the pFastBac plasmid with codon-optimized human full-length Lis1 (*PAFAH1B1*) fused to an amino-terminal His-ZZ-TEV tag and pFastBac containing human dynein monomer (amino acids 1320-4646 of DYNC1H1) were gifts from Andrew Carter (LMB-MRC, Cambridge, UK). BicD2 constructs were amplified from a human cDNA library generated from RPE1 cells and the other activating adaptor constructs were obtained as described previously[35]. Activating adaptors were fused to a ZZ-TEV-HaloTag (Promega) on the amino-terminus and inserted into a pET28a expression vector. All additional tags were added via Gibson assembly

and all mutations and truncations were made via site-directed mutagenesis (Agilent). For rapalog induced motility in cells, HaloTag-BicD2-S was cloned into the pcDNA5 backbone with a carboxy-terminal V5 epitope tag fused to FRB. The peroxisome tag PEX3 was cloned into pcDNA5 with a carboxy-terminal mEmerald fluorescent protein and FKBP.

Protein expression and purification

Human full-length dynein, human dynein monomer, and human Lis1 constructs were expressed in Sf9 cells as described previously[3,33]. Briefly, the pDyn3 plasmid containing the human dynein genes or the pFastBac plasmid containing full-length Lis1 or dynein monomer was transformed into DH10EmBacY chemically competent cells with heat shock at 42°C for 15 seconds followed by incubation at 37°C for 5 hours in S.O.C media (Thermofisher scientific). The cells were then plated on LB-agar plates containing kanamycin (50 µg/ml), gentamicin (7 µg/ml), tetracycline (10 µg/ml), BluoGal (100 µg/ml) and IPTG (40 µg/ml) and positive clones were identified by a blue/white color screen after 48 hours. For full-length human dynein constructs, white colonies were additionally tested for the presence of all six dynein genes using PCR. These colonies were then grown overnight in LB medium containing kanamycin (50 µg/ml), gentamicin (7 µg/ml) and tetracycline (10 µg/ml) at 37°C. Bacmid DNA was extracted from overnight cultures using an isopropanol precipitation method as described previously[12]. 2mL of Sf9 cells at $0.5x10^6$ cells/mL were transfected with 2µg of fresh bacmid DNA and FuGene HD transfection reagent (Promega) at a 3:1 transfection reagent to

DNA ratio according to the manufacturer's instructions. After three days, the supernatant containing the "V0" virus was harvested by centrifugation at 200 x g for 5 minutes at 4°C. To generate "V1", 1 mL of the V0 virus was used to transfect 50mL of Sf9 cells at $1x10^6$ cells/mL. After three days, the supernatant containing the V1 virus was harvested by centrifugation at 200 x g for 5 minutes at 4°C and stored in the dark at 4°C until use. For protein expression, 4 mL of the V1 virus were used to transfect 400 mL of Sf9 cells at $1x10^6$ cells/mL. After three days, the cells were harvested by centrifugation at 3000 x g for 10 minutes at 4°C. The pellet was resuspended in 10 mL of ice-cold PBS and pelleted again. The pellet was flash frozen in liquid nitrogen and stored at -80°C.

Protein purification steps were done at 4°C unless otherwise indicated. Full-length dynein and dynein monomer were purified from frozen Sf9 pellets transfected with the V1 virus as described previously[3]. Frozen cell pellets from a 400 mL culture were resuspended in 40 mL of Dynein-lysis buffer (50 mM HEPES [pH 7.4], 100 mM sodium chloride, 1 mM DTT, 0.1 mM Mg-ATP, 0.5 mM Pefabloc, 10% (v/v) glycerol) supplemented with 1 cOmplete EDTA-free protease inhibitor cocktail tablet (Roche) per 50 mL and lysed using a Dounce homogenizer (10 strokes with a loose plunger and 15 strokes with a tight plunger). The lysate was clarified by centrifuging at 183,960 x g for 88 min in Type 70 Ti rotor (Beckman). The clarified supernatant was incubated with 4 mL of IgG Sepharose 6 Fast Flow beads (GE Healthcare Life Sciences) for 3-4 hours on a roller. The beads were transferred to a gravity flow column, washed with 200 mL of Dynein-lysis buffer

and 300 mL of TEV buffer (50 mM Tris–HCl [pH 8.0], 250 mM potassium acetate, 2 mM magnesium acetate, 1 mM EGTA, 1 mM DTT, 0.1 mM Mg-ATP, 10% (v/v) glycerol). For fluorescent labeling of carboxy-terminal SNAPf tag, dynein-coated beads were labeled with 5 µM SNAP-Cell-TMR (New England Biolabs) in the column for 10 min at room temperature and unbound dye was removed with a 300 mL wash with TEV buffer at 4°C. The beads were then resuspended and incubated in 15 mL of TEV buffer supplemented with 0.5 mM Pefabloc and 0.2 mg/mL TEV protease (purified in the Reck-Peterson lab) overnight on a roller. The supernatant containing cleaved proteins was concentrated using a 100K MWCO concentrator (EMD Millipore) to 500 µL and purified via size exclusion chromatography on a TSKgel G4000SWXL column (TOSOH Bioscience) with GF150 buffer (25 mM HEPES [pH7.4], 150 mM KCl, 1mM MgCl2, 5 mM DTT, 0.1 mM Mg-ATP) at 1 mL/min. The peak fractions were collected, buffer exchanged into a GF150 buffer supplemented with 10% glycerol, concentrated to 0.1-0.5 mg/mL using a 100K MWCO concentrator (EMD Millipore) and flash frozen in liquid nitrogen.

Lis1 constructs were purified from frozen cell pellets from 400 mL culture. Lysis and clarification steps were similar to full-length dynein purification except Lis1-lysis buffer (30 mM HEPES [pH 7.4], 50 mM potassium acetate, 2 mM magnesium acetate, 1 mM EGTA, 300 mM potassium chloride, 1 mM DTT, 0.5 mM Pefabloc, 10% (v/v) glycerol) supplemented with 1 cOmplete EDTA-free protease inhibitor cocktail tablet (Roche) per 50 mL was used. The clarified

supernatant was incubated with 0.5 mL of IgG Sepharose 6 Fast Flow beads (GE Healthcare Life Sciences) for 2-3 hours on a roller. The beads were transferred to a gravity flow column, washed with 20 mL of Lis1-lysis buffer, 100 mL of modified TEV buffer (10 mM Tris–HCl [pH 8.0], 2 mM magnesium acetate, 150mM potassium acetate, 1 mM EGTA, 1 mM DTT, 10% (v/v) glycerol) supplemented with 100 mM potassium acetate, and 50 mL of modified TEV buffer. For fluorescent labeling of Lis1 constructs with amino-terminal HaloTags, Lis1-coated beads were labeled with 200 µM Halo-TMR (Promega) for 2.5 hours at 4°C on a roller and the unbound dye was removed with a 200 mL wash with modified TEV buffer supplemented with 250 mM potassium acetate. Lis1 was cleaved from IgG beads via incubation with 0.2 mg/mL TEV protease overnight on a roller. The cleaved Lis1 was filtered by centrifuging with an Ultrafree-MC VV filter (EMD Millipore) in a tabletop centrifuge and flash frozen in liquid nitrogen.

Dynactin was purified from stable HEK293T cell lines expressing p62-Halo-3xFlag as described previously[35]. Briefly, frozen pellets collected from 160 x 15cm plates were resuspended in 80 mL of Dynactin-lysis buffer (30 mM HEPES [pH 7.4], 50 mM potassium acetate, 2 mM magnesium acetate, 1 mM EGTA, 1 mM DTT, 10% (v/v) glycerol) supplemented with 0.5 mM Mg-ATP, 0.2% Triton X-100 and 1 cOmplete EDTA-free protease inhibitor cocktail tablet (Roche) per 50 mL and rotated slowly for 15 min. The lysate was clarified by centrifuging at 66,000 x g for 30 min in Type 70 Ti rotor (Beckman). The clarified supernatant was incubated with 1.5 mL of anti-Flag M2 affinity gel (Sigma-Aldrich) overnight on a roller. The

beads were transferred to a gravity flow column, washed with 50 mL of wash buffer (Dynactin-lysis buffer supplemented with 0.1 mM Mg-ATP, 0.5 mM Pefabloc and 0.02% Triton X-100), 100 mL of wash buffer supplemented with 250 mM potassium acetate, and again with 100 mL of wash buffer. For fluorescent labeling the HaloTag, dynactin-coated beads were labeled with 5 µM Halo-JF646 (Janelia) in the column for 10 min at room temperature and the unbound dye was washed with 100 mL of wash buffer at 4°C. Dynactin was eluted from beads with 1 mL of elution buffer (wash buffer with 2 mg/mL of 3xFlag peptide). The eluate was collected, filtered by centrifuging with Ultrafree-MC VV filter (EMD Millipore) in a tabletop centrifuge and diluted to 2 mL in Buffer A (50 mM Tris-HCl [pH 8.0], 2 mM MgOAc, 1 mM EGTA, and 1 mM DTT) and injected onto a MonoQ 5/50 GL column (GE Healthcare and Life Sciences) at 1 mL/min. The column was pre-washed with 10 CV of Buffer A, 10 CV of Buffer B (50 mM Tris-HCl [pH 8.0], 2 mM MgOAc, 1 mM EGTA, 1 mM DTT, 1 M KOAc) and again with 10 CV of Buffer A at 1 mL/min. To elute, a linear gradient was run over 26 CV from 35-100% Buffer B. Pure dynactin complex eluted from ~75-80% Buffer B. Peak fractions containing pure dynactin complex were pooled, buffer exchanged into a GF150 buffer supplemented with 10% glycerol, concentrated to 0.02-0.1 mg/mL using a 100K MWCO concentrator (EMD Millipore) and flash frozen in liquid nitrogen.

Activating adaptors containing amino-terminal HaloTags were expressed in BL-21[DE3] cells (New England Biolabs) at OD 0.4-0.6 with 0.1 mM IPTG for 16 hr at 18°C. Frozen cell pellets from 2 L culture were resuspended in 60mL of

activator-lysis buffer (30 mM HEPES [pH 7.4], 50 mM potassium acetate, 2 mM magnesium acetate, 1 mM EGTA, 1 mM DTT, 0.5 mM Pefabloc, 10% (v/v) glycerol) supplemented with 1 cOmplete EDTA-free protease inhibitor cocktail tablet (Roche) per 50 mL and 1 mg/mL lysozyme. The resuspension was incubated on ice for 30 min and lysed by sonication. The lysate was clarified by centrifuging at 66,000 x g for 30 min in Type 70 Ti rotor (Beckman). The clarified supernatant was incubated with 2 mL of IgG Sepharose 6 Fast Flow beads (GE Healthcare Life Sciences) for 2 hr on a roller. The beads were transferred to a gravity flow column, washed with 100 mL of activator-lysis buffer supplemented with 150 mM potassium acetate and 50mL of cleavage buffer (50 mM Tris–HCl [pH 8.0], 150 mM potassium acetate, 2 mM magnesium acetate, 1 mM EGTA, 1 mM DTT, 0.5 mM Pefabloc, 10% (v/v) glycerol). The beads were then resuspended and incubated in 15 mL of cleavage buffer supplemented with 0.2 mg/mL TEV protease overnight on a roller. The supernatant containing cleaved proteins were concentrated using a 50K MWCO concentrator (EMD Millipore) to 1 mL, filtered by centrifuging with Ultrafree-MC VV filter (EMD Millipore) in a tabletop centrifuge, diluted to 2 mL in Buffer A (30 mM HEPES [pH 7.4], 50 mM potassium acetate, 2 mM magnesium acetate, 1 mM EGTA, 10% (v/v) glycerol and 1 mM DTT) and injected onto a MonoQ 5/50 GL column (GE Healthcare and Life Sciences) at 1 mL/min. The column was pre-washed with 10 CV of Buffer A, 10 CV of Buffer B (30 mM HEPES [pH 7.4], 1 M potassium acetate, 2 mM magnesium acetate, 1 mM EGTA, 10% (v/v) glycerol and 1 mM DTT) and again

with 10 CV of Buffer A at 1 mL/min. To elute, a linear gradient was run over 26 CV from 0-100% Buffer B. The peak fractions containing Halo-tagged activating adaptors were collected and concentrated to using a 50K MWCO concentrator (EMD Millipore) to 0.2 mL. For fluorescent labeling the HaloTag, the concentrated peak fractions were incubated with 5 μM Halo-Alexa488 (Promega) for 10 min at room temperature. Unbound dye was removed by PD-10 desalting column (GE Healthcare and Life Sciences) according to the manufacturer's instructions. The labeled activating adaptor sample was concentrated using a 50K MWCO concentrator (EMD Millipore) to 0.2 mL, diluted to 0.5 mL in GF150 buffer and further purified via size exclusion chromatography on a Superose 6 Increase 10/300 GL column (GE Healthcare and Life Sciences) with GF150 buffer at 0.5 mL/min. The peak fractions were collected, buffer exchanged into a GF150 buffer supplemented with 10% glycerol, concentrated to 0.2-1 mg/mL using a 50K MWCO concentrator (EMD Millipore) and flash frozen in liquid nitrogen.

For the two-color dynein experiments shown in Figure 3, the labeling efficiency of TMR-dynein was 94% for one bioreplicate and 87% for the other, and the labeling efficiency of Alexa647-dynein was 96% for one bioreplicate and 100% for the other. For the two-color experiment in Figure 4 the labeling efficiency of Alexa-647 dynein and TMR-Lis1 was 100% and 93%, respectively. For the two-color experiment in Figure S4 the labeling efficiency of Alexa-647 dynein and TMR-Lis1-5A was 100% and 87%, respectively. For the two-color dynein

experiments shown in Figure 5, the labeling efficiency of both TMR-dynein and Alexa647-dynein was 100%.

Single-molecule TIRF microscopy

Single-molecule imaging was performed with an inverted microscope (Nikon, Ti-E Eclipse) equipped with a 100x 1.49 N.A. oil immersion objective (Nikon, Plano Apo) and a ProScan linear motor stage controller (Prior). The microscope was equipped with a LU-NV laser launch (Nikon), with 405 nm, 488 nm, 532 nm, 561 nm and 640 nm laser lines. The excitation and emission paths were filtered using appropriate single bandpass filter cubes (Chroma). For two-color colocalization imaging, the emission signals were further filtered and split using W-view Gemini image splitting optics (Hamamatsu). The emitted signals were detected with an electron multiplying CCD camera (Andor Technology, iXon Ultra 897). Illumination and image acquisition was controlled by NIS Elements Advanced Research software (Nikon).

Single-molecule motility and microtubule binding assays were performed in flow chambers assembled as described previously[50] using the TIRF microscopy set up described above. Either biotin-PEG-functionalized coverslips (Microsurfaces) or No. 1-1/2 coverslips (Corning) sonicated in 100% ethanol for 10 min were used for the flow-chamber assembly. Taxol-stabilized microtubules with ~10% biotin-tubulin and ~10% fluorescent-tubulin (Alexa405-, 488- or 647-labeled) were prepared as described previously[51]. Flow chambers were assembled with taxol-stabilized microtubules by incubating sequentially with the following

solutions, interspersed with two washes with assay buffer (30 mM HEPES [pH 7.4], 2 mM magnesium acetate, 1 mM EGTA, 10% glycerol, 1 mM DTT) supplemented with 20 µM Taxol in between: (1) 1 mg/mL biotin-BSA in assay buffer (3 min incubation); (2) 0.5 mg/mL streptavidin in assay buffer (3 min incubation) and (3) a fresh dilution of taxol-stabilized microtubules in assay buffer (3 min incubation). After flowing in microtubules, the flow chamber was washed twice with assay buffer supplemented with 1 mg/mL casein and 20 µM Taxol.

To assemble dynein-dynactin-activating adaptor complexes, purified dynein (10-20 nM concentration), dynactin and the activating adaptor were mixed at 1:2:10 molar ratio and incubated on ice for 10 min. These dynein-dynactin-activating adaptor complexes were then incubated with Lis1 or modified TEV buffer (to buffer match for experiments without Lis1) for 10 min on ice. Dynactin and the activating adaptors were omitted for the experiments with dynein alone. The mixtures of dynein, dynactin, activating adaptor or dynein alone and Lis1 were then flowed into the flow chamber assembled with taxol-stabilized microtubules. The final imaging buffer contained the assay buffer supplemented with 20 µM Taxol, 1 mg/mL casein, 71.5 mM β-mercaptoethanol, an oxygen scavenger system, and 2.5 mM Mg-ATP. The final concentration of dynein in the flow chamber was 0.5-1 nM for experiments with dynein-dynactin-activating adaptor complexes and 0.3-0.5 nM for dynein alone experiments. The final concentration of Lis1 was between 12 nM - 300 nM (as indicated in the main text) for experiments with unlabeled Lis1, and 50 nM for experiments with TMR-labeled

Lis1. For standard motility experiments our final imaging buffer contained 30mM KOAc and 7.5 mM KCl. For the experiments in Figures 2 and 3, the increased ionic strength buffer contained 60mM KOAc and 7.5 mM KCl. We selected this salt condition because it resulted in severely compromised the motility of dynein/ dynactin/ Hook3 complexes.

For single-molecule motility assays, microtubules were imaged first by taking a single-frame snapshot. Dynein and/or the activating adaptor labeled with fluorophores (TMR, Alexa647 or Alexa488) was imaged every 300 msec for 3 min. At the end, microtubules were imaged again by taking a snapshot to assess stage drift. Movies showing significant drift were not analyzed. Each sample was imaged no longer than 15 min. For single-molecule microtubule binding assays, the final imaging mixture containing dynein was incubated for an additional 5 min in the flow chamber at room temperature before imaging. After 5 min incubation, microtubules were imaged first by taking a single-frame snapshot. Dynein and/or activating adaptors labeled with fluorophores (TMR, Alexa647 or Alexa488) were imaged by taking a single-frame snapshot. Each sample was imaged at 4 different fields of view and there were between 5 and 10 microtubules in each field of view. In order to compare the effect of Lis1 on microtubule binding, the samples with and without Lis1 were imaged in two separate flow chambers made on the same coverslip on the same day with the same stock of polymerized tubulin as described previously[51].

Microtubule gliding assays

For microtubule gliding assays 30 nM TMR-dynein in GF150 was flowed into the chamber and non-specifically bound to the coverslip. After 3 minutes the chamber was washed twice with BRB80 buffer (80mM PIPES pH 6.8, 2mM $MgCl_2$, 1 mM EGTA) supplemented with 1 mg/mL casein, and then with the same buffer containing 5mg/mL casein for 3 minutes. The chamber was next washed twice with BRB80 buffer with casein. Finally, GMPCPP-stabilized microtubules (polymerized with 10% 488-tubulin) was added in the presence or absence of Lis1. The final imaging buffer contained BRB80 buffer supplemented with 20 µM Taxol, 1 mg/mL casein, 71.5 mM β-mercaptoethanol, an oxygen scavenger system, and 2.5 mM Mg-ATP. Microtubules were incubated for three minutes, and then two fields of view were imaged at 1s/frame for 3 minutes.

Single-molecule motility assay analysis

Kymographs were generated from motility movies and dynein velocity was calculated from kymographs using ImageJ macros as described[51]. Only runs that were longer than 4 frames (1.2 s) were included in the analysis. Bright aggregates, which were less than 5% of the population, were excluded from the analysis. Stationary and diffusive events were grouped as non-processive events when calculating the percent of events that were processive. For two-color colocalization analysis, kymographs from each channel were generated and merged in ImageJ and the number of colocalized runs was determined manually. For two-color colocalization and percent processive analysis data from all replicates was pooled

and a chi-squared test was performed. Data plotting and statistical analyses were performed in Prism8 (GraphPad).

Single-molecule microtubule binding assay analysis

Intensity profiles of dynein or activating adaptor spots from a single-frame snapshot were generated over a 5-pixel wide line drawn perpendicular to the long axis of microtubules in ImageJ. Intensity peaks at least 2-fold higher than the neighboring background intensity were counted as dynein or activating adaptor spots bound to microtubules. Bright aggregates that were 5-fold brighter than the neighboring intensity peaks were not counted. The average binding density was calculated as the total number of dynein or activating adaptor spots divided by the total microtubule length in each snapshot. Normalized binding density was calculated by dividing by the average binding density of dynein or activating adaptor without Lis1 collected on the same coverslip (see above). Data plotting and statistical analyses were performed in Prism7 (GraphPad).

Microtubule gliding assay analysis

Kymographs were generated by tracing the path of individual microtubules and velocity was calculated from kymographs using ImageJ macros as described[51]. Data plotting and statistical analyses were performed in Prism8 (GraphPad).

Protein binding assays

To assess dynein/ dynactin complex formation, BicD2-S was first coupled to 15 µL of Magne HaloTag Beads (Promega) in 2 mL Protein Lo Bind Tubes

(Eppendorf) using the following protocol. Beads were washed twice with 1 mL of GF150 without ATP supplemented with 10% glycerol and 0.1%NP40. BicD2-S was diluted in this buffer to 75 nM. 25 uL of diluted BicD2-S was added to the beads and gently shaken for one hour. 20 µL of supernatant were then analyzed via SDS-PAGE to confirm complete depletion of BicD2-S. The BicD2-S-conjugated beads were washed once with 1 mL GF150 with 10% glycerol and 0.1% NP40 and once with 1mL of binding buffer (30 mM HEPES [pH 7.4], 2 mM magnesium acetate, 1 mM EGTA, 10% glycerol, 1 mM DTT, 1 mg/mL casein, 0.1% NP40, 1mM ADP) supplemented with 15.7 mM KCl and 8.3 mM KOAc.. 10 nM dynein, 10nM dynactin and 150 nM Lis1 were diluted in binding buffer, which resulted in 15.7 mM KCl and 8.3 mM KOAc. We used a molar ratio of dynein, dynactin, and BicD2-S of 1:1:7.5 because at this ratio dynein bound to BicD2-S minimally in the absence of Lis1. This gave us a large dynamic range to observe the Lis1-induced increase in binding. For experiments lacking dynactin or Lis1 the protein dilutions were supplemented with the equivalent mass of BSA in the equivalent amount of their purification buffers. 25 µL of the dynein, dynactin and Lis1 mixture were added to the beads pre-bound with BicD2-S and gently agitated for 45 minutes. After incubation 20 µL of the supernatant was removed, and 6.67 µL of NuPAGE® LDS Sample Buffer (4X) and 1.33 µL of Beta-mercaptoethanol was added to each. The samples were boiled for 5 minutes before running on a 4-12% NuPAGE Bis-Tris gel at 4C. Depletion was determined using densitometry in ImageJ.

Lis1 binding curves were determined as above with minor variations. 25 µL of Magne HaloTag Beads were used, and washed twice with 1 mL modified TEV buffer. 0, 30, 60, 90, 120, 300 and 600 nM Lis1 were bound to beads for one hour at ambient temperature. Beads were then washed with 1 mL of modified TEV buffer and 1 mL of binding buffer supplemented with 30 mM KCl and 6 mM KOAc. 10 nM of dynein was diluted in binding buffer supplemented with salt to 30 mM KCl and 6 mM KOAc. Binding and determination of depletion were carried out as above. Binding curves were fit in Prism8 (Graphpad) with a nonlinear regression for one site binding with Bmax set to 1.

Cryo-EM sample preparation

A final concentration of 3.5 µM dynein monomer and 3.5 µM HaloTag-Lis1 were incubated in assay buffer supplemented with DTT, NP40, and $ATPVO_4$ for 10-20 minutes before grids were prepared. Proteins were diluted and mixed such that the final salt and additive concentrations were 52.5 mM KCl, 20 mM KOAc, 4.8% glycerol, 5 mM DTT, 0.005% NP40, and 2.5 mM $ATPVO_4$. 4 ul of sample was applied to UltraAuFoil R 1.2/1.3 300 mesh grids (Electron Microscopy Sciences) that were glow discharged with 20 mA negative current for 30 sec. Grids were plunge-frozen in a Vitrobot Mark IV robot (FEI Company), maintained at 100% humidity and 4 °C.

Cryo-EM data collection and image analysis

Data was collected on a Talos Arctica transmission electron microscope (FEI Company) operating at 200 keV with a K2 Summit direct electron detector

(Gatan Inc). Dose-fractionated movies were collected in counting mode, with a final calibrated pixel size of 1.16 Å/pixel, a dose rate of ~6 e^-/pixel/sec, and a total dose of ~60 $e^-/Å^2$. Leginon[52] was used for automated data collection and movies were processed on-the-fly using Appion[53]. Movie alignment was performed with MotionCor2 defocus estimations were performed with CTFFIND4[54], and particles were picked using DoG Picker[55] 403,439 particles were extracted from 2,422 aligned, dose weighted micrographs in Relion-3[56] with a box size of 288 x 288 pixels and binned by 2 for a final pixel size of 2.32 Å/pixel. The extracted particles were imported into cryoSPARC 2.4.2 for all subsequent analysis[57]. To generate the 2D-class averages shown in figure 2, two rounds of 2D classification were performed. In the first round, 2D classes containing clear density corresponding to the dynein ATPase ring and Lis1 (comprising 71,436 particles) were selected. In the second round, three classes, containing 22,621 total particles were selected for presentation in figure 2 (7,712 particles in the class on the left, 8,943 particles in the class in the middle, 6,506 particles in the class on the right).

To generate a model of human dynein bound to Lis1, we aligned human dynein-2 bound to ATP-vanadate (PDB: 4RH7[44]) with yeast dynein (AAA3-Walker B) in ATP-vanadate and Lis1 (PDB: 5VLJ[30]) using the part of the sequence that encompasses the two Lis1 binding sites in yeast dynein, from AAA3 until after the binding site for the second Lis1 in the stalk. We then deleted the dynein chain of 5VLJ and combined the remaining two copies of Lis1 with 4RH7. To highlight the

densities corresponding to Lis1, we also generated 2D projections of human dynein-2 alone (PDB: 4RH7) in the same orientations as our experimental data.

SEC-MALS

SEC-MALS experiments were performed using an ÄKTAmicro chromatography system hooked up to a Superdex 200 Increase 3.2/300 size exclusion chromatography column (GE Healthcare and Life Sciences) coupled in-line to a DAWN HELEOS II multiangle light scattering detector (Wyatt Technology) and an Optilab T-rEX refractive index detector (Wyatt Technology). SEC-MALS was performed in 25 mM HEPES [pH7.4], 30 mM KCl, 6mM KOAc, 1mM MgCl2, 5 mM DTT and 0.1 mM Mg-ATP flowed at 0.1 mL/min. A 50 µL sample of 4 µM dynein monomer and/or 2 µM Lis1 dimer or 4 µM Lis1ΔN was incubated on ice for 10 minutes prior to injection. Molar mass was calculated using ASTRA 6 software, with protein concentration derived from the Optilab T-rEX.

Peroxisome recruitment assay

Human U2OS cells were cultured in Dulbecco's modified Eagle's medium containing 10% fetal calf serum and 1% penicillin/streptomycin. One day before transfection the cells were plated on 35 mm fluorodishes (World Precision Instruments) coated with 100 µg/mL poly-D-lysine (Sigma Aldrich) and 4 µg/mL mouse laminin (Thermo Fisher Scientific). Cells were transfected with 120 ng PEX3-mEMerald-FKBP and BicD2NS-V5-FRB constructs per well as well as 20 pmol of either ON-TARGETplus Non-targeting siRNA #1 (Dharmacon), ON-TARGETplus PAFAH1B1 siRNA J-010330-07-0002 (Dharmacon), ON-

TARGETplus PAFAH1B1 siRNA J-010330-09-0002 (Dharmacon), or SMARTpool: ON-TARGETplus PAFAH1B1 siRNA (Dharmacon) using Lipofectamine 2000 (Thermo Fisher Scientific).

Cells were labelled with Halo-JF549 (Janelia) and imaged after 48 hours using a 100x Apo TIRF NA 1.49 objective on a Nikon Ti2 microscope with a Yokogawa-X1 spinning disk confocal system, MLC400B laser engine (Agilent), Prime 95B back-thinned sCMOS camera (Teledyne Photometrics), piezo Z-stage (Mad City Labs) and stage top environmental chamber (Tokai Hit). Cells were screened for the presence of JF549 signal with the 560 nm laser line and then mEmerald was imaged at 2 frames per second, 100 ms exposure with the 488 nm laser line. Dimerization of FKBP-FRB was induced with 1 µM rapalog (Takara Bio). Images were analyzed in ImageJ. Kymographs were generated from >5 peroxisomes that moved directionally for >3 frames in each cell and velocity was calculated from kymographs using ImageJ macros as described[51]. Data plotting and statistical analyses were performed in Prism8 (GraphPad).

Western analysis and antibodies

Lysates were run on 4–12% polyacrylamide gels (NuPage, Invitrogen) and transferred to PVDF (Immobilon-P, EMD Millipore; Billerica, MA) for 1.5 hr at 300 mA constant current. Blots were blocked for 10 min with TBS +5% dry milk (w/v), and immunoblotted with appropriate antibodies. All antibodies were diluted in TBST +5% milk (w/v). Primary antibodies were incubated overnight at 4˚C, while secondary antibodies were incubated for 1 hr at room temperature. Antibodies

used were mouse anti-Lis1 (sc-374586, Santa Cruz Biotechnology, 1:200 dilution), mouse anti-beta Actin (MA5-15739, Invitrogen, 1:2000 dilution), rabbit anti-V5 (V8137, Sigma-Aldrich, 1:2000 dilution), goat anti-rabbit HRP (7076, Cell Signaling Technology, 1:5000 dilution) and horse anti-mouse HRP (7074, Cell Signaling Technology, 1:5000 dilution). Westerns were visualized with Supersignal West Pico or Femto Chemiluminescent reagents (Thermo Fisher Scientific) and a VersaDoc imaging system (Bio-Rad Laboratories; Hercules, CA). Image intensity histograms were adjusted and images were converted to 8-bit with ImageJ before being imported into Adobe Illustrator to make figures.

Statistics and Reproducibility

Live-cell experiments were performed with two independent cell transfections. No commonly misidentified cell lines were used. At least three individual experiments were performed using two independent purifications of dynein for biochemistry and single-molecule results, with the exception of the SEC-MALS experiments that used a single purification. Each experiment was repeated independently with similar results. The n for each experiment is defined in the figure legends along with a description of the statistical tests performed.

2.6 Acknowledgements

Chapter 2, in full, is a reprint of Htet, ZM*; Gillies, JP*; Baker, RW.; Leschziner, AE; DeSantis, ME; Reck-Peterson, SL. LIS1 promotes the formation of activated cytoplasmic dynein-1 complexes. Nat. Cell Biol. 22, 518–525 (2020). The dissertation author was the co-primary author of this work.

We thank Jenna Christensen, Eva Karasmanis, Aga Kendrick, Anthony Roberts and John Salogiannis for comments on the manuscript and helpful discussions, the Nikon Imaging Center at UC San Diego where we collected data and received help with image analysis, and the UC San Diego cryo-EM facility, where cryo-EM data was collected. We also thank the Physics Computing Facility for IT support. SRP is supported by HHMI and NIH R01GM121772. Funding to SRP from the HHMI/Simons Faculty Scholars Program and R01GM107214 funded earlier parts of this work. AEL is supported by R01GM107214, ZMH by an NSF graduate research fellowship DGE1144152, JPG by the Molecular Biophysics Training Grant, NIH Grant T32 GM008326, RWB is a Damon Runyon Fellow supported by the Damon Runyon Cancer Research Foundation DRG-#2285-17, and MED by NIH K99GM127757 and previously by a Jane Coffin Childs Memorial Fund Postdoctoral Fellowship 61-1552-T.

2.7 Supplementary figures

Supplementary Data Figure 2.1. Effect of Lis1 on the motility and microtubule binding of activated dynein complexes. **a.** SDS-PAGE gel stained with Sypro Red of human dynein, dynactin and the activating adaptors BicD2-S (aa 25-398), BicD2-L (aa 1-598), Hook3 (aa 1-552), and Ninl (aa 1-702) used here. The dynein heavy chain was tagged with the SNAP tag, the dynactin subunit p62 with the HaloTag, and each activating adaptor with the HaloTag. The dynein light chains are too small to be seen on this low percentage gel. SDS-PAGE gels were run after all protein purifications. **b.** Example microscopy images for microtubule binding density data in the absence (white circles) or presence (black circles) of 300 nM Lis1 presented in Figure 1 d and e. Microtubules in magenta and dynein or activating adaptor foci in green. Scale bars are 10 µm. **c.** Example kymographs of dynein/ dynactin/ activating adaptor complexes in the absence (white circles) or presence (black circles) of 300 nM Lis1. Scale bars are 10 µm (x) and 20 sec (y). **d.** Percent processive runs of dynein/ dynactin/ activating adaptor complexes in standard motility buffer in the absence (white circles) or presence (black circles) of 300 nM Lis1. Statistical analysis was performed on data pooled from all replicates with a chi-squared test. **e.** Immunoblots of cell lysates from human U2OS cells co-transfected with PEX3-mEmerald-FKBP and BicD2-S-V5-FRB constructs, as well as either scramble siRNA or Lis1 siRNA 1 or 2. Blots were performed for each biorep with similar results. **f.** Peroxisome velocity in human U2OS cells with scrambled or Lis1 siRNA pool knockdown. The median and interquartile range are shown. At least 7 peroxisome motility events were measured per cell. **g.** Immunoblots of cell lysates from human U2OS cells co-transfected with PEX3-mEmerald-FKBP and BicD2-S-V5-FRB constructs and scramble or Lis1 siRNA pool. Two bio-replicates (1 and 2) are shown. An anti-V5 antibody detects BicD2-S-V5-FRB, an anti-Lis1 antibody assesses the efficiency of Lis1 knockdown, and an anti-actin antibody serves as a loading control for immunoblots shown in e and g

.

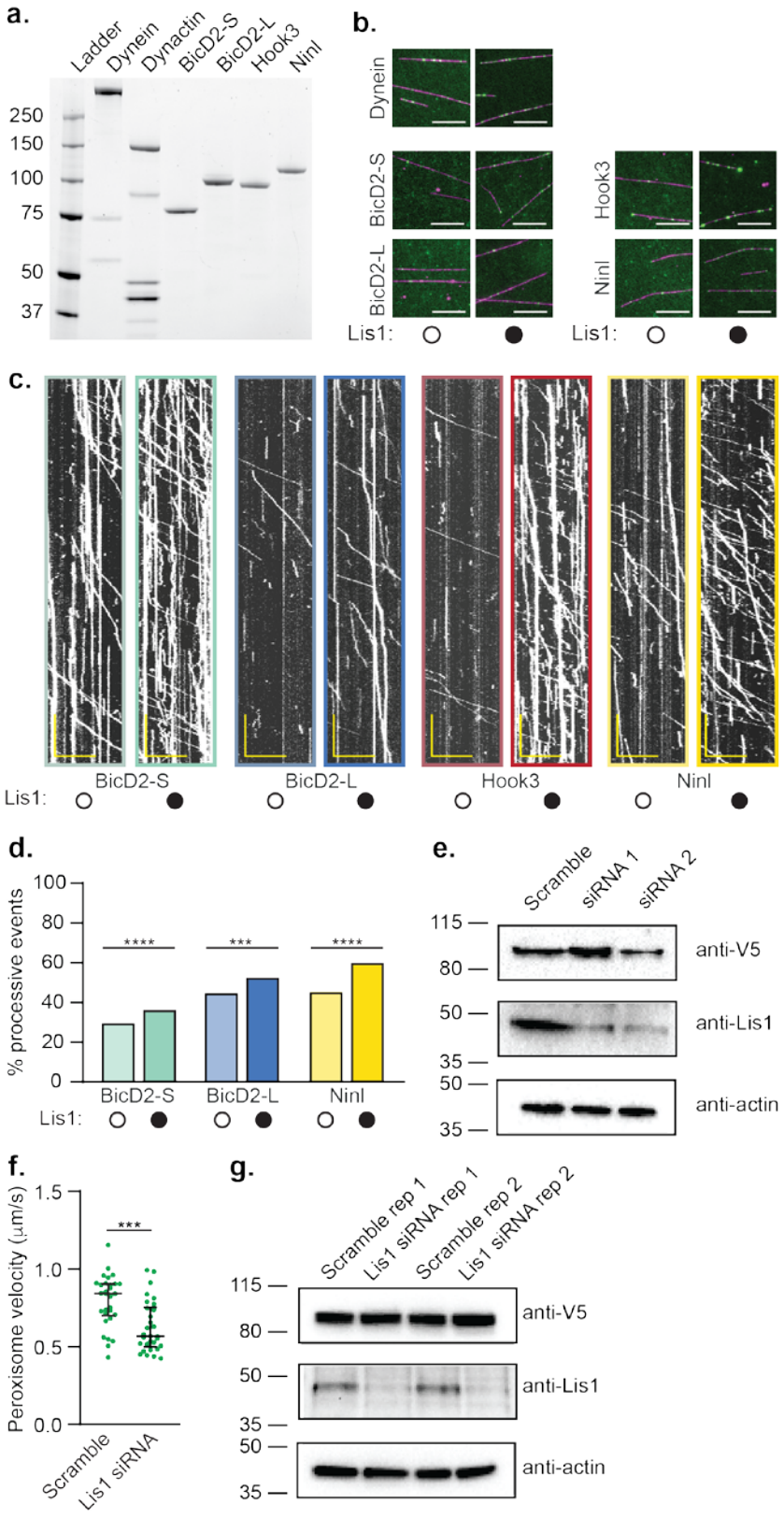
a.
Ladder
Dynein
Dynactin
BicD2-S
BicD2-L
Hook3
NinI
250
150
100
75
50
37
b.
Dynein
BicD2-S
BicD2-L
Hook3
NinI
Lis1:
Lis1:
c.
BicD2-S
BicD2-L
Hook3
NinI
Lis1:
d.
% processive events
100
80
60
40
20
0
****
***
****
BicD2-S
BicD2-L
NinI
Lis1:
e.
Scramble
siRNA 1
siRNA 2
115
80
50
35
50
35
anti-V5
anti-Lis1
anti-actin
f.
Peroxisome velocity (μm/s)
1.5
1.0
0.5
0.0
***
Scramble
Lis1 siRNA
g.
Scramble rep 1
Lis1 siRNA rep 1
Scramble rep 2
Lis1 siRNA rep 2
115
80
50
35
50
35
anti-V5
anti-Lis1
anti-actin

Supplementary Data Figure 2.2. Characterization of the dynein binding interface and dimerization domain of Lis1. a. Example SEC-MALS traces with Lis1 dimer (orange), dynein monomer (grey), and dynein monomer with Lis1 dimer (black). The intensity of the UV signal (solid line) and the molecular weight fit (dashed line) are shown. Dimeric Halo-tagged-Lis1 is expected to be 161.4 kDa and monomeric dynein is expected to be 380.4 kDa. In this experiment we observe Halo-tagged-Lis1 to be 157.6 kDa, monomeric dynein to be 489.5 kDa and the Lis1-dynein complex to be 700.1 kDa. The high apparent molecular weight of monomeric dynein may be due to a self-association species that appears as a shoulder in the UV trace. The experiment was repeated in triplicate yielding similar results, giving a stoichiometry of 1.2 +/- 0.3 Lis1 dimers per dynein monomer. Based on this data we cannot rule out that some dynein monomers are bound to two Lis1 dimers (which has been reported to occur[34]), but our data suggest that most dynein monomers bind a single Lis1 dimer, and that Lis1 does not tether two dynein monomers. **b.** Single-molecule velocity of dynein/ dynactin/ BicD2-S complexes with increasing concentrations of Lis1. The median and interquartile range are shown. **c.** Single-molecule velocity of dynein/ dynactin/ Hook3 complexes in the presence of a higher ionic strength buffer in the absence (white circles) or presence (black circles) of 300 nM Lis1 or Lis1-5A. The data in the presence and absence of WT Lis1 was also presented in Figure 1h. The median and interquartile range are shown. **d.** Example kymographs of dynein/ dynactin/ Hook3 complexes in a higher ionic strength buffer in the absence or presence of 300 nM Lis1 or Lis1-5A. Scale bars are 10 µm (x) and 20 sec (y). Data is quantified in Supplementary Data Figure 2C. **e.** Example SEC-MALS trace of Lis1ΔN (orange). The intensity of the UV signal (solid line) and the molecular weight fit (dashed line) are shown. Monomeric Halo-tagged-Lis1ΔN is expected to be 71.5kDa. In this experiment we observe Halo-tagged-Lis1ΔN to have a monomer peak at 72.0 kDa and a dimer peak at 141.2 kDa. The experiment was repeated in triplicate yielding similar results.

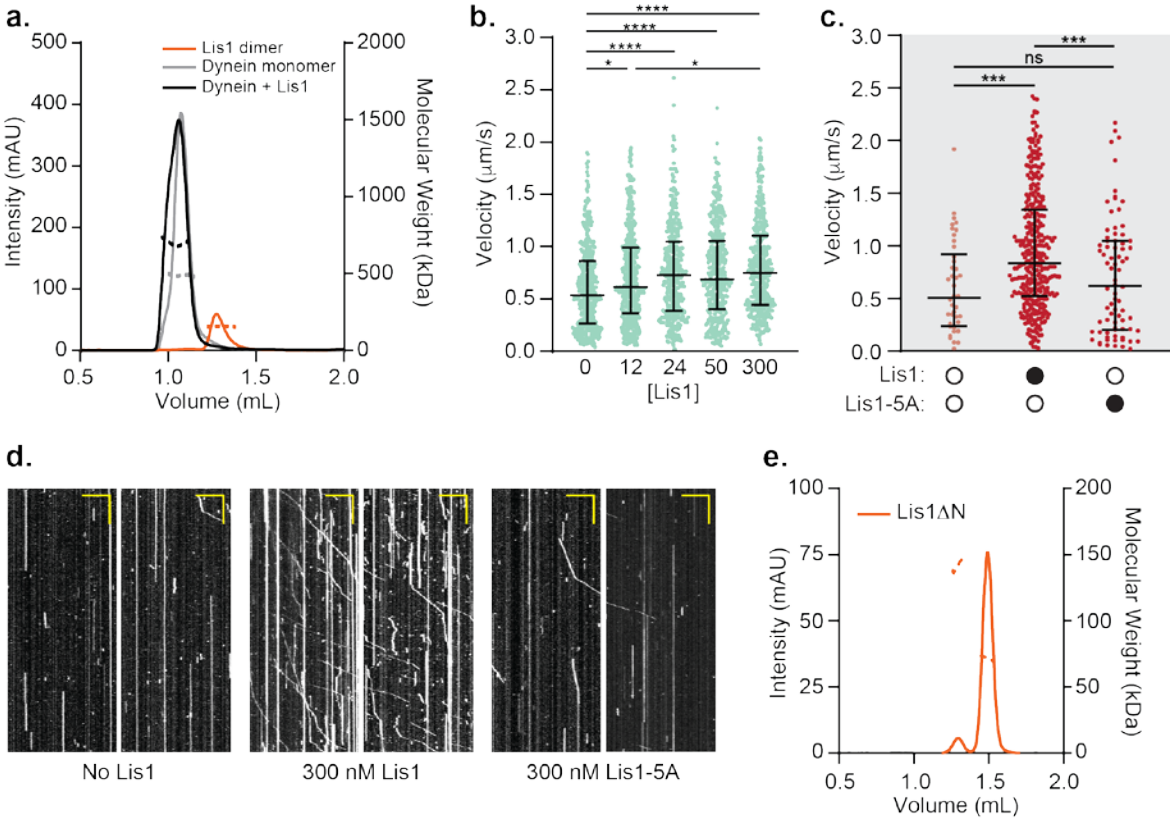
a.
Lis1 dimer
Dynein monomer
Dynein + Lis1
Intensity (mAU)
Molecular Weight (kDa)
Volume (mL)
b.
Velocity (µm/s)
[Lis1]
c.
ns
Lis1:
Lis1-5A:
d.
No Lis1
300 nM Lis1
300 nM Lis1-5A
e.
Lis1ΔN

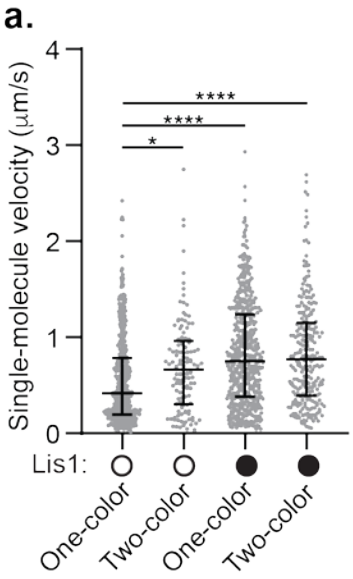

Supplementary Data Figure 2.3. Quantification of the velocity of one-color and two-color activated dynein complexes in the presence or absence of Lis1. a. Single-molecule velocity of dynein/ dynactin/ BicD2-S complexes in the absence (white circles) or presence (black circles) of 300 nM Lis1 with colocalized dynein (two color) or without observed colocalization (one color). The median and interquartile range are shown.

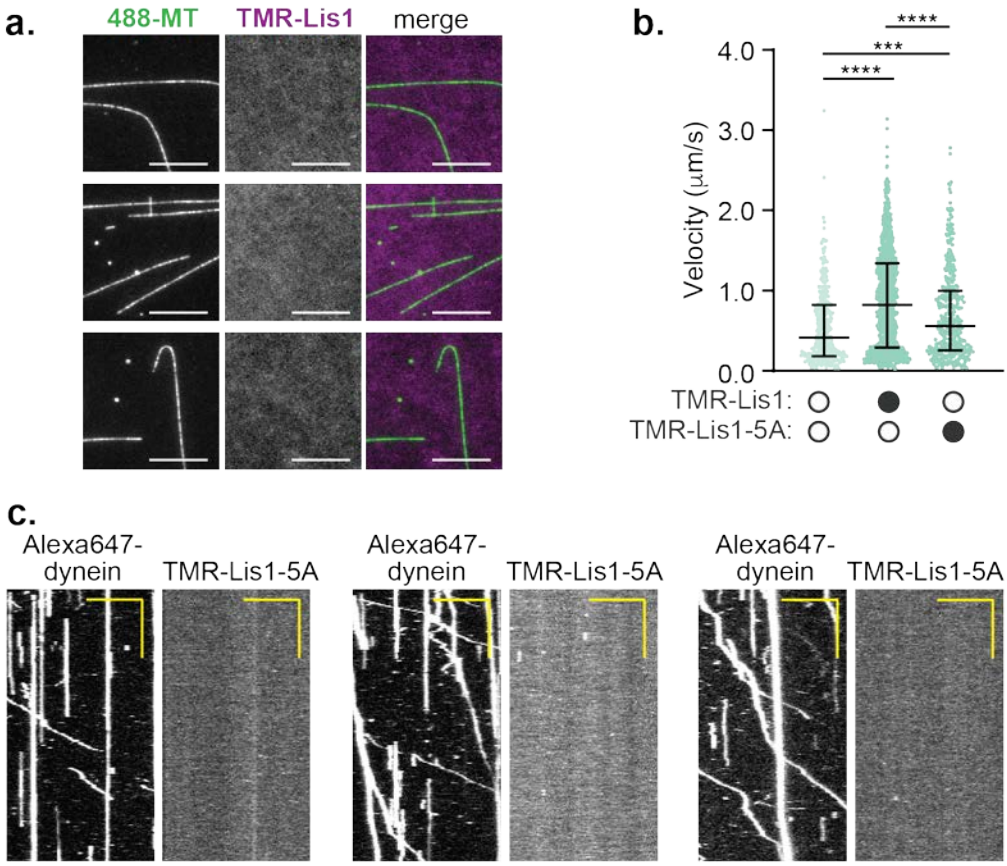

Supplementary Data Figure 2.4. Characterization of Lis1 binding to microtubules and activated dynein complexes. a. Example microscopy images for imaging 50 nM TMR-Lis1 (magenta in merge) in the presence of microtubules (green in merge). Lis1 does not colocalize with microtubules. Scale bars are 10 μm. The experiment was repeated in triplicate yielding similar results. **b.** Single-molecule velocity of dynein/ dynactin/ BicD2-S complexes in the absence (white circles) or presence (black circles) of 50 nM TMR-Lis1 or TMR-Lis1-5A. The median and interquartile range are shown. **c.** Representative kymographs of Alexa647-dynein/ dynactin/ BicD2-S complexes in the presence of 50 nM TMR-Lis1-5A. Scale bars are 10 μm (x) and 20 sec (y).

2.8 References

1. Raaijmakers, J. A. & Medema, R. H. Function and regulation of dynein in mitotic chromosome segregation. *Chromosoma* **123,** 407–422 (2014).

2. Reck-Peterson, S. L., Redwine, W. B., Vale, R. D. & Carter, A. P. The cytoplasmic dynein transport machinery and its many cargoes. *Nature Reviews Molecular Cell Biology* **19,** 1–17 (2018).

3. Schlager, M. A., Hoang, H. T., Urnavicius, L., Bullock, S. L. & Carter, A. P. In vitro reconstitution of a highly processive recombinant human dynein complex. *EMBO J* **33,** 1855–1868 (2014).

4. Mckenney, R. J., Huynh, W., Tanenbaum, M. E., Bhabha, G. & Vale, R. D. Activation of cytoplasmic dynein motility by dynactin-cargo adapter complexes. *Science* **345,** 337–341 (2014).

5. Urnavicius, L., Lau, C. K., Elshenawy, M. M., Morales-Rios, E., Motz, C., Yildiz, A. & Carter, A. P. Cryo-EM shows how dynactin recruits two dyneins for faster movement. bioRxiv (2017).

6. Grotjahn, D. A., Chowdhury, S., Xu, Y., McKenney, R. J., Schroer, T. A. & Lander, G. C. Cryo-electron tomography reveals that dynactin recruits a team of dyneins for processive motility. Nat. Struct. Mol. Biol. 25, 203–207 (2018).

7. Lipka, J., Kuijpers, M., Jaworski, J. & Hoogenraad, C. C. Mutations in cytoplasmic dynein and its regulators cause malformations of cortical development and neurodegenerative diseases. *Biochem Soc Trans* **41,** 1605–1612 (2013).

8. Olenick, M. A. & Holzbaur, E. L. F. Dynein activators and adaptors at a glance. *J Cell Sci* **132,** jcs227132 (2019).

9. Reck-Peterson, S. L., Yildiz, A., Carter, A. P., Gennerich, A., Zhang, N. & Vale, R. D. Single-Molecule Analysis of Dynein Processivity and Stepping Behavior. Cell 126, 335–348 (2006).

10. Trokter, M., Mücke, N. & Surrey, T. Reconstitution of the human cytoplasmic dynein complex. *Proc Natl Acad Sci USA* **109,** 20895–20900 (2012).

11. Moore, J. K., Stuchell-Brereton, M. D. & Cooper, J. A. Function of dynein in budding yeast: mitotic spindle positioning in a polarized cell. *Cell Motil Cytoskeleton* **66,** 546–555 (2009).

12. Zhang, K., Foster, H. E., Rondelet, A., Lacey, S. E., Bahi-Buisson, N., Bird, A. W. & Carter, A. P. Cryo-EM Reveals How Human Cytoplasmic Dynein Is Auto-inhibited and Activated. Cell 169, 1303-1314.e18 (2017).

13. Torisawa, T., Ichikawa, M., Furuta, A., Saito, K., Oiwa, K., Kojima, H., Toyoshima, Y. Y. & Furuta, K. Autoinhibition and cooperative activation mechanisms of cytoplasmic dynein. Nat. Cell Biol. 16, 1118–1124 (2014).

14. Geiser, J.R., Schott, E.J., Kingsbury, T.J., Cole, N.B., Totis, L.J., Bhattacharyya, G., He, L. and Hoyt, M.A. Saccharomyces cerevisiae genes required in the absence of the CIN8-encoded spindle motor act in functionally diverse mitotic pathways. *Mol Biol Cell* **8,** 1035–1050 (1997).

15. Xiang, X., Osmani, A. H., Osmani, S. A., Xin, M. & Morris, N. R. NudF, a nuclear migration gene in *Aspergillus nidulans*, is similar to the human LIS-1 gene required for neuronal migration. *Mol Biol Cell* **6,** 297–310 (1995).

16. Liu, Z., Xie, T. & Steward, R. Lis1, the Drosophila homolog of a human lissencephaly disease gene, is required for germline cell division and oocyte differentiation. *Development* **126,** 4477–4488 (1999).

17. Lam, C., Vergnolle, M. A. S., Thorpe, L., Woodman, P. G. & Allan, V. J. Functional interplay between LIS1, NDE1 and NDEL1 in dynein-dependent organelle positioning. *J Cell Sci* **123,** 202–212 (2010).

18. Splinter, D., Razafsky, D.S., Schlager, M.A., Serra-Marques, A., Grigoriev, I., Demmers, J., Keijzer, N., Jiang, K., Poser, I., Hyman, A.A. and Hoogenraad, C.C. BICD2, dynactin, and LIS1 cooperate in regulating dynein recruitment to cellular structures. *Mol Biol Cell* **23,** 4226–4241 (2012).

19. Lenz, J. H., Schuchardt, I., Straube, A. & Steinberg, G. A dynein loading zone for retrograde endosome motility at microtubule plus-ends. *EMBO J* **25,** 2275–2286 (2006).

20. Moughamian, A. J., Osborn, G. E., Lazarus, J. E., Maday, S. & Holzbaur, E. L. F. Ordered Recruitment of Dynactin to the Microtubule Plus-End is Required for Efficient Initiation of Retrograde Axonal Transport. *Journal of Neuroscience* **33,** 13190–13203 (2013).

21. Lee, W.-L., Oberle, J. R. & Cooper, J. A. The role of the lissencephaly protein Pac1 during nuclear migration in budding yeast. *J Cell Biol* **160,** 355–364 (2003).

22. Tsai, J.-W., Chen, Y., Kriegstein, A. R. & Vallee, R. B. LIS1 RNA interference blocks neural stem cell division, morphogenesis, and motility at multiple stages. *J Cell Biol* **170,** 935–945 (2005).

23. Tanaka, T., Serneo, F.F., Higgins, C., Gambello, M.J., Wynshaw-Boris, A. and Gleeson, J.G. Lis1 and doublecortin function with dynein to mediate coupling of the nucleus to the centrosome in neuronal migration. *J Cell Biol* **165,** 709–721 (2004).

24. Dix, C.I., Soundararajan, H.C., Dzhindzhev, N.S., Begum, F., Suter, B., Ohkura, H., Stephens, E. and Bullock, S.L. Lissencephaly-1 promotes the recruitment of dynein and dynactin to transported mRNAs. *J Cell Biol* **202,** 479–494 (2013).

25. Reiner, O., Carrozzo, R., Shen, Y., Wehnert, M., Faustinella, F., Dobyns, W.B., Caskey, C.T. and Ledbetter, D.H. Isolation of a Miller-Dieker lissencephaly gene containing G protein beta-subunit-like repeats. *Nature* **364,** 717–721 (1993).

26. Kim, M.H., Cooper, D.R., Oleksy, A., Devedjiev, Y., Derewenda, U., Reiner, O., Otlewski, J. and Derewenda, Z.S. The structure of the N-terminal domain of the product of the lissencephaly gene Lis1 and its functional implications. *Structure* **12,** 987–998 (2004).

27. Tarricone, C., Perrina, F., Monzani, S., Massimiliano, L., Kim, M.H., Derewenda, Z.S., Knapp, S., Tsai, L.H. and Musacchio, A. Coupling PAF signaling to dynein regulation: structure of LIS1 in complex with PAF-acetylhydrolase. *Neuron* **44,** 809–821 (2004).

28. Toropova, K., Zou, S., Roberts, A.J., Redwine, W.B., Goodman, B.S., Reck-Peterson, S.L. and Leschziner, A.E. Lis1 regulates dynein by sterically blocking its mechanochemical cycle. *Elife* **3,** e03372 (2014).

29. Huang, J. J., Roberts, A. J. A., Leschziner, A. E. A. & Reck-Peterson, S. L. S. Lis1 acts as a 'clutch' between the ATPase and microtubule-binding domains of the dynein motor. **150,** 975–986 (2012).

30. DeSantis, M.E., Cianfrocco, M.A., Htet, Z.M., Tran, P.T., Reck-Peterson, S.L. and Leschziner, A.E. Lis1 Has Two Opposing Modes of Regulating Cytoplasmic Dynein. *Cell* **170,** 1197–1208 (2017).

31. Yamada, M., Toba, S., Yoshida, Y., Haratani, K., Mori, D., Yano, Y., Mimori-Kiyosue, Y., Nakamura, T., Itoh, K., Fushiki, S. and Setou, M. LIS1 and NDEL1 coordinate the plus-end-directed transport of cytoplasmic dynein. *EMBO J* **27,** 2471–2483 (2008).

32. Mckenney, R. J., Vershinin, M., Kunwar, A., Vallee, R. B. & Gross, S. P. LIS1 and NudE induce a persistent dynein force-producing state. **141,** 304–314 (2010).

33. Baumbach, J., Murthy, A., McClintock, M.A., Dix, C.I., Zalyte, R., Hoang, H.T. and Bullock, S.L. Lissencephaly-1 is a context-dependent regulator of the human dynein complex. *Elife* **6,** e21768 (2017).

34. Gutierrez, P. A., Ackermann, B. E., Vershinin, M. & Mckenney, R. J. Differential effects of the dynein-regulatory factor Lissencephaly-1 on processive dynein-dynactin motility. *J Biol Chem* **292,** 12245–12255 (2017).

35. Redwine, W.B., DeSantis, M.E., Hollyer, I., Htet, Z.M., Tran, P.T., Swanson, S.K., Florens, L., Washburn, M.P. and Reck-Peterson, S.L. The human cytoplasmic dynein interactome reveals novel activators of motility. *Elife* **6,** e28257 (2017).

36. Hoogenraad, C.C., Akhmanova, A., Howell, S.A., Dortland, B.R., De Zeeuw, C.I., Willemsen, R., Visser, P., Grosveld, F. and Galjart, N. Mammalian Golgi-associated Bicaudal-D2 functions in the dynein-dynactin pathway by interacting with these complexes. *EMBO J* **20,** 4041–4054 (2001).

37. Hoogenraad, C.C., Wulf, P., Schiefermeier, N., Stepanova, T., Galjart, N., Small, J.V., Grosveld, F., de Zeeuw, C.I. and Akhmanova, A. Bicaudal D induces selective dynein-mediated microtubule minus end-directed transport. *EMBO J* **22,** 6004–6015 (2003).

38. orisawa, T., Nakayama, A., Furuta, K.Y., Yamada, M., Hirotsune, S. and Toyoshima, Y.Y. Functional dissection of LIS1 and NDEL1 towards understanding the molecular mechanisms of cytoplasmic dynein regulation. *J Biol Chem* **286,** 1959–1965 (2011).

39. Wang, S., Ketcham, S.A., Schön, A., Goodman, B., Wang, Y., Yates III, J., Freire, E., Schroer, T.A. and Zheng, Y. Nudel/NudE and Lis1 promote dynein and dynactin interaction in the context of spindle morphogenesis. *Mol Biol Cell* **24,** 3522–3533 (2013).

40. Kapitein, L.C., Schlager, M.A., Van der Zwan, W.A., Wulf, P.S., Keijzer, N. and Hoogenraad, C.C. Probing Intracellular Motor Protein Activity Using an Inducible Cargo Trafficking Assay. *Biophys J* **99,** 2143–2152 (2010).

41. Tai, C.-Y., Dujardin, D. L., Faulkner, N. E. & Vallee, R. B. Role of dynein, dynactin, and CLIP-170 interactions in LIS1 kinetochore function. *J Cell Biol* **156,** 959–968 (2002).

42. Sasaki, S., Shionoya, A., Ishida, M., Gambello, M.J., Yingling, J., Wynshaw-Boris, A. and Hirotsune, S. A LIS1/NUDEL/cytoplasmic dynein heavy chain complex in the developing and adult nervous system. *Neuron* **28,** 681–696 (2000).

43. Schmidt, H. & Carter, A. P. Review: Structure and mechanism of the dynein motor ATPase. *Biopolymers* **105,** 557–567 (2016).

44. Schmidt, H., Zalyte, R., Urnavicius, L. & Carter, A. P. Structure of human cytoplasmic dynein-2 primed for its power stroke. *Nature* **518,** 435–438 (2015).

45. Elshenawy, M.M., Kusakci, E., Volz, S., Baumbach, J., Bullock, S.L. and Yildiz, A. Lis1 activates dynein motility by pairing it with dynactin. *bioRxiv* 10.1101/685826 (2019).

46. Qiu, R., Zhang, J. & Xiang, X. LIS1 regulates cargo-adapter-mediated activation of dynein by overcoming its autoinhibition in vivo. *J Cell Biol* **218,** 3630–3646 (2019).

47. Marzo, M. G., Griswold, J. M. & Markus, S. M. Pac1/LIS1 promotes an uninhibited conformation of dynein that coordinates its localization and activity. *bioRxiv* 10.1101/684290 (2019).

48. Sheeman, B., Carvalho, P., Sagot, I., Geiser, J., Kho, D., Hoyt, M.A. and Pellman, D. Determinants of S. cerevisiae dynein localization and activation: implications for the mechanism of spindle positioning. *Curr Biol* **13,** 364–372 (2003).

49. Egan, M. J., Tan, K. & Reck-Peterson, S. L. Lis1 is an initiation factor for dynein-driven organelle transport. *J Cell Biol* **197,** 971–982 (2012).

50. Case, R. B., Pierce, D. W., Hom-Booher, N., Hart, C. L. & Vale, R. D. The directional preference of kinesin motors is specified by an element outside of the motor catalytic domain. *Cell* **90,** 959–966 (1997).

51. Roberts, A. J., Goodman, B. S. & Reck-Peterson, S. L. Reconstitution of dynein transport to the microtubule plus end by kinesin. *Elife* **3,** e02641 (2014).

52. Scheres, S. H. W. RELION: implementation of a Bayesian approach to cryo-EM structure determination. *J Struct Biol* **180,** 519–530 (2012).

53. Lander, G.C., Stagg, S.M., Voss, N.R., Cheng, A., Fellmann, D., Pulokas, J., Yoshioka, C., Irving, C., Mulder, A., Lau, P.W. and Lyumkis, D. Appion: an integrated, database-driven pipeline to facilitate EM image processing. *J Struct Biol* **166,** 95–102 (2009).

54. Zheng, S.Q., Palovcak, E., Armache, J.P., Verba, K.A., Cheng, Y. and Agard, D.A. MotionCor2: anisotropic correction of beam-induced motion for improved cryo-electron microscopy. *Nat Meth* **14,** 331–332 (2017).

55. Voss, N. R., Yoshioka, C. K., Radermacher, M., Potter, C. S. & Carragher, B. DoG Picker and TiltPicker: software tools to facilitate particle selection in single particle electron microscopy. *J Struct Biol* **166,** 205–213 (2009).

56. Zivanov, J., Nakane, T., Forsberg, B.O., Kimanius, D., Hagen, W.J., Lindahl, E. and Scheres, S.H. New tools for automated high-resolution cryo-EM structure determination in RELION-3. *Elife* **7,** e42166 (2018).

57. Punjani, A., Rubinstein, J. L., Fleet, D. J. & Brubaker, M. A. cryoSPARC: algorithms for rapid unsupervised cryo-EM structure determination. *Nat Meth* **14,** 290–296 (2017).

Chapter 3:

Structural Basis for Cytoplasmic Dynein-1 Regulation by Lis1

3.1 Introduction

Cytoplasmic dynein-1 (dynein) is a microtubule (MT)-based motor responsible for minus-end-directed transport. In humans and other eukaryotes dynein drives the movement of hundreds of different cargos, including endosomes, peroxisomes, mitochondria, and other membrane-bound compartments[1]. In addition, dynein positions nuclei and centrosomes and has a role in organizing the mitotic spindle and in the spindle assembly checkpoint[1]. Mutations in dynein and its regulatory machinery cause a range of neurological diseases[2].

In *S. cerevisiae* dynein has a single non-essential role in positioning the mitotic spindle, but the major dynein regulators are conserved, making it a valuable model to study dynein regulation[3]. Dynein anchored at the cell cortex pulls on microtubules attached to the spindle pole body (SPB), thereby aligning the mitotic spindle[18]. Dynein reaches the cortex by localizing to MT plus ends, either via kinesin-dependent transport or recruitment from the cytosol[19–21]. Deletion of any of the genes encoding the dynein subunits, dynactin subunits, Lis1 or NudE, all of which are conserved in yeast, results in defects in positioning the mitotic spindle. This ultimately results in some cells inheriting multiple nuclei after cell division.

Lis1 was first discovered as the primary gene mutated in type-1 lissencephaly, a neurodevelopmental disorder that results in a smooth cerebral surface and abnormal neuronal migration[4]. Lis1 consists of two β-propellers dimerized by a LisH domain[5,6]. It binds dynein at two sites, one site at AAA3/AAA4

(site$_{ring}$) and one on the dynein stalk (site$_{stalk}$)[7–9]. These sites can be bound simultaneously and the two Lis1 β-propellers likely interact with one another, although this has not been confirmed due to resolution constraints in previous structures[9].

Lis1 is the only known dynein regulator to bind directly to the motor domain, and it is therefore important to consider Lis1's regulation of dynein's mechanochemical cycle. Lis1 has been shown to have two modes of regulating dynein. The first is to induce a high microtubule binding affinity of dynein, which has been seen in organisms ranging from yeast to humans[7,10–14]. This state correlates with Lis1 bound only at site$_{ring}$[7,9]. In *S. cerevisiae* mutations at site$_{ring}$ result in an increase in cells that inherit multiple nuclei similar to deletion of Lis1[7].

The second mode of regulation occurs when Lis1 is bound to site$_{stalk}$ as well as site$_{ring}$, and results in a low microtubule affinity conformation of dynein. This regulation depends on the nucleotide state in dynein's AAA3. Using cryo-electron microscopy (cryo-EM), Lis1 bound to dynein's site$_{stalk}$ was observed when AAA3 was bound to ATP or ADP.Pi[9]. In *S. cerevisiae* mutating site$_{stalk}$ results in mislocalization of dynein[9].

Here, we use a combination of cryo-EM, single-molecule microscopy, *in vitro* reconstitution and *in vivo* assays to elucidate the mechanisms of the two modes of Lis1 regulation. Our previous structures were not of high enough resolution to unambiguously determine the orientation of the Lis1 β-propeller. With our new high-resolution structure, we set out to disrupt all of the observed dynein-

Lis1 interactions, as well as the interface between the two Lis1 β-propellers, and then determine the effects on dynein's mechanochemistry and function *in vivo* in *S. cerevisiae*.

3.2 A 3.1Å structure of a dynein-Lis1 complex

Previously, we determined structures of *S. cerevisiae* dynein motor domains bound to Lis1 at 7.7Å – 10.5Å resolution[9]. Here, we aimed to improve the overall resolution of the dynein-Lis1 complex. To limit conformational heterogeneity by capturing dynein with both Lis1 sites occupied we used a construct of the dynein motor domain containing a Walker B mutation in AAA3 that prevents the hydrolysis of ATP[9]. However, dynein's strong preferred orientation in open-hole cryo-EM grids limited our initial attempts at obtaining a higher resolution structure. To overcome this, we randomly biotinylated dynein and applied the sample to streptavidin affinity grids, which results in randomly oriented dynein complexes[15]. This allowed us to determine the structure of dynein bound to Lis1 in the presence of ATP vanadate (ATP-Vi) using cryo-EM to a nominal resolution of 3.1 Å (Figure 3.1A, B, C). Our high-resolution map revealed dynein in the closed ring state bound to two Lis1s, and allowed us to unambiguously assign the correct placement and orientation of both Lis1 β-propellers at site$_{ring}$ and site$_{stalk}$. Binding of Lis1 at site$_{ring}$ primarily involves the smaller face of the β-propeller in Lis1 and the alpha helix bridging AAA3 and AAA4 in dynein. Our previous lower resolution structures identified a contact between Lis1 and AAA5, but due to the limited

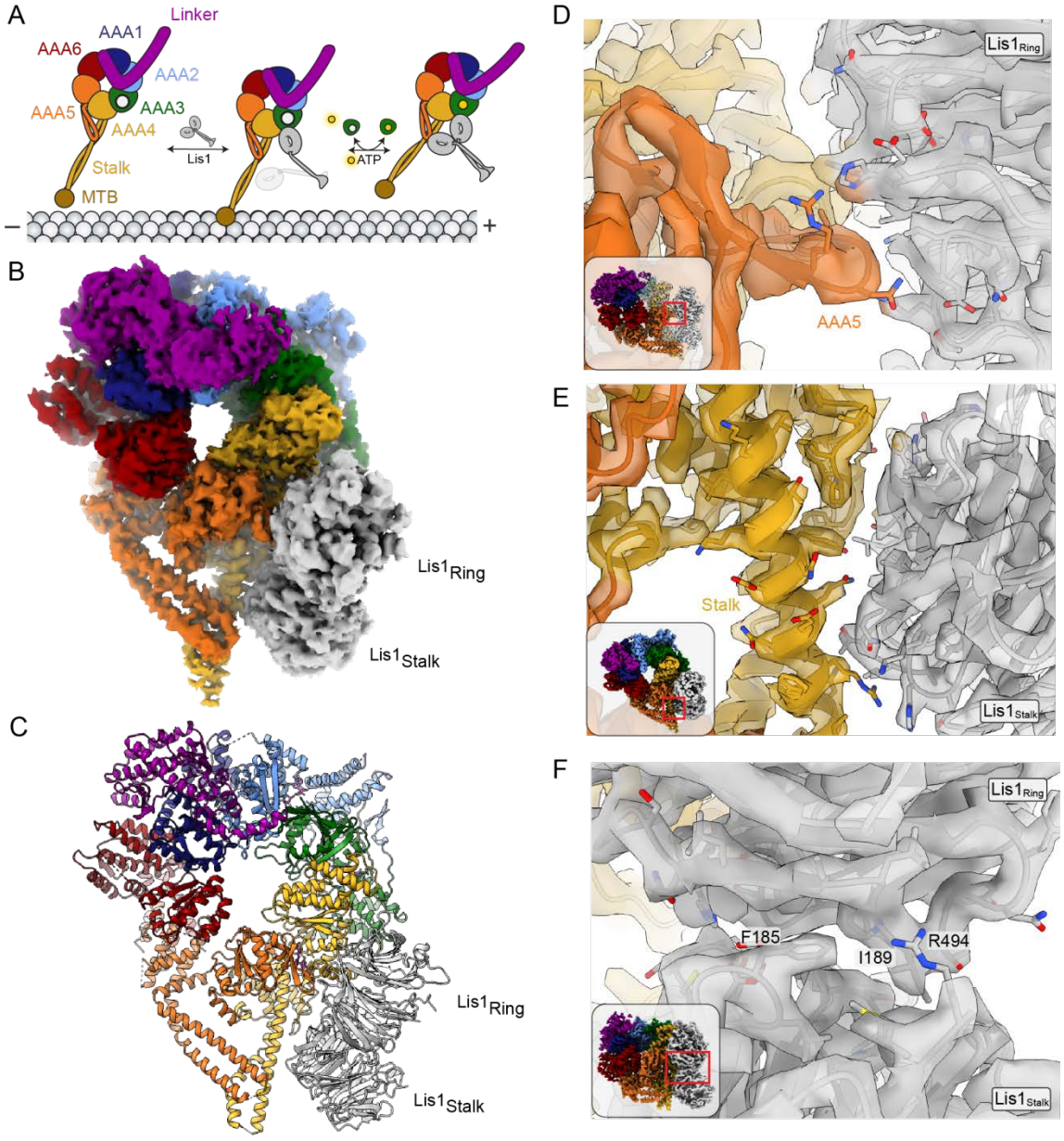

Figure 3.1. 3.1Å structure of a dynein-Lis1 complex A. Cartoon model of the two modes of dynein regulation by Lis1. B. EM density of Lis1 bound to dynein. C. Model of Lis1 bound to dynein. D. The interaction between $Lis1_{ring}$ and dynein's AAA5. E. Interaction between $Lis1_{stalk}$ and dynein's stalk and AAA4. F. Interaction between $Lis1_{ring}$ and $Lis1_{stalk}$.

resolution of these structures we could not unambiguously determine the nature of the contact[9]. Our new structure unambiguously revealed an additional contact site between $Lis1_{ring}$ and a loop in AAA5 (Figure 3.1D). Our structure also revealed an interaction between $Lis1_{stalk}$ and a loop in AAA4 (Figure 3.1E), in addition to the interaction with dynein's stalk helices that we observed previously[9]. The $Lis1_{ring}$-$Lis1_{stalk}$ β-propellers are also in close proximity. For the first time we are able to observe the interface between the two, which is mediated by hydrophobic interactions. Based on the proximity of the β-propellers in our structure and our inability to identify any additional density coming from a second Lis1 dimer, our data is most compatible with the two β-propellers coming from the same Lis1 dimer.

3.3 Lis1's interaction with dynein AAA5 contributes to regulation at $site_{ring}$

The dynein-Lis1 interface at $site_{ring}$ is mostly mediated through a helix bridging AAA3 and AAA4 of dynein, mutations in which completely abrogate Lis1 binding to dynein[7]. Here we set out to determine if the additional contact we observed between Lis1 and dynein at AAA5 also contributed to dynein regulation by Lis1 at $site_{ring}$. To disrupt this electrostatic interaction (Figure 3.2A), we made mutations in the endogenous copies of either Lis1 (*PAC1*) or dynein (*DYN1*). We mutated Lis1's glutamic acid 253 and histidine 254 to alanine and deleted dynein's asparagine 3475 and arginine 3476, which were both present in a short loop. To determine if these mutations had a phenotype *in vivo*, we performed

Figure 3.2 Lis1's interaction with dynein AAA5 contributes to regulation at site$_{ring}$ A. Close-up view of the interface between Lis1 and dynein AAA5 at site$_{ring}$. The residues mutated to inhibit this interaction on Lis1 (gray) and dynein (orange) are indicated. The inset shows the location of the close up in the full structure. B. Example images of normal and binucleate cells in wild type and Lis1 depleted strains. C. Determination of the percentage of cells displaying an aberrant binucleate phenotype for WT (medium grey), Lis1 deletion (light grey) and Lis1$^{E253A, H254A}$ (dark grey). n=3 replicates of at least 200 cells each per condition. D. Determination of the binding affinity of dynein^{WT} for Lis1^{WT} (light grey; K_d = 113.1 ± 9.0) and Lis1$^{E253A, H254A}$ (dark grey; K_d = 195.1 ± 16.0) and dynein$^{\Delta N3475, R3476}$ for Lis1^{WT} (orange; K_d = 200.7 ± 12.5) and Lis1$^{E253A, H254A}$ (brown; K_d = 205.0 ± 12.9). n = 3 replicates per condition. Statistical analysis was performed using an extra sum-of-squares F test; ***, p<0.0001. E. Binding density (mean ± s.e.m.) of dynein on microtubules with ATP in the absence (light grey) or presence of Lis1^{WT} (medium grey) or Lis1$^{E253A, H254A}$ (dark grey). Data was normalized to a density of 1.0 in the absence of Lis1. Statistical analysis was performed using an ANOVA; ****, p<0.0001; **, p = 0.0029. n = 12 replicates per condition. F. Binding density (mean ± s.e.m.) of dynein on microtubules with ATP-Vi in the absence (light grey) or presence of Lis1^{WT} (medium grey) or Lis1$^{E253A, H254A}$ (dark grey). Data was normalized to a density of 1.0 in the absence of Lis1. Statistical analysis was performed using an ANOVA; ****, p<0.0001; ***, p = 0.0001; ns = 0.9997. n = 12 replicates per condition. G. Single-molecule velocity of dynein with increasing concentrations of Lis1. Dynein^{WT} with Lis1^{WT} (light grey); Dynein^{WT} with Lis1$^{E253A, H254A}$ (dark grey); dynein$^{\Delta N3475, R3476}$ with Lis1^{WT} (orange); dynein$^{\Delta N3475, R3476}$ and Lis1$^{E253A, H254A}$ (brown).The median and interquartile range are shown. Data was normalized to a velocity of 1.0 in the absence of Lis1. At least 400 single molecule events were measured per condition.

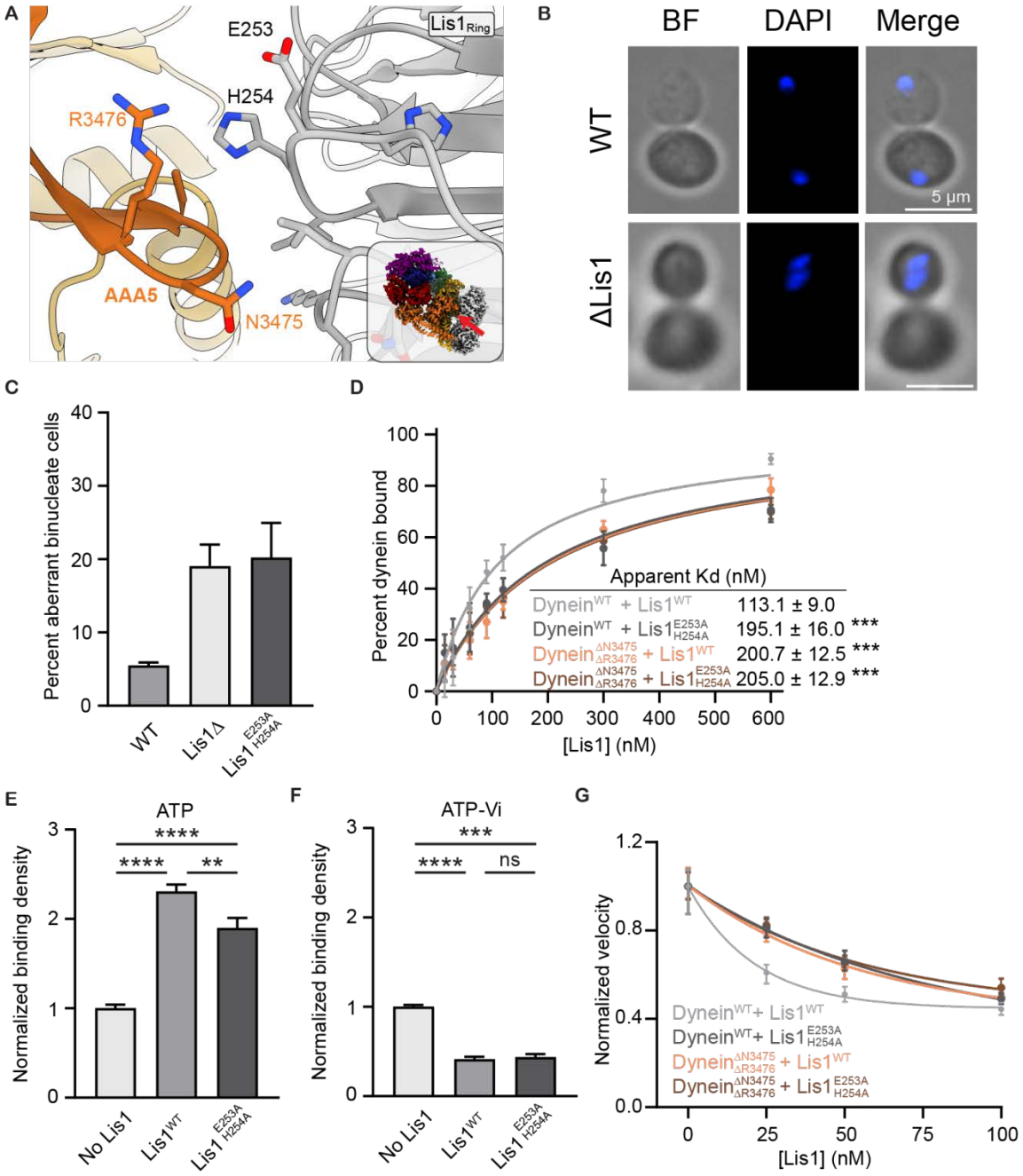
A
E253
Lis1 Ring
H254
R3476
AAA5
N3475
B
BF
DAPI
Merge
WT
ΔLis1
5 μm
C
Percent aberrant binucleate cells
WT
Lis1Δ
Lis1 E253A H254A
D
Percent dynein bound
[Lis1] (nM)
Apparent Kd (nM)
Dynein WT + Lis1 WT 113.1 ± 9.0
Dynein WT + Lis1 E253A H254A 195.1 ± 16.0 ***
Dynein ΔN3475 ΔR3476 + Lis1 WT 200.7 ± 12.5 ***
Dynein ΔN3475 ΔR3476 + Lis1 E253A H254A 205.0 ± 12.9 ***
E
ATP
Normalized binding density
No Lis1
Lis1 WT
Lis1 E253A H254A
F
ATP-Vi
ns
G
Normalized velocity
[Lis1] (nM)
Dynein WT + Lis1 WT
Dynein WT + Lis1 E253A H254A
Dynein ΔN3475 ΔR3476 + Lis1 WT
Dynein ΔN3475 ΔR3476 + Lis1 E253A H254A

nuclear segregation assays. In this assay, deletion of dynein subunits or Lis1 leads to an increase in binucleate mother cells, which arise from defects in mitotic spindle positioning. We found that Lis1$^{E253A, H254A}$ exhibits a binucleate phenotype that is equivalent to Lis1 deletion (Figure 3.2B, C), suggesting that the interaction between Lis1 and dynein at AAA5 is required for Lis1's ability to regulate dynein *in vivo*.

We next wanted to biochemically define the role of Lis1's interaction with AAA5. First, we measured the apparent binding affinity between purified Lis1 dimers and monomeric dynein motor domains. We captured SNAP-tagged Lis1 on magnetic beads and then determined the percentage of dynein bound. We found that Lis1$^{E253A, H254A}$ showed decreased binding to wild type dynein monomers and that wild type Lis1 showed decreased binding to dynein$^{\Delta N3475, R3476}$ monomers (Figure 3.2D). Next, we examined the ability of dynein to bind to microtubules in a single-molecule microtubule binding assay in the presence of ATP or ATP-Vi[9]. Previously, we showed that tight microtubule binding of dynein in the presence of ATP is mediated by site$_{ring}$, whereas Lis1-induced weak microtubule binding in the presence of ATP-Vi requires both site$_{ring}$ and site$_{stalk}$[9]. The dynein construct we used for this experiment is a well-characterized truncated and GST-dimerized dynein motor that behaves similarly to full-length dynein *in vitro*[16] ("dynein" here).We found that dynein shows a statistically significant decrease in microtubule binding in the presence of Lis1$^{E253A, H254A}$ compared to wild type Lis1 in the presence of ATP and is indistinguishable from wild type Lis1 in the presence of

ATP-Vi (Figure 3.2E and F). Finally, we measured the single-molecule velocity of dynein in the context of Lis1$^{E253A,\ H254A}$ and dynein$^{\Delta N3475,\ R3476}$. In this assay Lis1 slows the motility of dynein in a dose-dependent manner[7]. In the absence of Lis1, dynein$^{\Delta N3475,\ R3476}$ had a similar velocity to wild type dynein (Supplementary Data Figure 3.1). However, dynein$^{\Delta N3475,\ R3476}$ was less sensitive to the addition of Lis1 compared to wild type dynein. Similarly, wild type dynein was less sensitive to the addition of Lis1$^{E253A,\ H254A}$ compared to wild type Lis1 (Figure 3.2G). Thus, the interaction of Lis1 with dynein at AAA5 contributes to Lis1's regulation of dynein at site$_{ring}$.

3.4 Identification of Lis1 mutations that specifically disrupt regulation at site$_{stalk}$

In addition to revealing the molecular nature of Lis1's interaction with dynein at site$_{ring}$, our structure also allowed us to probe the interaction of Lis1 at site$_{stalk}$. Previously, we identified three amino acids in dynein' stalk domain (E3012, Q3014, and N3018) that were required for Lis1-mediated weak microtubule binding of dynein[9]. Our new structure reveals that the interaction between Lis1 and dynein at site$_{stalk}$ also includes a contact between Lis1 and a short loop in AAA4 of dynein. To determine if this contact plays a role in dynein regulation by Lis1, we mutated serine 248 in the endogenous copy of Lis1 to glutamine to introduce a steric clash with the loop in dynein's AAA4 (Figure 3.3A). In a nuclear segregation assay Lis1^{S248Q} had significantly more aberrant binucleate cells compared to a strain

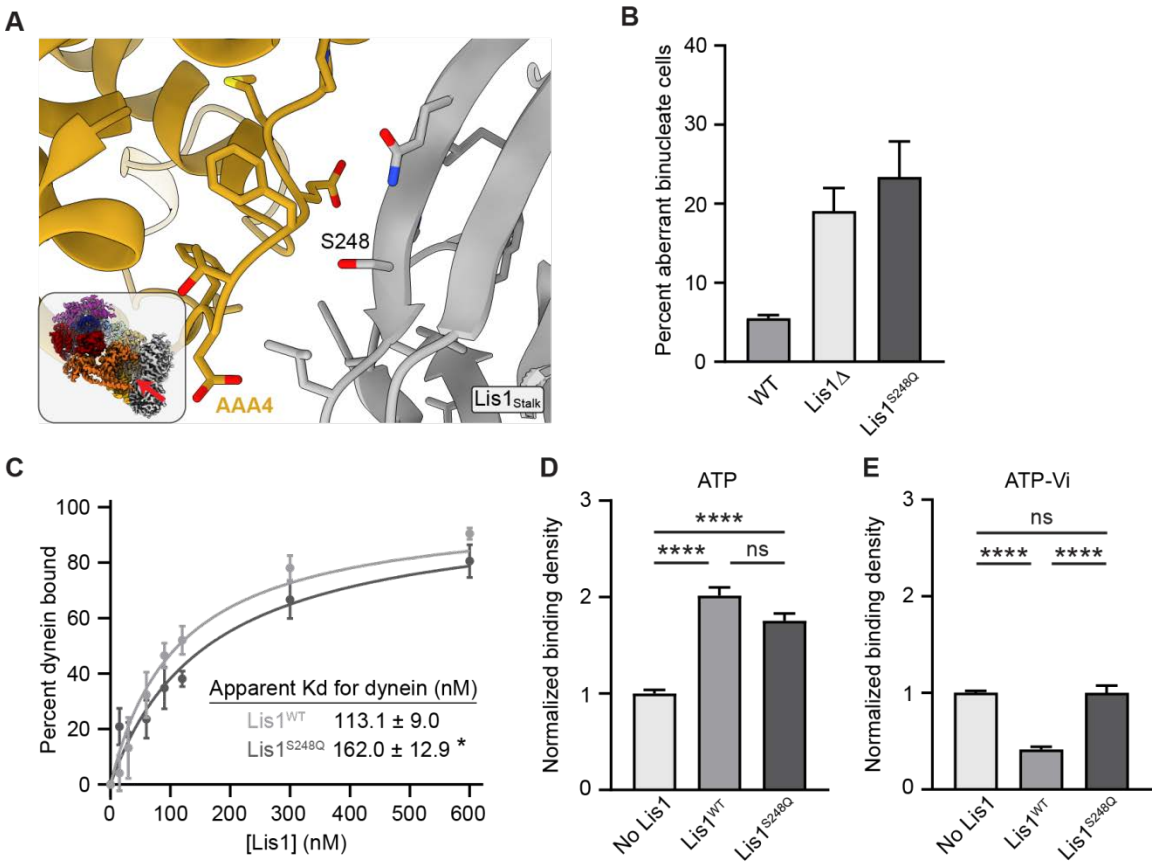

Figure 3.3 Identification of Lis1 mutations that specifically disrupt regulation at site$_{stalk}$ A. Close-up view of the Lis1-dynein interface at site$_{stalk}$. The residue mutated to inhibit Lis1 binding is indicated. The inset shows the location of the close up in the full structure. B. Determination of the percentage of cells displaying an aberrant binucleate phenotype for WT (medium grey), Lis1 deletion (light grey) and Lis1^{S248Q} (dark grey). n=3 replicates of at least 200 cells each per condition. C. Determination of the binding affinity of dynein for Lis1^{WT} (light grey; K_d = 113.1 ± 9.0) and Lis1^{S248Q} (dark grey; K_d = 162.0 ± 12.9). n = 3 replicates per condition. Statistical analysis was performed using an extra sum-of-squares F test; p = 0.0022. D. Binding density (mean ± s.e.m.) of dynein on microtubules with ATP in the absence (light grey) or presence of Lis1^{WT} (medium grey) or Lis1^{S248Q} (dark grey). Data was normalized to a density of 1.0 in the absence of Lis1. Statistical analysis was performed using an ANOVA; ****, p<0.0001; ns, p = 0.0614. n = 12 replicates per condition. E. Binding density (mean ± s.e.m.) of dynein on microtubules with ATP-Vi in the absence (light grey) or presence of Lis1^{WT} (medium grey) or Lis1^{S248Q} (dark grey). Data was normalized to a density of 1.0 in the absence of Lis1. Statistical analysis was performed using an ANOVA; ****, p<0.0001; ns, p > 0.9999. n = 12 replicates per condition.

expressing wild type Lis1 (Figure 3.3B). Thus, this contact on site$_{stalk}$ between dynein and Lis1 is also required for Lis1's ability to regulate dynein *in vivo*.

We also probed the role of this new contact *in vitro*. We found that Lis1^{S248Q} showed a moderate decrease in binding affinity for dynein monomers. Our previous studies showed that mutations in dynein's site$_{stalk}$ (E3012A, Q3014A, N3018A) abolished the ability of Lis1 to induce the weak microtubule binding state in dynein[9]. This same mutant was still sensitive to Lis1 binding at site$_{ring}$ as tight microtubule binding was observed in the presence of ATP. Here, we found that Lis1^{S248Q} demonstrated tight microtubule binding in the presence of ATP (regulation at site$_{ring}$) (Figure 3.3C) and no weakening of microtubule binding in ATP-Vi (loss of regulation at site$_{stalk}$) (Figure 3.3D). This is similar to dynein$^{E3012A, Q3014A, N3018A}$, although Lis1^{S248Q} did not fully display tight microtubule binding in ATP-Vi. This analysis reveals that Lis1^{S248Q} is the first Lis1 mutant capable of targeting regulation at site$_{stalk}$, making this mutant a valuable tool for dissecting the function of the two modes of Lis1 regulation.

3.5 The interface between the two Lis1 β-propellers is important for regulation at site$_{stalk}$

Our new structure revealed interactions between the two Lis1 β-propellers when they were bound to dynein at both site$_{ring}$ and site$_{stalk}$. Because this interface is largely hydrophobic we aimed to disrupt it by introducing charged residues in Lis1. We mutated Lis1's phenylalanine 185 and isoleucine 189 to aspartic acid.

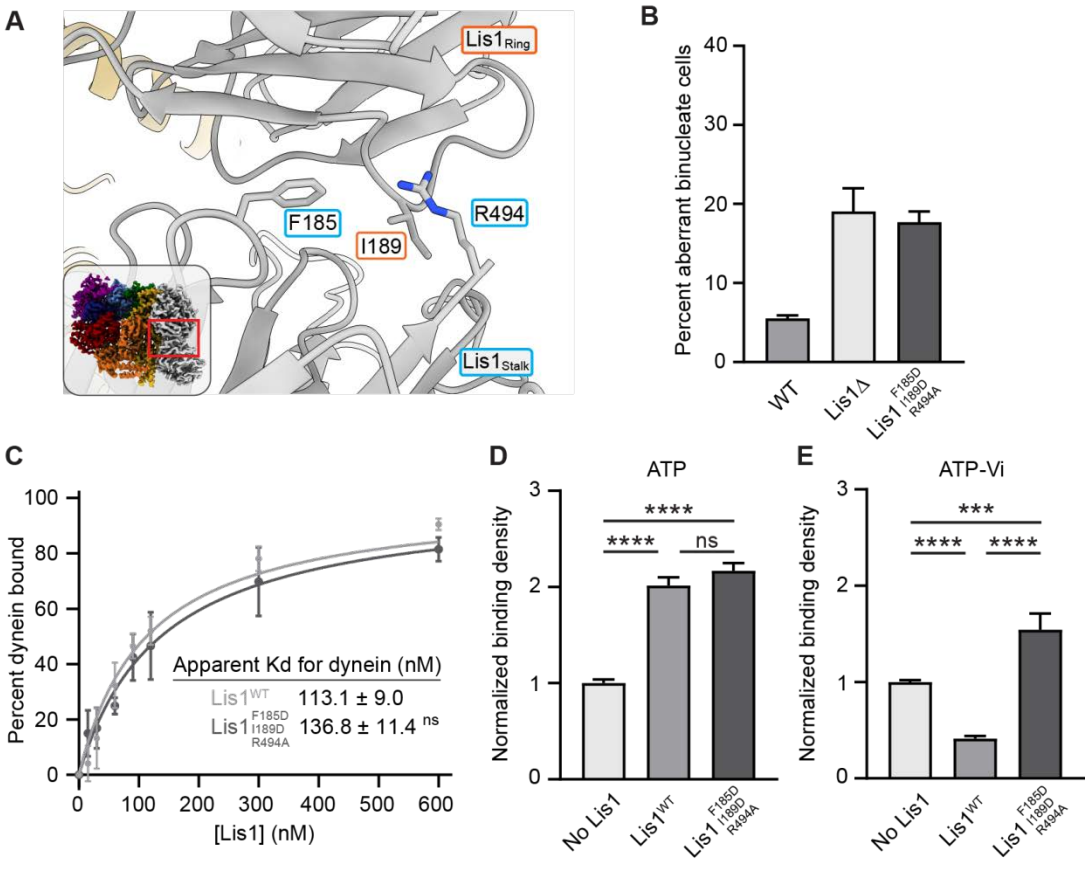

Figure 3.4. The interface between the two Lis1 β-propellers is important for regulation at site$_{stalk}$ A. Close-up view of the interface between the two Lis1 β-propellers. The residues mutated to inhibit this interaction are indicated. The inset shows the location of the close up in the full structure. B. Determination of the percentage of cells displaying an aberrant binucleate phenotype for WT (medium grey), Lis1 deletion (light grey) and Lis1$^{F185D, I189D, R494A}$ (dark grey). n=3 replicates of at least 200 cells each per condition. C. Determination of the binding affinity of dynein for Lis1^{WT} (grey; K_d = 113.1 ± 9.0) and Lis1$^{F185D, I189D, R494A}$ (green; K_d = 136.8 ± 11.4). n = 3 replicates per condition. Statistical analysis was performed using an extra sum-of-squares F test; p = 0.0974. Binding affinity of dynein for Lis1^{WT} repeated from figure 2. D. Binding density (mean ± s.e.m.) of dynein on microtubules with ATP in the absence (light grey) or presence of Lis1^{WT} (medium grey) or Lis1$^{F185D, I189D, R494A}$ (dark grey). Data was normalized to a density of 1.0 in the absence of Lis1. Statistical analysis was performed using an ANOVA; ****, p<0.0001; ns, p = 0.4445. n = 12 replicates per condition. E. Binding density (mean ± s.e.m.) of dynein on microtubules with ATP-Vi in the absence (light grey) or presence of Lis1^{WT} (medium grey) or Lis1$^{F185D, I189D, R494A}$ (dark grey). Data was normalized to a density of 1.0 in the absence of Lis1. Statistical analysis was performed using an ANOVA; ****, p<0.0001; ***, p = 0.0002. n = 12 replicates per condition.

In addition, to avoid the formation of new favorable contacts, we mutated arginine 494 to alanine (Figure 3.4A). In a nuclear segregation assay Lis1$^{F185D,\ I189D,\ R494A}$ had significantly more aberrant binucleate cells compared to a strain expressing wild type Lis1 (Figure 3.4B). Thus, the interaction between Lis1 β-propellers is required for Lis1's ability to regulate dynein *in vivo*. In vitro we found that Lis1$^{F185D,\ I189D,\ R494A}$ shows a very minor reduction in binding affinity for dynein (Figure 3.4C). In microtubule binding assays this mutant behaved similarly to dynein$^{E3012A,\ Q3014A,\ N3018A}$, demonstrating tight microtubule binding in the presence of both ATP (regulation at site$_{ring}$) (Figure 3.4C) and ATP-Vi (loss of regulation at site$_{stalk}$) (Figure 3.4D). This is the first evidence that the interaction between Lis1's β-propellers is important for Lis1's ability to regulate dynein.

3.6 Lis1 regulation is required for dynein localization in *S. cerevisiae*.

To understand how these mutants affect dynein in vivo we looked at dynein localization in dividing cells. In *S. cerevisiae,* dynein positions the mitotic spindle by pulling on SPB-anchored MTs from the cell cortex[18] (Figure 3.5A). Lis1 is required for dynein's localization to SPBs, plus ends and the cortex[9,21–26]. We imaged full length dynein-3xGFP and determined co-localization with the SPB (SPC110-tdTomato) and microtubules (CFP-TUB1) (Figure 3.5B). Deletion of Lis1 causes a significant decrease in dynein puncta at SPBs, plus ends and the cortex (Figure 3.5C-E). Lis1$^{E253A,\ H254A}$ decreases dynein puncta similarly to the deletion at all localizations (Figure 3.5C-E). Lis1$^{F185D,\ I189D,\ R494A}$ and Lis1^{S248Q} both have

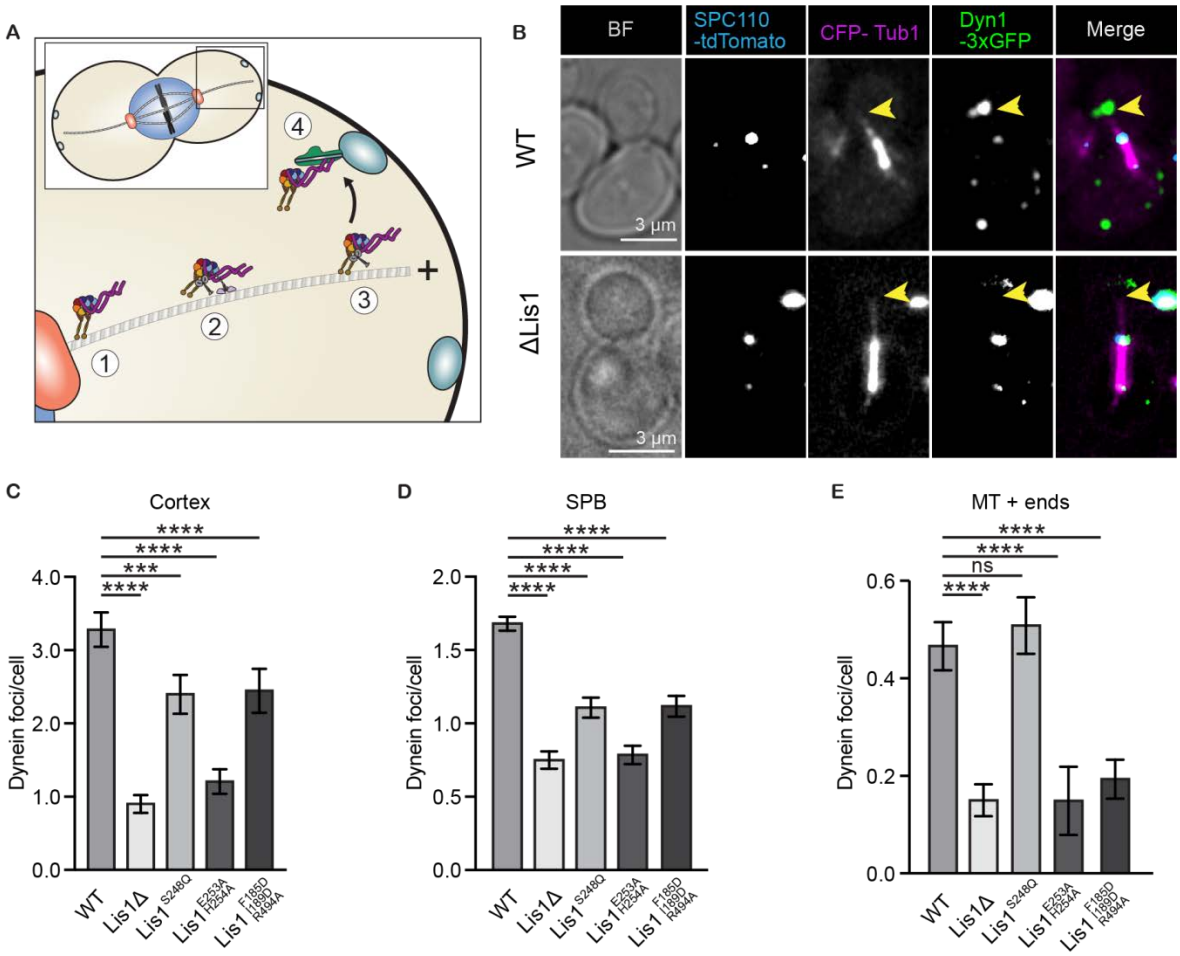

Figure 3.5 Lis1 regulation is required for dynein localization in *S. cerevisiae*. A. Cartoon of dynein and Lis1 during spindle positioning in *S. cerevisiae*. Dynein is localized to the SPB (1), transported to the MT plus end by a kinesin in a Lis1-dependent manner (2), maintained at the MT plus end (3), and off-loaded to the cell cortex (4), where it pulls on SPB-attached MTs to position the mitotic spindle. B. Example images of dynein localization in dividing *S. cerevisiae* cells. Yellow arrowheads point to MT plus tips. (C-E) Quantification of dynein localization. Bar graphs show the average number of dynein foci per cell localized to the cortex (C), SPB (D) and MT plus ends (E) in wild type, Lis1 deletion (ΔLis1), Lis1$^{E253A, H254A}$, Lis1$^{F185D, I189D, R494A}$ and Lis1^{S248Q} strains. Statistical analysis was performed using a Kruskal-Wallis test; ****, p<0.0001; ***, p = 0.0001; ns, p > 0.9999. n = 120 cells per condition.

intermediate phenotypes, significantly decreasing dynein puncta at the cortex and SPBs relative to WT but not to the level of the Lis1 deletion (Figure 3.5C-E). Interestingly while Lis1$^{F185D, I189D, R494A}$ also exhibits a loss of dynein puncta at MT plus ends, Lis1^{S248Q} has a WT amount of dynein puncta at that localization (Figure 3.5E).

3.7 Discussion

Lis1 directly binds to cytoplasmic dynein-1's motor domain and regulates dynein's mechanochemistry and cellular function. Here we solved a 3.1Å structure of Lis1 bound to dynein that revealed novel interactions required for the two modes of dynein regulation. Based on our structure we mutated each of these contacts and determined their role in regulating dynein's mechanochemistry and their *in vivo* role in positioning the mitotic spindle in *S. cerevisiae*. We identified new dynein-Lis1 and Lis1-Lis1 contacts that were required for Lis1's ability to regulate dynein.

We identified a new dynein-Lis1 interaction at site ring that involved dynein's AAA5 domain. We identified mutations in both dynein and Lis1 that abolished regulation via this interaction, showing that this interaction was required for Lis1's ability to increase dynein's microtubule binding affinity. In addition, this interaction was important for dynein regulation by Lis1 *in vivo,* with the mutant resulting in mislocalization of dynein and ultimately an increase in aberrant binucleate cells.

We also identified the molecular nature of interactions between Lis1 and dynein's AAA4 domain, as well as the interaction between the two Lis1 β-propellers. We found that both interactions were required for the Lis1-induced reduction in dynein's microtubule binding affinity. Both sites of interaction were also required for dynein's function *in vivo* in *S. cerevisiae*; they inhibited dynein's ability to reach its site of action on the cell cortex and caused an increase in binucleate cells. Interestingly, Lis1^{S248Q} had a similar amount of dynein puncta at MT plus ends compared to Lis1^{WT}, in contrast to the other mutants. This may indicate that this mutant has a defect in forming dynein complexes at the cortex, similar to the role of Lis1 in forming activated dynein complexes observed *in vitro* with human proteins[13,14].

A recent report hypothesized that Lis1 bound at site$_{ring}$ may slow dynein's velocity due to Lis1 binding to microtubules[17], thereby crosslinking dynein to microtubules via Lis1. This hypothesis requires either 1) one Lis1 β-propeller in a dimer would interact with dynein and the other with the microtubule or 2) a single Lis1 β-propeller would need to interact simultaneously with both dynein and the microtubule. If the first case were true, monomers of Lis1 would be predicted to have no effect on dynein's velocity. To test this, we measured the velocity of dynein in the presence of either dimeric or monomeric Lis1 and found that both Lis1 dimers and monomers could slow dynein motility in a dose-dependent manner (Supplementary Data Figure 3.2A), in agreement with previous studies[7]. Thus, if Lis1 crosslinks dynein to microtubules, it must do so in the context of a

single β-propeller, with one face of Lis1 interacting with dynein and another with microtubules. This model predicts that mutants that disrupt Lis1 binding to dynein would not disrupt Lis1 microtubule binding. To test this, we used a Lis1 mutant where 5 amino acids that face site$_{ring}$ were mutated to alanine (Supplementary Data Figure 3.2B). We previously demonstrated that Lis1^{5A} does not bind to dynein[8]. Using a microtubule co-pelleting assay, we found that Lis1^{5A} also does not bind to microtubules (Supplementary Data Figure 3.2C), suggesting that Lis1 would not be capable of crosslinking dynein to microtubules. This, along with the finding that human Lis1 does not interact with microtubules but does increase dynein's microtubule binding affinity[11,13], suggest it is unlikely that a Lis1-microtubule interaction plays a role in the mechanism of dynein regulation.

Finally, the new sites of interaction between dynein and Lis1 that we identified here and the mutants that we described that disrupts these interactions will be valuable tools for dissecting the multiple modes of dynein regulation by Lis1. How Lis1's mechanochemical regulation of dynein relates to dynein's trafficking roles in other organisms is unclear. The Lis1-induced tight microtubule binding mode of dynein is conserved in humans[10–14], but what role this plays in trafficking is unknown. Lis1 binding at site$_{stalk}$ is also conserved in humans[13], although the effects of this interaction have not been determined *in vitro* or *in vivo*. One possibility is that binding at both sites is required for dynein to form an activated motor complex with dynactin and activating adaptor. The mutants we have

developed can now be used to determine the mechanism of Lis1 regulation in other models of dynein-based cellular trafficking.

3.8 Methods

S. cerevisiae Strain Construction

The endogenous genomic copies of *DYN1* and *PAC1* (encoding the dynein heavy chain and Lis1) were modified or deleted using PCR-based methods as previously described[27]. Transformations were performed using the lithium acetate method[28] and screened by colony PCR. Point mutants were generated using QuikChange site-directed mutagenesis (Stratagene) and verified by DNA sequencing.

Nuclear segregation assay

Log-phase cells growing at 30^{o}C were transferred to 16^{o}C for 16 hr. Cells were fixed with 75% ethanol and stained with DAPI. Imaging was performed using a 100x Apo TIRF NA 1.49 objective on a Nikon Ti2 microscope with a Yokogawa-X1 spinning disk confocal system, MLC400B laser engine (Agilent), Prime 95B back-thinned sCMOS camera (Teledyne Photometrics), and a piezo Z-stage (Mad City Labs). The percentage of aberrant binucleate cells was calculated as the number of binucleate cells divided by the sum of dividing wild-type and binucleate cells.

Protein purification

Protein purification steps were done at 4ºC unless otherwise indicated. Dynein constructs were purified from *S. cerevisiae* using a ZZ tag as previously described[16]. Briefly, liquid nitrogen-frozen cell pellets were lysed by grinding in a chilled coffee grinder and resuspended in dynein lysis buffer (DLB: final concentration 30 mM HEPES [pH 7.4], 50 mM potassium acetate, 2 mM magnesium acetate, 1 mM EGTA, 10% glycerol, 1 mM DTT) supplemented with 0.1 mM Mg-ATP, 0.5 mM Pefabloc, 0.05% Triton and cOmplete EDTA-free protease inhibitor cocktail tablet (Roche). The lysate was clarified by centrifuging at 264,900 x g for 1 hr or at 125,100 x g for 2 hr. The clarified supernatant was incubated with IgG Sepharose beads (GE Healthcare Life Sciences) for 1 hr. The beads were transferred to a gravity flow column, washed with DLB buffer supplemented with 250 mM potassium chloride, 0.1 mM Mg-ATP, 0.5 mM Pefabloc and 0.1% Triton, and with TEV buffer (10 mM Tris–HCl [pH 8.0], 150mM potassium chloride, 10% glycerol, 1 mM DTT, and 0.1 mM Mg-ATP). GST-dimerized dynein constructs were labeled with 5 mM Halo- TMR (Promega) in the column for 10 min at room temperature and unbound dyes were washed out with TEV buffer at 4ºC. Dynein was cleaved from IgG beads via incubation with 0.15 mg/mL TEV protease for 1 hr at 16ºC. For dynein monomer constructs, the TEV cleavage step was done overnight at 4ºC and the cleaved proteins were concentrated using 100K MWCO concentrator (EMD Millipore). Cleaved proteins

were filtered by centrifuging with Ultrafree-MC VV filter (EMD Millipore) in a tabletop centrifuge and flash frozen in liquid nitrogen.

Lis1 constructs were purified from *S. cerevisiae* using their His_8 and ZZ tags as previously described[7]. Lysis and clarification steps were similar to dynein purification except for the lysis buffer used was buffer A (final concentration: 50 mM potassium phosphate [pH 8.0], 150 mM potassium acetate, 150 mM sodium chloride, 2 mM magnesium acetate, 5 mM b-mercaptoethanol, 10% glycerol, 0.2% Triton, 0.5 mM Pefabloc) supplemented with 10 mM imidazole (pH 8.0) and cOmplete EDTA-free protease inhibitor cocktail tablet. The clarified supernatant was incubated with Ni-NTA agarose (QIAGEN) for 1 hr. The Ni beads were transferred to a gravity column, washed with buffer A + 20 mM imidazole (pH 8.0) and eluted with buffer A + 250 mM imidazole (pH 8.0). The eluted protein was incubated with IgG Sepharose beads for 1 hr. IgG beads were transferred to a gravity flow column, washed with buffer A + 20 mM imidazole (pH 8.0) and with modified TEV buffer (50 mM Tris–HCl [pH 8.0], 150 mM potassium acetate, 2 mM magnesium acetate, 1 mM EGTA, 10% glycerol, 1 mM DTT). Lis1 was cleaved from the IgG beads via incubation with 0.15 mg/mL TEV protease for 1 hr at 16^{o}C. Cleaved proteins were filtered by centrifuging with Ultrafree-MC VV filter (EMD Millipore) in a tabletop centrifuge and flash frozen in liquid nitrogen.

Electron microscopy sample preparation

Dynein was buffer exchanged into Modification Buffer (100 mM sodium phosphate, pH 8.0, 150 mM NaCl) and biotinylated using water soluble Sulfo ChromaLink biotin (Sulfo ChromaLINK Biotin, Cat #B-1007) in a 1:2 molar ratio for 2 hr at room temperature. Biotinylated protein was dialyzed into TEV buffer overnight. Biotinylation of dynein was verified using a pull-down assay with streptavidin magnetic beads (Thermo Fisher).

Streptavidin affinity grids (SA grids) were prepared as previously described[15]. Just prior to use, the SA grids were washed by touching the SA side of the grid to three drops (2x 50 µL, 1 x 100 µL) of rehydration buffer (150 mM KCl, 50 mM HEPES pH 7.4, 5 mM EDTA) to remove the storage trehalose layer. For complete removal of the protective trehalose layer, rehydration buffer was manually pipetted up and down onto the SA side of the grid, and then the grid was placed onto a 100 µL drop of rehydration buffer for 10 minutes. This process was repeated once, and then the grid was buffered exchanged into sample buffer using five 50 µL drops of sample buffer. 4 µL of sample (150 nM dynein, 150 nM Lis1) was applied to each grid and incubated for ~10 minutes inside a humidity chamber. Unbound protein was washed away by touching the sample side of the grid to three 100 µL drops of sample buffer containing 200 nM Lis1. Grids were vitrified using a Vitrobot (FEI) set to 20°C and 100% humidity. Vitrobot tweezers were kept cold on ice between samples. The sample was first manually wicked inside the Vitrobot using a Whatman No. 1 filter paper, followed by the addition of 1.5 µL of

sample buffer before standard blotting and vitrification proceeded (Blot time: 4s and blot force: 20).

Image collection and processing

Vitrified grids were imaged on a Titan Krios (FEI) operated at an accelerating voltage of 300 kV and the images were recorded with a K2 Summit direct electron detector (Gatan Inc.). We collected 2378 movies in super resolution mode (0.655 Å/super-resolution pixel at the object level) dose-fractionated into 200 ms frames for a total exposure of 10 s with a dose rate of 10 electrons/pixel/s for a total fluence of 58.3 electrons/Å2. The defocus of the images varied within a range of -2.0 µm to -2.7 µm. Automated data collection was executed by SerialEM[29].

Movie frames were aligned using the dose-weighted frame alignment option in UCSF MotionCor2[30] as employed in Relion 3.0[31]. At this stage the individual frames were corrected for the anisotropic magnification distortion inherent to the electron microscope[32]. The signal from the streptavidin lattice was removed from aligned micrographs using Fourier filtering as described previously[15]. Micrographs were manually inspected for defects including sub-optimal ice thickness and incomplete removal of the SA lattice signal and 46 micrographs were removed leaving 2332 micrographs for further processing. CTF estimation was carried out on the non-dose weighted micrographs using GCTF[33] using the local CTF estimation option as implemented in Appion[34]. Images with CTF fits having 0.5 confidence resolution worse than 5 Å were excluded from further processing.

Particles were picked using crYOLO[35] using a training model generated from manually picked particles. The particles were extracted with a down sampled pixel size of 3.93 Å/pixel, and a single round of two-dimensional (2D) classification were carried out in Relion 3.0 to identify bad particles. Particles belonging to good 2D class averages were recentered and extracted (1.31 Å/pixel), and further processed in cryoSPARC. Ab initio models were generated with the majority of particles going into one good class displaying the characteristic features of the dynein motor domain and the WD40 rings of Lis1. Those particles were refined using the non-uniform refinement routine of cryoSPARC[36], against the best ab initio model. This resulted in a 3.2 Å map containing 233 476 particles. We performed per-particle CTF refinement and beam tilt refinement in Relion 3.0 followed by a single round of three-dimensional (3D) classification without alignment. The particles contributing to one of the classes lead to a high resolution reconstruction of the dynein-Lis1 complex and those particles were further refined in Relion 3.0 to generate the final 3.0 Å map (based on the 0.143 cutoff of the gold-standard FSC curve) of the dynein-Lis1 complex. For visualization purposes the map was sharpened with an automatically estimated negative B-factor of 33 (as determined from the “PostProcess” routine of Relion 3.0). The local resolution of the map was estimated using the “local-resolution” routine of Relion 3.0 and the map was low pass filtered according to the local resolution prior to analysis. The 3-D FSC was calculated by 3dfsc version 2.5[37] using the half-maps and the mask used for the PostProcess routine in Relion 3.0.

Model building

The dynein-Lis1 map was segmented using Seggar[38] as implemented in UCSF chimera[39] and the atomic models of the different components were initially built to account for their respective segmented maps. A homology of the Lis1 WD40 domain was generated using I-TASSER[40] and this model was rigid body docked into the corresponding segmented map using the “fit in map” routing in UCSF Chimera. Regions of the model that did not agree with the EM map were manually rebuilt using Coot[41]. The resulting model was used as a reference for Rosetta CM[42] and 1200 models were generated. A hybrid model was made using the two lowest energy output models from Rosetta CM. This model was then manually placed using Coot into both Lis1 sites, and areas of disagreement between the map and the model were resolved manually.

A homology model of the *S. cerevisiae* dynein motor domain was created in Swiss-Model[43] by using the human dynein atomic model in the closed conformation (PDB 5NUG)[44] as a template. The resulting model was fit in the segmented map corresponding to the dynein motor domain using the “fit to map” command in UCSF Chimera, and manually rebuilt in Coot to improve the agreement between the atomic model and the map. The resulting model was used as a template for Rosetta CM and 700 models were generated. The lowest energy model was selected and manually placed into the map, followed by an additional round of manual rebuilding

The resulting models of the dynein motor domain and Lis1 WD40 domains were combined, and further refined against the unsegmented dynein-Lis1 map using an using an iterative process between Phenix Real Space Refine[45] and manual rebuilding in Coot.

Binding curves

To assess dynein/Lis1 binding, Lis1 was first covalently coupled to 16 µL of SNAP-Capture Magnetic Beads (NEB) in 2 mL Protein Lo Bind Tubes (Eppendorf) using the following protocol. Beads were washed twice with 1 mL of modified TEV buffer. Lis1 (0-600nM) was added to the beads and gently shaken for one hour. The supernatant was analyzed via SDS-PAGE to confirm complete depletion of Lis1. The Lis1-conjugated beads were washed once with 1 mL modified TEV buffer and once with 1mL of binding buffer (10 mM Tris–HCl [pH 8.0], 150mM potassium chloride, 2mM magnesium chloride, 10% glycerol, 1 mM DTT, 0.1% NP40, 1mM ADP). 20 nM dynein diluted in binding buffer was added to the Lis1-conjugated beads and gently agitated for 30 minutes. The supernatant was analyzed via SDS-PAGE and depletion was determined using densitometry in ImageJ. Binding curves were fit in Prism8 (Graphpad) with a nonlinear regression for one site binding with Bmax set to 1.

Single-molecule TIRF microscopy

Single-molecule imaging was performed with an inverted microscope (Nikon, Ti-E Eclipse) equipped with a 100x 1.49 N.A. oil immersion objective (Nikon, Plano Apo), a ProScan linear motor stage controller (Prior) and a LU-NV laser launch (Nikon), with 405 nm, 488 nm, 532 nm, 561 nm and 640 nm laser lines. The excitation and emission paths were filtered using appropriate single bandpass filter cubes (Chroma). The emitted signals were detected with an electron multiplying CCD camera (Andor Technology, iXon Ultra 897). Illumination and image acquisition was controlled by NIS Elements Advanced Research software (Nikon).

Single-molecule motility and microtubule binding assays were performed in flow chambers assembled as described previously (Case 1997) using the TIRF microscopy set up described above. Either biotin-PEG-functionalized coverslips (Microsurfaces) or No. 1-1/2 coverslips (Corning) sonicated in 100% ethanol for 10 min were used for the flow-chamber assembly. Taxol-stabilized microtubules with ~10% biotin-tubulin and ~10% fluorescent-tubulin (Alexa405- or 488-labeled) were prepared as described previously[46]. Flow chambers were assembled with taxol-stabilized microtubules by incubating sequentially with the following solutions, interspersed with two washes with assay buffer (30 mM HEPES [pH 7.4], 50 mM potassium acetate, 2 mM magnesium acetate, 1 mM EGTA, 10% glycerol, 1 mM DTT) supplemented with 20 µM Taxol in between: (1) 1 mg/mL biotin-BSA in assay buffer (3 min incubation, ethanol washed coverslips only); (2) 1 mg/mL

streptavidin in assay buffer (3 min incubation) and (3) a fresh dilution of taxol-stabilized microtubules in assay buffer (3 min incubation). After flowing in microtubules, the flow chamber was washed twice with assay buffer supplemented with 1 mg/mL casein and 20 μM Taxol.

Dynein was incubated with Lis1 or modified TEV buffer (to buffer match for Lis1) in assay buffer for 10 minutes before flowing into the assembled flow chamber. The final assay buffer was supplemented with 1 mg/mL casein, 71.5 mM β-mercaptoethanol, an oxygen scavenger system (0.4% glucose, 45 mg/ml glucose catalase, and 1.15 mg/ml glucose oxidase), and 2.5 mM Mg-ATP. For experiments in the presence of vanadate 2.5 mM sodium vanadate was included. The final concentration of dynein was 2-15 pM. For single-molecule microtubule binding assays, the final imaging mixture containing dynein was incubated for an additional 5 min in the flow chamber at room temperature before imaging. After 5 min incubation, microtubules were imaged first by taking a single-frame snapshot. Dynein was imaged by taking a single-frame snapshot. Each sample was imaged at 4 different fields of view and there were between 5 and 10 microtubules in each field of view. In order to compare the effect of Lis1 on microtubule binding, the samples with and without Lis1 were imaged in two separate flow chambers made on the same coverslip on the same day with the same stock of polymerized tubulin as described previously[46]. For single-molecule motility assays, microtubules were imaged first by taking a single-frame snapshot. Dynein was imaged every 1s for 5 min. At the end, microtubules were imaged again by taking a snapshot to assess

stage drift. Movies showing significant drift were not analyzed. Each sample was imaged no longer than 15 min.

Single-molecule microtubule binding assay analysis

Intensity profiles of dynein spots from a single-frame snapshot were generated over a 5-pixel wide line drawn perpendicular to the long axis of microtubules in ImageJ. Intensity peaks at least 2-fold higher than the neighboring background intensity were counted as dynein bound to microtubules. Bright aggregates that were 5-fold brighter than the neighboring intensity peaks were not counted. The average binding density was calculated as the total number of dynein spots divided by the total microtubule length in each snapshot. Normalized binding density was calculated by dividing by the average binding density of dynein without Lis1 collected on the same coverslip (see above). Data plotting and statistical analyses were performed in Prism8 (GraphPad).

Single-molecule motility assay analysis

Kymographs were generated from motility movies and dynein velocity was calculated from kymographs using ImageJ macros as described[46]. Only runs that were longer than 4 frames (4 s) were included in the analysis. Bright aggregates, which were less than 5% of the population, were excluded from the analysis. Data plotting and statistical analyses were performed in Prism8 (GraphPad).

Microtubule co-pelleting assay

Unlabeled Taxol-stabilized MTs were polymerized as above and free tubulin was removed by centrifugation through a 60% glycerol gradient in BRB80 (80 mM PIPES-KOH pH 6.8, 1 mM magnesium chloride, 1mM EGTA, 1mM DTT, 20µM Taxol) for 15min at 100000g and 37ºC. The MT pellet was resuspended in DLB supplemented with 20 µM Taxol. MTs (0-600nM tubulin) were incubated with 100nM Lis1 for 10 minutes before being pelleted for 15min at 100000g and 25ºC. The supernatant was analyzed via SDS-PAGE and depletion was determined using densitometry in ImageJ. Binding curves were fit in Prism8 (Graphpad) with a nonlinear regression for one site binding with Bmax set to 1.

3.9 Acknowledgments

Chapter 3, in full, is a manuscript in preparation: Gillies, JP*; Reimer, JM*; Lahiri I; Karasmanis E; Htet ZM; Leschziner, AE; Reck-Peterson, SL. Structural Basis for Cytoplasmic Dynein-1 Regulation by Lis1. (In preparation). The dissertation author was the co-primary author of this work.

3.10 Supplementary figures

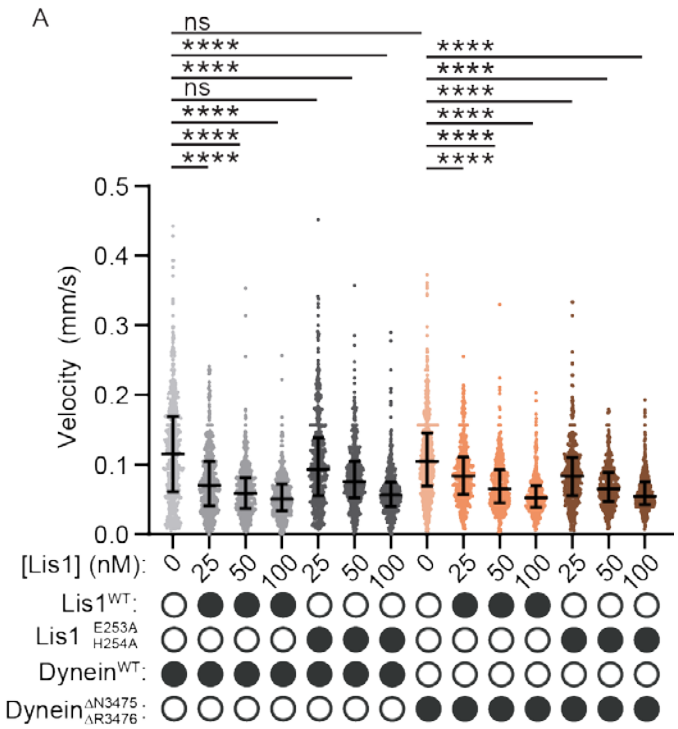

Supplementary Data Figure 3.1. Single-molecule velocity data. A. Raw single-molecule velocity data from Figure 3.2G. The median and interquartile range are shown. n > 400 events per condition. Statistical analysis was performed with a Kruskal-Wallis test; ****, p > 0.0001; ns for Dynein^{WT} + 0 vs + 25nM Lis1$^{E253A, H254A}$ p = 0.8792; ns for Dynein^{WT} vs dynein$^{\Delta N3475,}$ R3476, p > 0.9999.

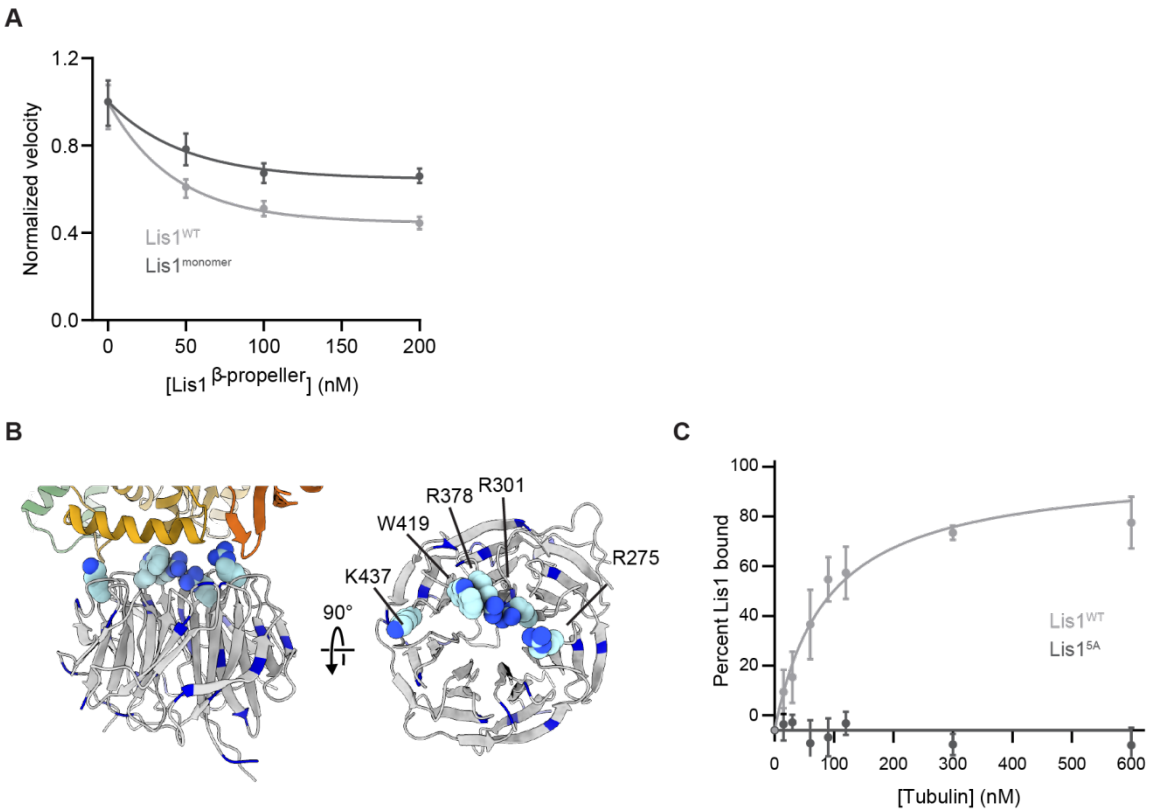

Supplementary Data Figure 3.2. Lis1's interaction with microtubules is not required for dynein regulation at site$_{ring}$. A. Single-molecule velocity of dynein with increasing concentrations of Lis1^{WT} (light grey) or Lis1^{monomer} (dark grey). The median and interquartile range are shown. Data was normalized to a velocity of 1.0 in the absence of Lis1. At least 400 single molecule events were measured per condition. B. The structure of Lis1 at site$_{ring}$ (left) and alone (right) with the five residues mutated in Lis1^{5A} shown as spheres and all Lys and Arg residues in blue. C. Microtubule co-pelleting assay with Lis1^{WT} (light grey) and Lis1^{5A} (dark grey).

3.11 References

1. Reck-Peterson, S. L., Redwine, W. B., Vale, R. D. & Carter, A. P. The cytoplasmic dynein transport machinery and its many cargoes. *Nat. Rev. Mol. Cell Biol.* (2018) doi:10.1038/s41580-018-0004-3.

2. Lipka, J., Kuijpers, M., Jaworski, J. & Hoogenraad, C. C. Mutations in cytoplasmic dynein and its regulators cause malformations of cortical development and neurodegenerative diseases. *Biochem. Soc. Trans.* **41**, 1605–12 (2013).

3. Cianfrocco, M. a., DeSantis, M. E., Leschziner, A. E. & Reck-Peterson, S. L. Mechanism and Regulation of Cytoplasmic Dynein. *Annu. Rev. Cell Dev. Biol.* **31**, annurev-cellbio-100814-125438 (2015).

4. Reiner, O., Carrozzo, R., Shen, Y., Wehnert, M., Faustinella, F., Dobyns, W. B., Caskey, C. T. & Ledbetter, D. H. Isolation of a Miller-Dieker lissencephaly gene containing G protein beta-subunit-like repeats. *Nature* **364**, 717–721 (1993).

5. Tarricone, C., Perrina, F., Monzani, S., Massimiliano, L., Kim, M. H., Derewenda, Z. S., Knapp, S., Tsai, L. H. & Musacchio, A. Coupling PAF signaling to dynein regulation: Structure of LIS1 in complex with PAF-acetylhydrolase. *Neuron* **44**, 809–821 (2004).

6. Kim, M. H., Cooper, D. R., Oleksy, A., Devedjiev, Y., Derewenda, U., Reiner, O., Otlewski, J. & Derewenda, Z. S. The structure of the N-terminal domain of the product of the lissencephaly gene Lis1 and its functional implications. *Structure* **12**, 987–998 (2004).

7. Huang, J., Roberts, A. J., Leschziner, A. E. & Reck-Peterson, S. L. Lis1 acts as a ‘clutch’ between the ATPase and microtubule-binding domains of the dynein motor. *Cell* **150**, 975–986 (2012).

8. Toropova, K., Zou, S., Roberts, A. J., Redwine, W. B., Goodman, B. S., Reck-Peterson, S. L. & Leschziner, A. E. Lis1 regulates dynein by sterically blocking its mechanochemical cycle. *Elife* **3**, 1–25 (2014).

9. DeSantis, M. E., Cianfrocco, M. A., Htet, Z. M., Tran, P. T., Reck-Peterson, S. L. & Leschziner, A. E. Lis1 Has Two Opposing Modes of Regulating Cytoplasmic Dynein. *Cell* **170**, 1197-1208.e12 (2017).

10. Yamada, M., Toba, S., Yoshida, Y., Haratani, K., Mori, D., Yano, Y., Mimori-Kiyosue, Y., Nakamura, T., Itoh, K., Fushiki, S., Setou, M., Wynshaw-Boris, A., Torisawa, T., Toyoshima, Y. Y. & Hirotsune, S. LIS1 and NDEL1 coordinate the plus-end-directed transport of cytoplasmic dynein. *EMBO J.*

27, 2471–2483 (2008).

11. McKenney, R. J., Vershinin, M., Kunwar, A., Vallee, R. B. & Gross, S. P. LIS1 and NudE induce a persistent dynein force-producing state. *Cell* **141**, 304–314 (2010).

12. Baumbach, J., Murthy, A., McClintock, M. A., Dix, C. I., Zalyte, R., Hoang, H. T. & Bullock, S. L. Lissencephaly-1 is a context-dependent regulator of the human dynein complex. *Elife* **6**, 1–31 (2017).

13. Htet, Z. M., Gillies, J. P., Baker, R. W., Leschziner, A. E., DeSantis, M. E. & Reck-Peterson, S. L. LIS1 promotes the formation of activated cytoplasmic dynein-1 complexes. *Nat. Cell Biol.* **22**, 518–525 (2020).

14. Elshenawy, M. M., Kusakci, E., Volz, S., Baumbach, J., Bullock, S. L. & Yildiz, A. Lis1 activates dynein motility by modulating its pairing with dynactin. *Nat. Cell Biol.* (2020) doi:10.1038/s41556-020-0501-4.

15. Han, B. G., Walton, R. W., Song, A., Hwu, P., Stubbs, M. T., Yannone, S. M., Arbeláez, P., Dong, M. & Glaeser, R. M. Electron microscopy of biotinylated protein complexes bound to streptavidin monolayer crystals. *J. Struct. Biol.* **180**, 249–253 (2012).

16. Reck-Peterson, S. L., Yildiz, A., Carter, A. P., Gennerich, A., Zhang, N. & Vale, R. D. Single-Molecule Analysis of Dynein Processivity and Stepping Behavior. *Cell* **126**, 335–348 (2006).

17. Marzo, M. G., Griswold, J. M. & Markus, S. M. Pac1/LIS1 stabilizes an uninhibited conformation of dynein to coordinate its localization and activity. *Nat. Cell Biol.* (2020) doi:10.1038/s41556-020-0492-1.

18. Adames, N. R. & Cooper, J. A. Microtubule interactions with the cell cortex causing nuclear movements in Saccharomyces cerevisiae. *J. Cell Biol.* **149**, 863–874 (2000).

19. Carvalho, P., Gupta, M. L., Hoyt, M. A. & Pellman, D. Cell cycle control of kinesin-mediated transport of Bik1 (CLIP-170) regulates microtubule stability and dynein activation. *Dev. Cell* **6**, 815–829 (2004).

20. Caudron, F., Andrieux, A., Job, D. & Boscheron, C. A new role for kinesin-directed transport of Bik1p (CLIP-170) in Saccharomyces cerevisiae. *J. Cell Sci.* **121**, 1506–1513 (2008).

21. Markus, S. M., Punch, J. J. & Lee, W. L. Motor- and Tail-Dependent Targeting of Dynein to Microtubule Plus Ends and the Cell Cortex. *Curr. Biol.* **19**, 196–205 (2009).

22. Lee, W. L., Oberle, J. R. & Cooper, J. A. The role of the lissencephaly protein Pac1 during nuclear migration in budding yeast. *J. Cell Biol.* **160**, 355–364 (2003).

23. Li, J., Lee, W. L. & Cooper, J. A. NudEL targets dynein to microtubule ends through LIS1. *Nat. Cell Biol.* **7**, 686–690 (2005).

24. Markus, S. M. & Lee, W. L. Regulated offloading of cytoplasmic dynein from microtubule plus ends to the cortex. *Dev. Cell* **20**, 639–651 (2011).

25. Markus, S. M., Plevock, K. M., St. Germain, B. J., Punch, J. J., Meaden, C. W. & Lee, W. L. Quantitative analysis of Pac1/LIS1-mediated dynein targeting: Implications for regulation of dynein activity in budding yeast. *Cytoskeleton* **68**, 157–174 (2011).

26. Sheeman, B., Carvalho, P., Sagot, I., Geiser, J., Kho, D., Hoyt, M. A. & Pellman, D. Determinants of S. cerevisiae dynein localization and activation: Implications for the mechanism of spindle positioning. *Curr. Biol.* **13**, 364–372 (2003).

27. Longtine, M. S., McKenzie, A., Demarini, D. J., Shah, N. G., Wach, A., Brachat, A., Philippsen, P. & Pringle, J. R. Additional modules for versatile and economical PCR-based gene deletion and modification in Saccharomyces cerevisiae. *Yeast* **14**, 953–961 (1998).

28. Guthrie, Christine, and G. R. F. *Methods in enzymology: guide to yeast genetics and molecular biology*. (1991).

29. Mastronarde, D. N. Automated electron microscope tomography using robust prediction of specimen movements. *J. Struct. Biol.* **152**, 36–51 (2005).

30. Zheng, S. Q., Palovcak, E., Armache, J.-P., Verba, K. A., Cheng, Y. & Agard, D. A. MotionCor2: anisotropic correction of beam-induced motion for improved cryo-electron microscopy. *Nat. Methods* **14**, 331–332 (2017).

31. Zivanov, J., Nakane, T., Forsberg, B. O., Kimanius, D., Hagen, W. J., Lindahl, E. & Scheres, S. H. New tools for automated high-resolution cryo-EM structure determination in RELION-3. *Elife* **7**, (2018).

32. Grant, T. & Grigorieff, N. Measuring the optimal exposure for single particle cryo-EM using a 2.6 Å reconstruction of rotavirus VP6. *Elife* **4**, (2015).

33. Zhang, K. Gctf: Real-time CTF determination and correction. *J. Struct. Biol.* **193**, 1–12 (2016).

34. Lander, G. C., Stagg, S. M., Voss, N. R., Cheng, A., Fellmann, D., Pulokas,

J., Yoshioka, C., Irving, C., Mulder, A., Lau, P.-W., Lyumkis, D., Potter, C. S. & Carragher, B. Appion: An integrated, database-driven pipeline to facilitate EM image processing. *J. Struct. Biol.* **166**, 95–102 (2009).

35. Wagner, T., Merino, F., Stabrin, M., Moriya, T., Antoni, C., Apelbaum, A., Hagel, P., Sitsel, O., Raisch, T., Prumbaum, D., Quentin, D., Roderer, D., Tacke, S., Siebolds, B., Schubert, E., Shaikh, T., Lill, P, Gatsogiannis, C, & Raunser, S. SPHIRE-crYOLO is a fast and accurate fully automated particle picker for cryo-EM. Commun. Biol. 2, 218 (2019).36. Punjani, A., Zhang, H. & Fleet, D. Non-uniform refinement: Adaptive regularization improves single particle cryo-EM reconstruction.1–20 (2019) doi:10.1101/2019.12.15.877092.

37. Tan, Y. Z., Baldwin, P. R., Davis, J. H., Williamson, J. R., Potter, C. S., Carragher, B. & Lyumkis, D. Addressing preferred specimen orientation in single-particle cryo-EM through tilting. *Nat. Methods* **14**, 793–796 (2017).

38. Pintilie, G. D., Zhang, J., Goddard, T. D., Chiu, W. & Gossard, D. C. Quantitative analysis of cryo-EM density map segmentation by watershed and scale-space filtering, and fitting of structures by alignment to regions. *J. Struct. Biol.* **170**, 427–438 (2010).

39. Pettersen, E. F., Goddard, T. D., Huang, C. C., Couch, G. S., Greenblatt, D. M., Meng, E. C. & Ferrin, T. E. UCSF Chimera--a visualization system for exploratory research and analysis. *J. Comput. Chem.* **25**, 1605–12 (2004).

40. Roy, A., Kucukural, A. & Zhang, Y. I-TASSER: a unified platform for automated protein structure and function prediction. *Nat. Protoc.* **5**, 725–738 (2010).

41. Emsley, P., Lohkamp, B., Scott, W. G. & Cowtan, K. Features and development of Coot. *Acta Crystallogr. Sect. D Biol. Crystallogr.* **66**, 486–501 (2010).

42. Song, Y., DiMaio, F., Wang, R. Y.-R., Kim, D., Miles, C., Brunette, T., Thompson, J. & Baker, D. High-Resolution Comparative Modeling with RosettaCM. *Structure* **21**, 1735–1742 (2013).

43. Waterhouse, A., Bertoni, M., Bienert, S., Studer, G., Tauriello, G., Gumienny, R., Heer, F. T., de Beer, T. A. P., Rempfer, C., Bordoli, L., Lepore, R. & Schwede, T. SWISS-MODEL: homology modelling of protein structures and complexes. *Nucleic Acids Res.* **46**, W296–W303 (2018).

44. Zhang, K., Foster, H. E., Rondelet, A., Lacey, S. E., Bahi-Buisson, N., Bird, A. W. & Carter, A. P. Cryo-EM Reveals How Human Cytoplasmic Dynein Is Auto-inhibited and Activated. *Cell* **169**, 1303-1314.e18 (2017).

45. Afonine, P. V., Poon, B. K., Read, R. J., Sobolev, O. V., Terwilliger, T. C., Urzhumtsev, A. & Adams, P. D. Real-space refinement in PHENIX for cryo-EM and crystallography. *Acta Crystallogr. Sect. D Struct. Biol.* **74**, 531–544 (2018).

46. Roberts, A. J., Goodman, B. S. & Reck-Peterson, S. L. Reconstitution of dynein transport to the microtubule plus end by kinesin. *Elife* **2014**, 1–16 (2014).

Chapter 4:

Discussion and Future Directions

4.1 Regulation of activated dynein complexes by Lis1

We and others[1] have shown that Lis1 promotes formation of activated dynein complexes composed of dynein, dynactin and an activating adaptor (Figure 4.1 #1-3). Contemporaneous work in the model organism *A. nidulans* came to a similar conclusion using a genetic approach[2], suggesting that this is a conserved mechanism of Lis1. Dynein has also been shown to form the autoinhibited phi conformation in organisms ranging from yeast to humans[3,4], leading to the attractive model that Lis1 relieves dynein's autoinhibited phi conformation to promote the assembly of activated dynein complexes (Figure 4.1 #1).

Mutations that disrupt the autoinhibited phi conformation do not completely rescue the loss of Lis1[2,5]. This raises the possibility that Lis1 promotes dynein complex assembly in other ways. For example, Lis1 binding to dynein may have allosteric effects that promote the formation of activated dynein complexes, such as inducing the parallel conformation of dynein that is observed when it interacts with dynactin and activating adaptors[6,7] (Figure 4.1 #1). To determine if this is the case, future work could use negative stain EM to score the dynein conformation as phi, parallel or open in the presence of Lis1 as has been done previously for dynein alone[3]. Alternatively, a FRET pair could be inserted into dynein so that FRET occurs when dynein is in the parallel conformation. This could be used to measure the percentage of dynein in the parallel conformation in the presence of Lis1 as well as other dynein regulators such as dynactin or activating adaptors.

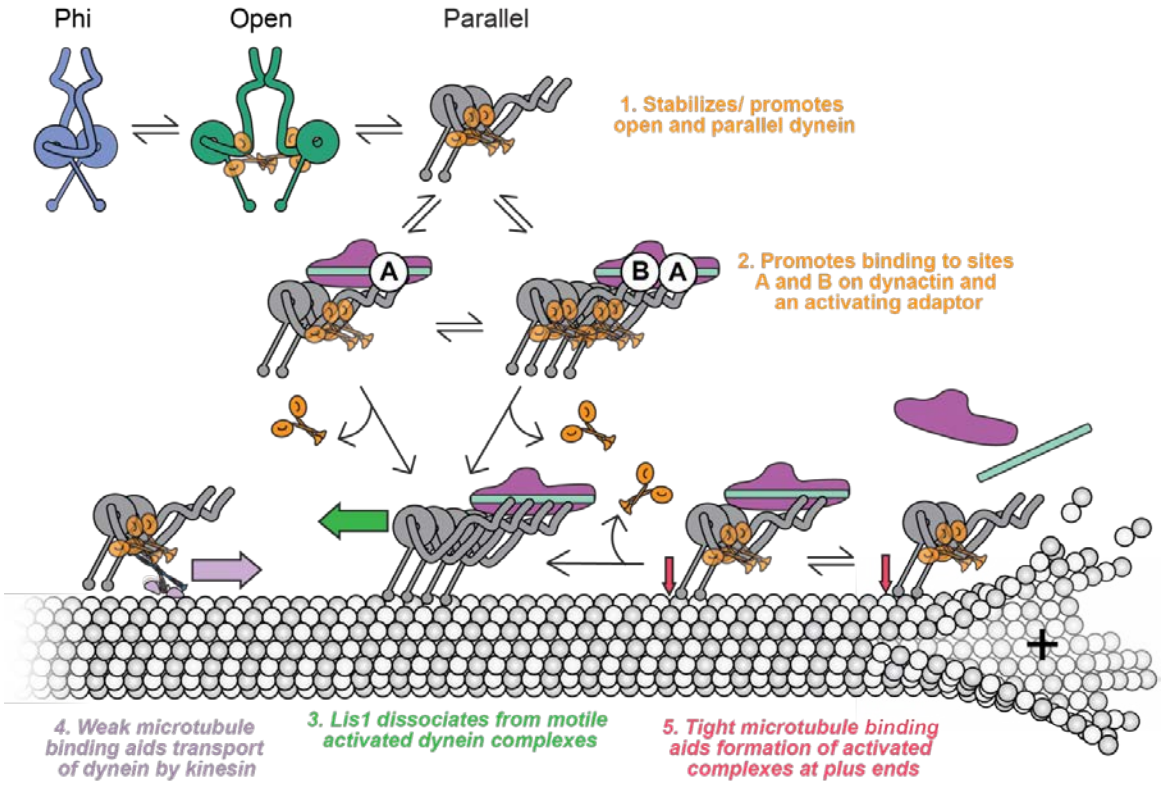

Figure 4.1. Activation of dynein by Lis1. Lis1 may promote assembly of activated dynein complexes through the following methods. **1.** Lis1 may promote the open dynein conformation and favor a parallel conformation of dynein that is primed to assemble the fully activated complex. **2.** Lis1 favors the recruitment of dynein to both binding sites of dynactin and an activating adaptor. **3.** Once a fully activated dynein/ dynactin/ activating adaptor complex is formed, Lis1 dissociates from the moving complex. Lis1's regulation of dynein's mechanochemistry may support its role in forming activated dynein complexes. **4.** The Lis1-induced weak microtubule binding state of dynein aids in the transport of dynein to the plus ends of microtubules. **5.** Lis1-induced tight microtubule binding may serve to retain dynein at the plus ends of microtubules to aid in the formation of a complex with two dynein dimers, dynactin and an activating adaptor.

4.2 Regulation of dynein mechanochemistry by Lis1

We have further explored Lis1's regulation of dynein mechanochemistry. We found that Lis1's contact with AAA5 supports, but is not required for, the Lis1-induced strengthening of dynein's microtubule binding (Figure 4.1 #5). This mode of regulation is conserved from yeast to humans, as are the binding sites required for it. *In vivo* tight microtubule binding may aid the formation of activated dynein complexes (Figure 4.1). For example, Lis1 has a role in initiating transport from microtubule plus ends[8–10], where tight microtubule binding and reduced motility is likely important for maintaining dynein at these sites and aiding in the challenging kinetics of loading two dynein motors on to dynactin before transport begins. Binding of Lis1 to dynein at microtubule plus ends could also promote the opening of the phi conformation to lead to the formation of activated dynein complexes containing two dynein dimers. This will need to be further tested in organisms such as *A. nidulans,* which has been used extensively to study the mechanism of dynein-based organelle transport *in vivo*[2,10,11]. *A. nidulans* dynein is responsible for the transport of endosomes, and loss of Lis1 results in clusters of endosomes at microtubule plus ends[10]. Based on our work, I hypothesize that loss of Lis1-dependent tight microtubule binding at plus ends would make it more difficult for dynein to load onto endosomes, resulting in a similar clustering phenotype.

Lis1 is also able to lower dynein's microtubule binding affinity (Figure 4.1 #4), and we showed that a Lis1 contact at dynein's AAA4 as well as the interface between the two Lis1 β-propellers are both required for this mode of regulation. In

yeast, this function of Lis1 correlates with defects in dynein being transported as a cargo to the plus end by kinesins, during which it is advantageous for dynein to have weak microtubule binding affinity[12]. Lis1 also enhances targeting of dynein to the microtubule plus end in mammalian cells[13]. However in some organisms, such as *A. nidulans,* dynein localization at microtubule plus ends requires kinesin but is independent of Lis1[14]. This is surprising because the Lis1 binding site on dynein's stalk is conserved from yeast to humans[5,12], so it remains to be seen what additional roles this regulation may have. Future work using mutations based on those we have made in yeast will be able to determine this. The conservation of the Lis1-induced release of dynein from the microtubule could be tested using human proteins in single-molecule assays, similar to the ones in chapter 3. For determining the role this form of Lis1 regulation has in cargo transport, these mutations could be made in *A. nidulans* and the effect on endosome localization and velocity could be measured.

It will also be important to determine which of the Lis1 binding sites on dynein aide in the assembly of activated dynein complexes. In chapter 3, and in previous work from our lab[12,15,16], we have designed a number of mutants that abrogate Lis1 binding to either dynein's ring or stalk. These mutants could be made in human proteins and tested in the recruitment assays presented in chapter 2 to determine which sites are responsible for the formation of activated dynein complexes. It may be necessary to solve a high-resolution structure of human dynein and Lis1 to make mutations that will disrupt this interaction in the human

proteins. Additionally, it has been reported previously, using yeast two-hybrid assays, that mammalian Lis1 may interact with the tail and accessory chains of dynein[17]. Neither the tail of dynein nor its associated chains were present in our structural work with yeast proteins. It is possible that Lis1's interaction with dynein's tail could orient dynein into a parallel conformation.

4.3 Regulation of dynein by Lis1 and Nudel

We now have a good molecular model for how Lis1 regulates dynein. Going forward it will be important to understand how another set of regulatory factors, members of the conserved protein family Nudel, function in this framework since they are known to be key members of the dynein-Lis1 regulatory pathway. This family of proteins was first discovered as a nuclear migration mutant gene in *Neurospora*[18]. In mammals there are two homologs, NudE and NudeL (Referred to collectively as "Nudel" here). Both homologs are critical; in mice knockout of NudE results in reduced brain volume while knockout of NudeL results in embryonic lethality[19,20]. Nudel was linked to the dynein pathway in *Aspergillus nidulans* in a Lis1 mutant suppressor screen[21], and has been shown to bind to both dynein and Lis1[22–24]. This suggests that Nudel may act as a tether, effectively increasing the local Lis1 concentration. In support of this, in *Aspergillus nidulans* it has been shown that overexpression of Lis1 can rescue the growth defects caused by Nudel deletion[25]. Furthermore, supplementing Nudel-depleted *Xenopus* extracts with Lis1 rescued defects in spindle morphogenesis[26]. Nudel has also been found to induce

slowing of dynein velocity at lower concentrations of Lis1 using purified yeast proteins[15]. In addition, with mammalian proteins Nudel was found to retain Lis1 on dynein coated beads and maintain Lis1-induced prolongation of force generation after washes that remove Lis1 in the absence of Nudel[27].

However, experiments with mammalian dynein have found opposing effects of Nudel and Lis1 on microtubule binding. Nudel decreases dynein's microtubule binding affinity and increases dynein's velocity in microtubule gliding assays[27–29]. This indicates that in addition to any role of tethering Lis1 to dynein, Nudel appears to directly affect dynein's mechanochemistry on its own. It will be important to fully characterize how Nudel regulates dynein on its own before working on how Lis1 and Nudel work in tandem. This includes determining how factors such as the concentration of Nudel, the nucleotide state of dynein's AAA domains, or the force that is put on dynein by cargoes affects Nudel regulation. In addition, given our work that implicates Lis1 in the formation of dynein complexes, it will be important to investigate Nudel's role in the context of activated dynein complexes. If Nudel does not influence the formation of activated dynein complexes on its own, it may be important for increasing the local Lis1 concentration to help Lis1 perform this role. Alternatively, Nudel could help remove Lis1 from dynein once complexes form and begin moving on the microtubule since Lis1 inhibits the motility of the complex if it remains bound.

4.4 Concluding remarks

In summary, the results I have presented in this thesis highlight the sophisticated nature of dynein regulation by Lis1 and provide novel insight into the nature of this regulation. We have identified a new role for Lis1 in forming activated dynein complexes. We have also elucidated the mechanisms of Lis1's two modes of regulation of dynein's mechanochemical cycle. We have now begun to bridge the gap between our mechanistic knowledge of dynein's regulation by Lis1 with the many known *in vivo* roles, allowing us to continue to build our understanding of the complex web of dynein regulation.

4.5 References

1. Elshenawy, M. M., Kusakci, E., Volz, S., Baumbach, J., Bullock, S. L. & Yildiz, A. Lis1 activates dynein motility by modulating its pairing with dynactin. *Nat. Cell Biol.* (2020) doi:10.1038/s41556-020-0501-4.

2. Qiu, R., Zhang, J. & Xiang, X. LIS1 regulates cargo-adapter-mediated activation of dynein by overcoming its autoinhibition in vivo. *J. Cell Biol.* **218**, 3630–3646 (2019).

3. Zhang, K., Foster, H. E., Rondelet, A., Lacey, S. E., Bahi-Buisson, N., Bird, A. W. & Carter, A. P. Cryo-EM Reveals How Human Cytoplasmic Dynein Is Auto-inhibited and Activated. *Cell* **169**, 1303-1314.e18 (2017).

4. Marzo, M. G., Griswold, J. M. & Markus, S. M. Pac1/LIS1 stabilizes an uninhibited conformation of dynein to coordinate its localization and activity. *Nat. Cell Biol.* (2020) doi:10.1038/s41556-020-0492-1.

5. Htet, Z. M., Gillies, J. P., Baker, R. W., Leschziner, A. E., DeSantis, M. E. & Reck-Peterson, S. L. LIS1 promotes the formation of activated cytoplasmic dynein-1 complexes. *Nat. Cell Biol.* **22**, 518–525 (2020).

6. Urnavicius, L., Lau, C. K., Elshenawy, M. M., Morales-Rios, E., Motz, C., Yildiz, A. & Carter, A. P. Cryo-EM shows how dynactin recruits two dyneins for faster movement. *Nature* **554**, 202–206 (2018).

7. Grotjahn, D. A., Chowdhury, S., Xu, Y., McKenney, R. J., Schroer, T. A. & Lander, G. C. Cryo-electron tomography reveals that dynactin recruits a team of dyneins for processive motility. *Nat. Struct. Mol. Biol.* **25**, 203–207 (2018).

8. Lenz, J. H., Schuchardt, I., Straube, A. & Steinberg, G. A dynein loading zone for retrograde endosome motility at microtubule plus-ends. *EMBO J.* **25**, 2275–2286 (2006).

9. Moughamian, A. J., Osborn, G. E., Lazarus, J. E., Maday, S. & Holzbaur, E. L. F. Ordered recruitment of Dynactin to the microtubule plus-end is required for efficient initiation of retrograde axonal transport. *J. Neurosci.* **33**, 13190–13203 (2013).

10. Egan, M. J., Tan, K. & Reck-Peterson, S. L. Lis1 is an initiation factor for dynein-driven organelle transport. *J. Cell Biol.* **197**, 971–982 (2012).

11. Xiang, X. & Qiu, R. Cargo-Mediated Activation of Cytoplasmic Dynein in vivo. *Front. Cell Dev. Biol.* **8**, 1–15 (2020).

12. DeSantis, M. E., Cianfrocco, M. A., Htet, Z. M., Tran, P. T., Reck-Peterson, S. L. & Leschziner, A. E. Lis1 Has Two Opposing Modes of Regulating Cytoplasmic Dynein. *Cell* **170**, 1197-1208.e12 (2017).

13. Splinter, D., Razafsky, D. S., Schlager, M. A., Serra-Marques, A., Grigoriev, I., Demmers, J., Keijzer, N., Jiang, K., Poser, I., Hyman, A. A., Hoogenraad, C. C., King, S. J. & Akhmanova, A. BICD2, dynactin, and LIS1 cooperate in regulating dynein recruitment to cellular structures. *Mol. Biol. Cell* **23**, 4226–4241 (2012).

14. Zhang, J., Han, G. & Xiang, X. Cytoplasmic dynein intermediate chain and heavy chain are dependent upon each other for microtubule end localization in Aspergillus nidulans. *Mol. Microbiol.* **44**, 381–392 (2002).

15. Huang, J., Roberts, A. J., Leschziner, A. E. & Reck-Peterson, S. L. Lis1 acts as a ‘clutch’ between the ATPase and microtubule-binding domains of the dynein motor. *Cell* **150**, 975–986 (2012).

16. Toropova, K., Zou, S., Roberts, A. J., Redwine, W. B., Goodman, B. S., Reck-Peterson, S. L. & Leschziner, A. E. Lis1 regulates dynein by sterically blocking its mechanochemical cycle. *Elife* **3**, 1–25 (2014).

17. Tai, C. Y., Dujardin, D. L., Faulkner, N. E. & Vallee, R. B. Role of dynein, dynactin, and CLIP-170 interactions in LIS1 kinetochore function. *J. Cell Biol.* **156**, 959–968 (2002).

18. Minke, P. F., Lee, I. H., Tinsley, J. H., Bruno, K. S. & Plamann, M. Neurospora crassa ro-10 and ro-11 genes encode novel proteins required for nuclear distribution. *Mol. Microbiol.* **32**, 1065–1076 (1999).

19. Feng, Y. & Walsh, C. A. Mitotic spindle regulation by Nde1 controls cerebral cortical size. *Neuron* **44**, 279–293 (2004).

20. Sasaki, S., Mori, D., Toyo-oka, K., Chen, A., Garrett-beal, L., Muramatsu, M., Miyagawa, S., Hiraiwa, N., Yoshiki, A., Wynshaw-boris, A. & Hirotsune, S. Complete Loss of Ndel1 Results in Neuronal Migration Defects and Early Embryonic Lethality. *Mol. Cell. Biol.* **25**, 7812–7827 (2005).

21. Efimov, V. P. & Morris, N. R. The LIS1-related NUDF protein of Aspergillus nidulans interacts with the coiled-coil domain of the NUDE/RO11 protein. *J. Cell Biol.* **150**, 681–688 (2000).

22. Wang, S. & Zheng, Y. Identification of a novel dynein binding domain in nudel essential for spindle pole organization in Xenopus egg extract. *J. Biol. Chem.* **286**, 587–593 (2011).

23. Sasaki, S., Shionoya, A., Ishida, M., Gambello, M. J., Yingling, J., Wynshaw-Boris, A. & Hirotsune, S. A LIS1/NUDEL/cytoplasmic dynein heavy chain complex in the developing and adult nervous system. *Neuron* **28**, 681–696 (2000).

24. Derewenda, U., Tarricone, C., Choi, W. C., Cooper, D. R., Lukasik, S., Perrina, F., Tripathy, A., Kim, M. H., Cafiso, D. S., Musacchio, A. & Derewenda, Z. S. The Structure of the Coiled-Coil Domain of Ndel1 and the Basis of Its Interaction with Lis1, the Causal Protein of Miller-Dieker Lissencephaly. *Structure* **15**, 1467–1481 (2007).

25. Efimov, V. P. Roles of NUDE and NUDF Proteins of Aspergillus nidulans: Insights from Intracellular Localization and Overexpression Effects. *Mol. Biol. Cell* **14**, 871–888 (2003).

26. Wang, S., Ketcham, S. A., Schon, A., Goodman, B., Wang, Y., Yates, J., Freire, E., Schroer, T. A. & Zheng, Y. Nudel/NudE and Lis1 promote dynein and dynactin interaction in the context of spindle morphogenesis. *Mol. Biol. Cell* **24**, 3522–3533 (2013).

27. McKenney, R. J., Vershinin, M., Kunwar, A., Vallee, R. B. & Gross, S. P. LIS1 and NudE induce a persistent dynein force-producing state. *Cell* **141**, 304–314 (2010).

28. Yamada, M., Toba, S., Yoshida, Y., Haratani, K., Mori, D., Yano, Y., Mimori-Kiyosue, Y., Nakamura, T., Itoh, K., Fushiki, S., Setou, M., Wynshaw-Boris,

A., Torisawa, T., Toyoshima, Y. Y. & Hirotsune, S. LIS1 and NDEL1 coordinate the plus-end-directed transport of cytoplasmic dynein. *EMBO J.* **27**, 2471–2483 (2008).

29. Torisawa, T., Nakayama, A., Furuta, K., Yamada, M., Hirotsune, S. & Toyoshima, Y. Y. Functional dissection of LIS1 and NDEL1 towards understanding the molecular mechanisms of cytoplasmic dynein regulation. *J. Biol. Chem.* **286**, 1959–1965 (2011).